ANALYSIS AND CALCULATION OF INTERNAL SEPARATED FLOW AT LARGE REYNOLDS NUMBER

BY

ANAND KUMAR

ME
1976
D
KUM
ANA

TH.
ME/1976/D
K96a

DEPARTMENT OF MECHANICAL ENGINEERING
INDIAN INSTITUTE OF TECHNOLOGY KANPUR

JUNE 1976

ANALYSIS AND CALCULATION OF INTERNAL SEPARATED FLOW AT LARGE REYNOLDS NUMBER

A Thesis Submitted
in Partial Fulfilment of the Requirements
for the Degree of
DOCTOR OF PHILOSOPHY

BY

ANAND KUMAR

3182

to the

DEPARTMENT OF MECHANICAL ENGINEERING
INDIAN INSTITUTE OF TECHNOLOGY KANPUR

JUNE 1976

CERTIFICATE

Certified that this work has been carried out under our supervision and that this has not been submitted elsewhere for a degree.

Dr. K.S. YAJNIK,
Scientist E, Aerodynamics,
National Aeronautical Laboratory,
Bangalore 560017.

(Formerly, Associate Professor,
Departmemt of Mechanical Engineering,
Indian Institute of Technology,
Kanpur 208016.)

Prof. V.K. STOKES,
Professor and Head,
Department of Mechanical Engineering,
Indian Institute of Technology,
Kanpur 208016.

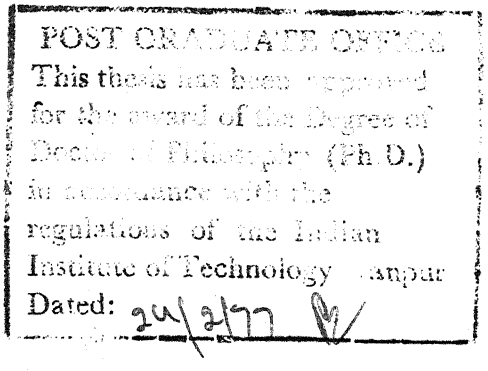

I. I. T. KANPUR
CENTRAL LIBRARY
Acc. No. 51152
22 SEP 1977

ME-1976-D-KUM-ANA.

ACKNOWLEDGEMENTS

I am indebted to my teachers Prof. V.K. Stokes, Dr. K.S. Yajnik, Prof. M.M. Oberai and Prof. R.K. Jain who have been early architects of my academic pursuit.

Dr. K.S. Yajnik has been my principal advisor. Subsequent to his resignation from the staff of the IIT, it became necessary to appoint another advisor. Prof. V.K. Stokes was kind enough to have agreed to it. I express my thanks to both of them.

This work was started at IIT Kanpur. Later I joined NAL Bangalore as a Scientist. I am thankful to SFGC, IIT Kanpur and Director, NAL Bangalore to have permitted me to continue this work.

I am also thankful to Shri M.B. Ananda for a good job of typing and to late Shri S.S. Rao and the staff of Drawing Office, Aero. Divn., NAL for the drawings.

Anand Kumar

ACKNOWLEDGEMENTS

I am indebted to my teachers Prof. V.K. Stokes, Dr. K.S. Yajnik, Prof. M.M. Oberai and Prof. R.K. Jain who have been early architects of my academic pursuit.

Dr. K.S. Yajnik has been my principal advisor. Subsequent to his resignation from the staff of the IIT, it became necessary to appoint another advisor. Prof. V.K. Stokes was kind enough to have agreed to it. I express my thanks to both of them.

This work was started at IIT Kanpur. Later I joined NAL Bangalore as a Scientist. I am thankful to SFGC, IIT Kanpur and Director, NAL Bangalore to have permitted me to continue this work.

I am also thankful to Shri M.B. Ananda for a good job of typing and to late Shri S.S. Rao and the staff of Drawing Office, Aero. Divn., NAL for the drawings.

Anand Kumar

TABLE OF CONTENTS

LIST OF TABLES

LIST OF FIGURES

ANALYSIS AND CALCULATION OF INTERNAL SEPARATED FLOW AT LARGE REYNOLDS NUMBER

A Thesis Submitted
In Partial Fulfilment of the Requirements
for the Degree of
DOCTOR OF PHILOSOPHY

by
ANAND KUMAR
to the
DEPARTMENT OF MECHANICAL ENGINEERING
INDIAN INSTITUTE OF TECHNOLOGY KANPUR
June 1976

ABSTRACT

Large Reynolds number approximations are examined for certain internal separated flows by considering various limits. It is argued that the equation governing the flows except possibly for some subregions, has the form of the boundary-layer equation, as the inertial and viscous forces are of the same order. A method of calculation is then developed which uses the eigenfunctions of the linear problem governing the far-downstream flow. It leads to a set of coupled, first order, ordinary differential equations. It is first tested for two cases for which results based on the Navier-Stokes equations are available. Details of the flow including streamlines in the recirculating regions are well predicted. It is concluded that the equation represents the large Reynolds number behaviour of the flows considered. Flow problems with three types of wall geometry are then solved. They are a channel having symmetric sudden expansion,

a channel having asymmetric sudden expansion and a base placed symmetrically in a channel. Calculations are performed for various values of the ratio of the upstream channel width to that downstream. Also two types of entry conditions representing a long and a short inlet are considered. Results which are presented include centreline velocity, velocity profiles, development length, streamlines, skin friction, pressure distribution and pressure recovery coefficient.

CHAPTER 1

INTRODUCTION

Separated flows constitute an important but difficult area of fluid mechanics. Boundary-layer approximations provide substantial simplifications in attached flows at large Reynolds number. In particular, the outer flow can be obtained to the lowest order, by an inviscid calculation in which the condition of zero normal velocity at the wall is satisfied. This is because the boundary-layer and the wake where the viscous forces and the inertial forces are of the same order, are rather thin and their effect on the outer flow is of a higher order. Separated flows, on the other hand, have quite thick rotational regions and the outer flow is affected substantially. Consequently, the outer flow calculation presents certain difficulties which have yet to be fully resolved.

The present thesis deals with a simpler class of separated flows which has one ingredient in common with external separated flows, namely that they have thick rotational regions. We consider the flows confined between two walls (Figure 1), which belong to the category of internal separated flows. One such flow is the flow in a channel having a sudden expansion in which recirculating regions are formed downstream of the expansion. As we shall see in Chapter 2, there are two types of internal separated

flows which differ in their streamwise length scales.

Limiting equations for various longitudinal and transverse length scales are examined as $R \to \infty$ (Chapter 2). It turns out that for the type of internal separated flow problem referred to earlier, the streamwise length scale is of order R. As the inertial forces are of the order of the viscous forces in the limit considered, the equation has the form of the boundary-layer equation. However, the longitudinal and transverse length scales of the present problem are different from the classical boundary-layer scales. Also, the pressure gradient is an additional unknown which is determined by using four boundary conditions arising from the walls unlike the boundary-layer problem.

A calculation procedure of the equation, which is developed in Chapter 3, exploits the ultimate development of the flow into Poiseuille flow ψ_p by taking the solution in the form

$$\psi(x,y;R) = \psi_p(y) + \sum_i a_i(x/R)\,\phi_i(y) \ ,$$

where x and y are the streamwise and transverse coordinates and ψ is the stream function. Usually in an integral relations method, the expansion set ϕ_i and the weighting functions are chosen for their analytical properties and computational simplicity. We however, adopt a different approach here. The flow at large downstream distances is

a small perturbation of the Poiseuille flow which leads to an eigenvalue problem. Its eigenfunctions form an efficient expansion set as the resulting set of coupled ordinary differential equations tend to get decoupled with increasing x. The weighting functions are the natural ones arising from the eigenvalue problem. The given flow problem then reduces to integrating these differential equations which are coupled quasi-linear and of first order. The initial condition has to be obtained by matching the far-flow field with the near-flow field. In the absence of any rigorous description of the near-flow field, a hypothesis is made to give the initial condition.

The scheme of calculation is first applied to two test cases for which numerical results based on the complete Navier-Stokes equations are available, and can be compared with the present calculation. The first problem to be taken up is the now classical entry flow problem (Chapter 4). Its simple geometry forms a suitable testing ground for theories and methods and hence is considered here, although no recirculating regions are present. The second test case is the flow in a channel having a symmetric sudden expansion with an expansion ratio of two. Comparison of the present calculation with that based on the Navier-Stokes equations for large R (Hung and Macagno, 1966) is found to be very good. Not only the gross quantities of interest such as the length of the recirculating region and the total recirculat

are found to agree well, but also the streamline pattern is well predicted. These results are discussed in Chapter 5.

The above comparison shows that the present method of expansion into eigenfunctions of the far downstream flow provides a suitable calculation procedure, and it also demonstrates the applicability of the limiting equation. We thus conclude that the streamwise length scale for such flows is of order R, the viscous term and the inertia term are of the same order, and the governing equation is parabolic despite the presence of recirculating regions.

Flow problems with three different types of wall geometry are solved by using the present method (see Figure 1). One type illustrates the applicability of the method to asymmetric flow problems. Another type models a base between two walls. Calculations are made for various values of the geometrical parameter h, and are included in Chapter 5. The results of these calculations are believed to be new.

As the method uses an eigenfunction expansion, the calculation, in principle, should be continued with increasing number of terms until a satisfactory convergent trend is obtained. However, we have used a rather small number of terms in the calculations. For example, the favourable comparison in the case of the symmetric sudden

expansion mentioned earlier is obtained with only three terms. The maximum number of terms used in the present calculations is therefore limited to five. Obviously the choice of the number of terms would depend on the wall geometry, the entry profile and the desired accuracy.

If the number of terms to be used in a calculation is fixed, a difficulty may be encountered in the integration of the ordinary differential equations. This difficulty is essentially due to the non-linear evolution term and is a general feature whenever a moment method or an integral relations method is applied to the present type of partial differential equation. This issue is discussed in Section 3.5. Phase plane analysis of the ordinary differential equation when two terms are used, is given to illustrate this feature.

We have restricted our attention to steady laminar two-dimensional flow of a Newtonian incompressible fluid, although the basic elements of the analysis would be applicable to a larger class of problems. We have however chosen to apply the method to three types of wall geometry, for a range of the parameter h, two type of entry conditions, and three choices of the number of terms with a view to obtain insight into the performance and the applicability of the method.

CHAPTER 2

LIMIT EQUATION FOR LARGE REYNOLDS NUMBER

2.1 GOVERNING EQUATION

The equation governing the two-dimensional plane steady laminar motion of a Newtonian incompressible fluid is

$$J(\nabla^2\psi, \psi) = R^{-1}\nabla^2\nabla^2\psi \quad , \tag{2.1}$$

where ψ is the stream function. The two cartesian coordinates are denoted by x and y, and ∇^2 and J denote the Laplacian and the Jacobian operators respectively. The above equation is written in the non-dimensional form, R being the Reynolds number. Equation (2.1), known as the vorticity transport equation, is obtained from the two momentum equations and the equation of continuity. The above equation, without any approximation, will be denoted by NSE.

2.2 LARGE REYNOLDS NUMBER LIMITS

Let the scales of x, y and ψ be denoted by L_x, L_y and γ respectively. Then the orders of the various terms in equation (2.1) are

$$(\gamma^2/L_x^3L_y, \ \gamma^2/L_xL_y^3), \ (\gamma/RL_x^4, \ \gamma/RL_x^2L_y^2, \ \gamma/RL_y^4) \ .$$

The first bracket shows the orders of inertia terms, while the orders of viscous terms are shown in the second bracket.

Terms of the lowest order in either group will depend on the order relation between the two length scales L_x and L_y. Therefore three sets of limits are possible depending on whether $L_x \sim L_y$*, $L_y \subset L_x$, or $L_x \subset L_y$. Possible limit equations are given below and each limit equation has been designated by E, V, B or N standing for inviscid, viscous, boundary-layer or Navier-Stokes types of limits.

$$L_x \sim L_y$$

E : $J(\nabla^2 \psi, \psi) = 0$

N : $J(\nabla^2 \psi, \psi) = R^{-1} \nabla^2 \nabla^2 \psi$

V : $\nabla^2 \nabla^2 \psi = 0$

$$L_y \subset L_x$$

E_y : $J(\psi_{yy}, \psi) = 0$

B_y : $J(\psi_{yy}, \psi) = R^{-1} \psi_{yyyy}$

V_y : $\psi_{yyyy} = 0$

---

* The order symbols used here have the following meaning.

$L_x \sim L_y$: $0 < \lim_{R \to \infty} L_x/L_y < \infty$

$L_x \subset L_y$: $\lim_{R \to \infty} L_x/L_y = 0$

$L_x \supset L_y$: $L_y \subset L_x$

$$L_x \subset L_y$$

$$E_x \quad : \quad J(\psi_{xx}, \psi) = 0$$

$$B_x \quad : \quad J(\psi_{xx}, \psi) = R^{-1} \psi_{xxxx}$$

$$V_x \quad : \quad \psi_{xxxx} = 0 \qquad (2.2)$$

Suffixes x and y following ψ denote respective partial derivatives.

Limit equations E_y and V_y can be obtained from B_y, and E_x and V_x from B_x. Limit equations E_y and E_x are contained in E and V contains V_x and V_y. Distinguished limits are those corresponding to E, V, B_y and B_x and N is the complete equation of motion.

E is the Euler equation governing inviscid fluid flow. Stokes equation in which only viscous terms are retained is designated by V. Interestingly, Stokes equation is obtained for large Reynolds number R. However, the appropriate Reynolds number γR goes to zero. B_y is the familiar boundary-layer equation differentiated once with respect to y to eliminate the pressure term. E_y is sometimes referred to as the inviscid boundary-layer equation. B_x and E_x are x counterparts of B_y and E_y respectively.

The domains of validity of the various limit equations can be readily visualised with the help of a three-dimensional plot with axes L_x, L_y and γ (Figure 2). This plot

is of a special nature as the axes are order axes. That is, a point, say $(R, \sqrt{R}, 1)$, denotes $L_x \sim R$, $L_y \sim \sqrt{R}$ and $\gamma \sim 1$. The choice of a log scale for the axes makes the representation simpler. A suitable unit for the plot is R. In Figure 2, OA = OB = OP = R.

$L_x \sim L_y$ represents the plane IGHJ in Figure 2. $\gamma \sim 1/R$ on the line EF in this plane, and the limit equation N is valid on this line. The domains of validity of the limit equations E and V are the portion above and below the line EF of the plane $L_x \sim L_y$, that is EGHF and IEFJ respectively, excluding the line EF in both cases.

As equation (2.1) is symmetric in x and y, the order space plot is symmetric about the plane $L_x \sim L_y$. Consider the case when $L_y \subset L_x$. The order of the inertia term is $\gamma^2/L_x L_y^3$ and that of the viscous term is γ/RL_y^4. When the two terms are of the same order, $\gamma L_y/L_x \sim R^{-1}$ which represents the plane EKLF due to the choice of log scales for the axes. This plane, to be called B_y, meets the plane $L_x \sim L_y$ along the line EF. Since $L_y \subset L_x$, B_y is restricted to only one side of the plane $L_x \sim L_y$. Limit equation B_y is valid on this plane except for the line EF. The domain of validity of the limit equation E_y and V_y are regions above and below the plane B_y such that $L_y \subset L_x$, that is, regions between the planes EGHF and EKLF and between the planes EIJF and EKLF respectively. A similar construction

is carried out when $L_x \subset L_y$. Each plane in the figure is infinite or semi-infinite. The construction of the figure is restricted to $\gamma \lesssim 1$ for clarity.

The line joining O and Q in Figure 2 is in the plane $L_x \sim 1$ and such that $u = \psi_y \sim \gamma/L_y \sim 1$. OQ meets the line of intersection PC of the plane $L_x \sim 1$ and the plane B_y (EKLF), at Q. Therefore the point Q represents the classical boundary-layer limit. Order coordinates of the point Q are $(1, R^{-\frac{1}{2}}, R^{-\frac{1}{2}})$.

It is clearly seen from Figure 2 which shows the possible limits of NSE, that although there are infinitely many limit processes (each point of the figure corresponds to a limit process) the possible outcomes are finite in number. The domain of validity of the limit equations E, V, B_y and B_x are planes whereas those for E_x, E_y, V_x and V_y are three-dimensional regions. Each of these regions is bounded by two of the four planes EGHF, EKLF, EIJF, and EMNF. For example, the domain of validity of V_x is the region between the planes EMNF and EIJF. Therefore limit equations E_x, E_y, V_x and V_y are each contained in the limit equations corresponding to the planes which bound their respective domains of validity. That is V_x is contained in V and B_x and so on. The four planes mentioned above meet along the line EF which corresponds to NSE. The limit equations corresponding to these planes are therefore principal limit equations of

NSE. B_x and B_y differ only in the definition of the coordinate axes. Thus we have only three principal limit equations of NSE. They are the Euler equation, the Stokes equation and a third equation with which we associate the classical boundary-layer. However, this limit equation is more general.

The above construction of the order space helps in visualising various limits of NSE. A somewhat different construction of the order space can be one where we choose the order axes to be L_x, L_y and instead of γ the order of the streamwise velocity. This, however, represents a linear transformation in the order space.

2.3 PHYSICAL PROBLEM

The flow is considered to be confined between two walls. A simple example of an internal separated flow is the flow in a channel having a symmetric sudden expansion (Figure 1). Recirculating regions are formed downstream of the expansion, and flow reattaches some distance downstream and finally evolves into a Poiseuille flow. An essential feature of this problem is that the flow is bounded in the transverse direction and, therefore, this length scale can be taken to be of order one. Two types of internal separated flows are identified later in Section 2.6.

In external separated flow, the interplay of the

recirculating flow and the outer irrotational flow requires that the shape of the bubble or the boundary of the irrotational flow be determined as a part of the problem. As a result the transverse length scale of the separated wake is difficult to ascertain. However, the boundary conditions on the two walls are sufficient to formulate the present problem.

2.4 LIMIT EQUATIONS WHEN $L_y \sim 1$

When $L_y \sim 1$, (i.e. the plane normal to L_y axis in Figure 2) possible limit equations with their domain of validity are shown in Figure 3. The limit equation N is valid at P. E and V are valid on the $\mathcal{Y}$ axis above and below P respectively. B_y is valid on PA whereas B_x on PD. Domains of validity of E_y, E_x, V_y and V_x are regions OPA, OPD, APT and DPT respectively. Line OG in Figure 3 is such that $v = -\psi_x \sim \mathcal{Y}/L_x \sim 1$. Also, along the L_x axis $u \sim 1$. Therefore, if the flow velocities are bounded for large R, the region of interest is that below AOG in Figure 3. Point G corresponds to the usual boundary-layer when the y axis is along the surface.

For the physical problems considered the total flow across any section remains constant and in its non-dimensional form is independent of R. Therefore, $\mathcal{Y} \sim 1$. From Figure 3 we see that there are then two principal limits.

They correspond to point O and point A.

The limit equation corresponding to point O(1,1,1) is the Euler equation

$$J(\nabla^2 \psi, \psi) = 0 \qquad (2.3)$$

The flow in this limit is inviscid. The above equation is elliptic in nature. Consequently, if the solution is disturbed at any point, its effect is felt at all other points of the region.

The limit equation corresponding to point A (R,1,1) in Figure 3 is

$$\psi_y \psi_{yyx} - \psi_x \psi_{yyy} = R^{-1} \psi_{yyyy} \ . \qquad (2.4)$$

The length scale in the x direction is of order R. The above equation is parabolic so that there is a direction at every point, called the characteristic direction. The effect of a perturbation introduced at any point in the region is sensed along this local direction.

2.5 DEVELOPMENT OF POISEUILLE FLOW

We first consider the development of Poiseuille flow as a prelude to the internal separated flow problems, as the flow between the two parallel walls develops ultimately into Poiseuille flow. Wilson (1969) has considered the development of Poiseuille flow using NSE. A small

perturbation analysis is carried out with the perturbation assumed in the form $\phi(y) \exp(-\lambda x)$, where x and y are the streamwise and transverse coordinates. An eigenvalue problem is obtained for ϕ, λ being the eigenvalue. For large R, two sequences of eigenvalues are obtained. The members of the first sequence are of order one, while those of the second are of order 1/R. An eigenvalue of order one indicates that the perturbation is effective over a distance of order one. The eigenvalues of this class are positive as well as negative. The perturbations are, therefore, sensed in both the upstream and the downstream directions over a distance of order one. The streamwise extent over which the perturbations corresponding to the second sequence are felt is of order R. These eigenvalues are such that the perturbations decay in only the downstream direction.

It then follows that if a small disturbance is introduced on the Poiseuille flow, it propogates both upstream as well as downstream. However, the extent of upstream propagation is of order one and that downstream is of order R. Also, it is the second mechanism which is dominant in the downstream propagation of any disturbance as its decay rate is considerably slower.

The eigenvalue problem for the second type of eigenfunction can be derived from the limit equation (2.4). Qualitatively the mechanism of propagation of the

disturbance should therefore be similar to that of equation (2.4). Since the equation has a characteristic direction, the disturbances are expected to propagate in only one direction.

It can then be argued on the basis of the nature and length scales of limit equations, and the analysis of Wilson that there are two modes by which disturbances are propagated through the flow. If there is an upstream influence then this flow is expected to be governed by the limit equation (2.3). The second mechanism is dominant for downstream flow, and is described by the limit equation (2.4).

2.6 TWO TYPES OF INTERNAL SEPARATED FLOWS

Two simple geometrical arrangements causing separation in internal flows are sudden contraction and sudden expansion (see Figure 4). The separated flows in these configurations are qualitatively different. In the case of sudden contraction, the flow separates upstream of the geometrical configuration responsible for it. The streamwise length scale is, therefore, of order one, and the separation bubble appearing ahead of the contraction will be of order one.

The second type of separated flow is that downstream of a sudden expansion. The dominant mode of propagation of the effect of the sudden expansion in the downstream direction is that corresponding to equation (2.4). The

streamwise length scale is of order R, that is a typical length, say, the length of the separated bubble, behaves as R. Viscous diffusion over a distance R is significant. Therefore, viscous forces are not negligible in the dynamics of the flow in the bubble. The appropriate limit equation is (2.4). Separated flows of this class are dealt with in the present work.

The above rather intuitive conclusion can also be reached by the following argument. When $L_x \sim 1$ and $L_y \sim 1$, viscous terms are of higher order. In the 'near' limit, the flow is governed by the Euler equation. Discontinuous surfaces are allowed. One such surface is along the separating streamline. A vorticity layer is required for the vorticity to diffuse in the bubble. The thickness of this layer is of order $(x/R)^{1/3}$ and therefore for any fixed x, it shrinks to zero in the limit. When $x \sim R$, the vorticity layer thickness is of the order of the transverse length scale of the channel itself. The 'near' limit is, therefore, inapplicable when $x \sim R$. A 'far' limit given by $L_x \sim R$ is required which leads to equation (2.4).

2.7 EARLIER RESULTS ON STREAMWISE LENGTH SCALE

We examine the behaviour of a typical streamwise distance for large Reynolds number in the earlier numerical calculations with a view to test the above conclusion

regarding the nature of separated flow.

Hung and Macagno (1966) have calculated internal separated flow in a channel having a symmetric sudden expansion. Their calculation is based on NSE and uses a finite-difference scheme. Two methods have been used to study the problem. In the first, steady state equations are solved, while the second approach is based on unsteady equations and the calculation is continued till a steady state is reached. The second approach is considered to have advantages over the first for large R. The ratio of expansion (downstream to upstream width) is two and the calculation is performed for R (based on the average velocity and the half-width of the channel downstream of the expansion) upto about 160. Flow slightly upstream of the expansion is taken to be fully developed i.e. a Poiseuille flow. Two typical streamwise lengths are shown as functions of R in Figure 5. They are, the distance of the point of reattachment and the distance of the centre of the 'eddy' measured from the expansion. They clearly show a linear trend for sufficiently large R. This problem is also considered by Morihara (1972). Calculations of NSE are performed upto R = 20, using a different numerical scheme. The length of the 'eddy' obtained by Morihara is also shown in the figure. His results also show a linear trend. Flow in a gradually widening channel has been calculated by Dorodnitsyn and

Meller (1970). Their Figure 6 shows the length of the reversed flow region which increases approximately linearly with R.

We thus conclude that the earlier calculations based on NSE support the view that the streamwise length scale is of order R and it is then expected that equation (2.4) should govern the large Reynolds number flow except possibly for some small sub-regions.

2.8 FORMULATION OF THE PROBLEM

We shall consider the flow in a sudden expansion as a prototype for our discussion, although the conclusions are expected to be more general and applicable to other similar problems such as shown in Figure 1.

The flow downstream of the expansion is divided into two sub-regions corresponding to $L_x \sim 1$ and $L_x \sim R$. The limit equation for the 'far' region ($L_x \sim R$) is (2.4). As a result of the limiting process, three derivatives in x are lost. Equation (2.4) can therefore satisfy only one condition in x which is obtained on matching with the solution for the 'near' region ($L_x \sim 1$). The 'near' region solution is somewhat difficult to construct. As the limit equation for this region is elliptic in nature, it would further require matching with the far upstream flow. To obtain the initial condition for equation (2.4) in the absence of matching, we

make a working hypothesis which is to be tested subsequently, that the initial velocity profile is the same as the far upstream flow.

We now eliminate R in equation (2.4) by scaling the x coordinate by R. It then becomes

$$\psi_y \psi_{yyx} - \psi_x \psi_{yyy} = \psi_{yyyy} . \qquad (2.5)$$

Unless otherwise stated, x would henceforth imply the contracted streamwise coordinate. In this work R is taken to be based on the average velocity and the half-width of the channel downstream of the expansion.

The initial condition required for the integration of equation (2.5) is given as

$$\psi(x = 0, y) = \psi_0(y) . \qquad (2.6)$$

This condition is equivalent to prescribing the streamwise velocity at the initial section. The no-slip condition at the walls requires

$$\psi = \pm 1, \quad \psi_y = 0 \quad \text{at} \quad y = \pm 1 . \qquad (2.7)$$

In the coordinate system x (contracted) and y, the 'near' region shrinks to a plane, x = 0. Equation (2.5) can then be regarded as the field equation valid for $x > 0$. At x = 0 an initial condition (2.6) is prescribed. Equation (2.5) along with conditions (2.6) and (2.7) constitute

the mathematical problem and subsequently we test if they form a sufficient basis to calculate the flow.

Equation (2.5) can be integrated once with respect to y. The constant of integration is the pressure gradient. However, as we will see, it is preferable to work with the higher order equation (2.5) than with its integrated version.

2.9 FURTHER COMMENTS

The equation obtained for the calculation of flow development is similar to Prandtl's boundary-layer equation BLE. However, it should be noted that the viscous region has a thickness of order one whereas the thickness of the classical boundary-layer is of order $R^{-\frac{1}{2}}$. Also, instead of pressure being impressed by the external flow, it has to be obtained as a part of the calculation here. However, there are four boundary conditions in y to be satisfied. The confinement of the flow can thus be said to generate its own pressure field. Strong interaction of the separated region with the mainflow which is a feature of the external separated flow is absent in the present internal separated flow.

It may appear surprising that the equation which we intend to use for flows having recirculating regions is of the boundary-layer type. BLE are known to possess a singularity at the point of zero skin friction (Goldstein, 1948),

and it is believed that the continuation of the calculation beyond this point is generally not possible (Brown & Stewartson, 1969). Flow reversal occurs beyond the separation point. Since the argument used in deriving BLE does not require the absence of reversed flow, BLE permit reversed flow as long as the boundary-layer thickness is of order $R^{-\frac{1}{2}}$. Briley (1971) obtained the NS solution for the flow in a separation bubble by means of a finite-difference scheme, which with increasing R appears to approach the corresponding solution of BLE.

Consider Figure 6 (taken from Brown & Stewartson, 1969). The conditions on an initial section AB, the wall AF and the edge of the boundary-layer BD are given. Since the flow in GEF is reversed, the convective propagation of a disturbance in the sense of decreasing x is possible. In such circumstances, the parabolic equation is said to be of the mixed type. There seems to be an intimate connection between the theory of parabolic equations of the mixed type and separated flow. Apparently, the requirements on the boundary condition are severe for such equations. The theory of such equations has not yet been sufficiently developed to give conditions which the given data must satisfy in order that the problem is well posed and a solution exists. In the absence of any formal theory, qualitative arguments are advanced for the appropriate

boundary conditions. It may appear that in addition to the already specified conditions on AB, BD and AF, a condition on EF (Figure 6) is required in order to determine the solution over ABDF. However, if the boundary conditions were to be completely arbitrary, flow upto point G will be affected by changing the condition over GF and EF, and possibly the separation point G itself will shift; but the flow in ABCG uniquely determines the point G. Perhaps some condition on EF is needed in general to determine the eigen-solutions if any. The above argument also suggests that the boundary condition to be prescribed should be in a certain class for the solution to be regular. The regularity of the solution imposes certain restrictions on the boundary condition, even when the region of interest is ABCG. When the given condition is otherwise, the flow manifests a singularity.

Based on the above discussion, the appearance of a singularity can be viewed from two angles. If we are looking for 'thin' separation (the contention here is that it is regular), the singularity represents the incompatible nature of the supplied data. Catherall and Mangler (1966) designed a thoughtful scheme in which the supplied data had partial freedom to adjust in order that the solution be continued in a regular way at each step. On the other hand, the singularity would mean the failure of the boundary-layer

limit as an approximation to the actual physical phenomenon ('thick' separation).

There are two distinct issues in the calculation of separated flow, namely, the equation and the boundary conditions required for the formulation of the mathematical problem, and a method of calculation for the formulated mathematical problem. Equation (2.5) is considered to be appropriate for the present class of problems. The boundary conditions prescribed on the walls (2.7) seem to be of the simplest type. If any difficulty arises, it can be attributed to the initial condition (2.6). We shall regard the problem as well posed and assume that a solution exists.

The usual methods of integration of parabolic equation are not expected to be applicable in the presence of reversed flow. An iterative technique is used by Klemp and Acrivos (1972) in which the shape of the reversed flow region is assumed, and then the solution in the forward direction and backward direction are obtained separately by a marching technique suitable for parabolic equations. The shape of the reversed flow region is iterated to match the flow quantities across it. In solving a parabolic equation of mixed type, Ban and Kuerti (1969) have used a numerical scheme which is normally applied to elliptic equations.

Integral relations methods or methods of weighted residuals are well known for solving partial differential equations. Their convergence can be shown under certain circumstances. The method of calculation used in the present work to solve equations (2.5 - 7) belongs to this class and is developed in the next chapter. However, the approximating and weighting functions are eigenfunctions of a related problem, unlike the usual functions which are often selected for their analytical properties and computational simplicity.

CHAPTER 3

METHOD OF CALCULATION

3.1 INTRODUCTION

This chapter deals with the formulation of a method to calculate the flow development between two parallel walls, which can be applied to internal separated flows. The governing equation and the required boundary conditions are given in Section 2.8.

Since the flow evolves ultimately into Poiseuille flow, equation (2.5) can be linearised about this flow for sufficiently large downstream distances. It then leads to an eigenvalue problem and the perturbations decay exponentially with increasing streamwise distance. In the region where the flow differs markedly from Poiseuille flow, the linear approximation does not hold, and nonlinear terms must be retained. However, if the nonlinear interaction terms between the modes decay rapidly, an expansion in the eigenfunctions could lead to an efficient computing procedure.

3.2 LINEAR PROBLEM

As $x \to \infty$, the channel flow develops into Poiseuille flow given by

$$\psi_p = 1/2\ (3y - y^3) \qquad (3.1)$$

Let the flow be expressed as a sum of Poiseuille flow and a perturbation Ψ_1, given by

$$\Psi = \Psi_p + \Psi_1 \quad . \tag{3.2}$$

Substituting (3.2) in equation (2.5), we get

$$\Psi_{1yyyy} - \Psi'_p \Psi_{1yyx} + \Psi'''_p \Psi_{1x} = \Psi_{1y} \Psi_{1yyx} - \Psi_{1x} \Psi_{1yyy} . \tag{3.3}$$

Dash indicates differentiation with respect to the argument. Neglecting the quadratic terms in Ψ_1 and substituting for Ψ_p from (3.1), we get the linearised equation

$$\Psi_{1yyyy} - 3/2(1 - y^2) \Psi_{1yyx} - 3 \Psi_{1x} = 0 \quad . \tag{3.4}$$

The form of the above equation suggests a solution of the form

$$\Psi_1 = \phi(y) \, e^{-\lambda x} \quad , \tag{3.5}$$

for some λ. Substituting (3.5) in (3.4) we get

$$\phi^{iv} + \lambda \left[3/2(1 - y^2) \phi'' + 3\phi \right] = 0 \quad , \tag{3.6a}$$

where λ is an eigenvalue. The wall conditions require that

$$\phi = \phi' = 0 \quad \text{at} \quad y = \pm 1 \quad . \tag{3.6b}$$

Linearization about the Poiseuille flow thus leads to an eigenvalue problem EVP, and the perturbations decay exponentially in the positive x direction, if λ is positive.

3.3 THE EIGENVALUE PROBLEM

The form of (3.6) suggests that its solutions can be separated into odd and even solutions. An eigenfunction is called odd or even depending on the antisymmetry or the symmetry of the associated streamwise velocity component.

EVP (3.6) has been studied earlier by Gillis and Brandt (1964) and by Wilson (1969). Gillis and Brandt have made a direct numerical computation of even eigenfunctions. Wilson has obtained equation (3.6) as the equation governing the leading term in a large Reynolds number expansion.

Equation (3.6) can be integrated once to give

$$\phi''' + \lambda \left[3/2(1 - y^2)\phi' + 3y\phi \right] = \text{Constant} . \qquad (3.7)$$

The constant of integration in (3.7), when multiplied by $e^{-\lambda x}$, gives the associated pressure gradient. Evaluating the left side of (3.7) at $y = 0$, the constant of integration turns out to be zero for odd eigenfunctions. Therefore the pressure field associated with an odd eigenfunction is uniform.

It has been shown by Wilson that the odd eigenvalues are real. It has not been possible to prove a similar result for even eigenvalues. However all the eigenvalues calculated by using numerical methods are real (Wilson, 1969).

The real eigenvalues of (3.6) can be shown to be positive by multiplying (3.6) by Φ and integrating by parts, which leads to

$$\int_{-1}^{1} \Phi''^2 \, dy - 3/2 \lambda \left[\int_{-1}^{1} (1 - y^2) \Phi'^2 \, dy - \int_{-1}^{1} \Phi^2 dy \right] = 0. \quad (3.8)$$

Now consider

$$\alpha = \int_{-1}^{1} (1 - y^2) \Phi'^2 \, dy / \int_{-1}^{1} \Phi^2 dy$$

Stationary value of α leads to Legendre's equation. The minimum value of α, therefore, is two. Hence the term in the bracket of (3.8) is positive. Therefore λ is positive.

Wilson has reported that machine calculations have shown no real eigenvalues in the range $-200 < \lambda < 0$. Although it has not been definitively established that all the eigenvalues are real, it is conjectured that they are real and therefore positive.

Appendix 1 contains an outline of a scheme for calculation of eigenvalues and eigenfunctions. Fourth order Runge-Kutta-Gills method has been used to integrate the differential equation (3.6). Eigenfunctions of higher order oscillate more rapidly and consequently have larger derivatives, which require a suitable method of integration. Estimates of λ for higher modes have been obtained in Section 3.3.1. Table 1 contains the first few eigenvalues. They are numbered in increasing order and are alternatively

odd and even. The lowest eigenvalue is odd in nature, and hence the velocity perturbation which persists the longest is antisymmetrical.

m	λ_m
1	14.4535
2	18.8146
3	48.8857
4	57.5463
5	104.572

TABLE 1 EIGENVALUES OF EQUATION (3.6)

3.3.1 ESTIMATES FOR LARGE λ

Analysis of equation (3.6) for large λ is somewhat similar to that of the Orr-Sommerfeld equation. There are four independent solutions, two of which correspond to length scale one, and are denoted by $\bar{\Phi}_A$ and $\bar{\Phi}_B$. The differential equation governing $\bar{\Phi}_A$ and $\bar{\Phi}_B$, in the limit $\lambda \to \infty$, is

$$(1 - y^2)\phi'' + 2\phi = 0 . \qquad (3.9)$$

One of the solutions, Φ_A, is a regular function. However Φ_B is singular at the wall (log singularity) and therefore an appropriate 'wall solution' is required.

The other two solutions are rapidly varying. These solutions are obtained using the WKBJ method. We denote these solutions by Φ_C and Φ_D. They are obtained by writing

$$\Phi_{C,D} = \exp\left(\int g\,dy\right) . \tag{3.10}$$

We assume a series solution of g in powers of $\lambda^{-\frac{1}{2}}$,

$$g = \lambda^{\frac{1}{2}} g_0 + g_1 + \cdots\cdots\cdots\cdots . \tag{3.11}$$

The series solution so obtained is

$$g = \pm\, i\, \lambda^{\frac{1}{2}} \sqrt{3/2}\,(1-y^2)^{\frac{1}{2}} + 5/2\; y(1-y^2) + \cdots , \tag{3.12}$$

which is valid only if

$$\left|\lambda^{1/3}(1 - y^2)\right| \gg 1 . \tag{3.13}$$

Substituting (3.12) in (3.10), we get

$$\Phi_{C,D} \sim (1-y^2)^{-5/4} \begin{matrix}\text{Cos}\\ \text{Sin}\end{matrix} \left[\tfrac{1}{2}(3/2\,\lambda)^{\frac{1}{2}}\,(y\sqrt{(1-y^2)} + \text{Sin}^{-1}y)\right] . \tag{3.14}$$

Condition (3.13) is violated near the walls and therefore the above solutions are invalid there. The proper stretching for the solutions near the wall can be obtained by considering the limit of (3.14) when y approaches the wall. Let

$$s = 1 + y . \tag{3.15}$$

Then as $s \to 0$, the limit of (3.14) is

$$\Phi_{C,D} \sim (2s)^{-5/4} \begin{matrix} \text{Cos} \\ \text{Sin} \end{matrix} \left[\tfrac{1}{2} (3/2\lambda)^{\frac{1}{2}} \left(-\pi/2 + 4\sqrt{2/3}.\ s^{3/2} \right) \right] . \quad (3.16)$$

The proper stretching required near the wall, therefore, is $\lambda^{-1/3}$. This can also be obtained by considering equation (3.6) or (3.13). The 'near wall' solutions are obtained in terms of Airy's function and matched with the WKBJ solutions, which gives

$$\lambda_n \sim n^2 \quad . \quad (3.17)$$

Detailed calculation leads to

$$\text{Odd} \quad : \quad \lambda_n \sim 32/3 \ (n + 1/12)^2 \ , \quad (3.18a)$$

$$\text{Even} \quad : \quad \lambda_n \sim 32/3 \ (n + 1/4)^2 \quad . \quad (3.18b)$$

It should be noted that the leading term of eigenvalues are real and positive, and the eigenvalues are countably infinite. For a given n, the odd eigenvalue is smaller than the even. If the eigenvalues are arranged in the increasing order, they are alternately odd and even.

3.3.2 ORTHOGONALITY RELATIONS

The present eigenvalue problem is of the form

$$\mathcal{L} \Phi + \lambda \mathcal{M} \Phi = 0 \ , \quad (3.19)$$

$$\mathcal{B} \Phi = 0 \ , \quad (3.20)$$

where $\mathcal{L}$ and $\mathcal{M}$ are the linear operators

$$\mathcal{L} = d^4/dy^4 \ , \ \mathcal{M} = 3/2(1 - y^2)\, d^2/dy^2 + 3 \ , \quad (3.21a)$$

and $\mathcal{B}$ represents the boundary conditions

$$\mathcal{B}\Phi = 0 \ ; \ \Phi = \Phi' = 0 \text{ at } y = \pm 1 \ . \quad (3.21b)$$

The eigenvalue problem encountered here is not of the usual type. It can be considered to be of a more general nature and reduces to an ordinary eigenvalue problem, when $\mathcal{M}$ is one. We shall assume that the eigenvalues are real and therefore positive and denumerably infinite. Now a scalar product is defined by

$$(\Phi, \Theta) = \int_{-1}^{1} \Phi\Theta \, dy. \quad (3.22)$$

Corresponding to $\mathcal{L}$ and $\mathcal{M}$, we define the adjoint operators by the relation

$$\Theta\mathcal{L}\Phi - \Phi\mathcal{L}^*\Theta = dP_1(\Phi,\Theta)/dy \ ,$$

$$\Theta\mathcal{M}\Phi - \Phi\mathcal{M}^*\Theta = dP_2(\Phi,\Theta)/dy \ ,$$

where Φ and Θ are any two suitably continuous functions and $P_1(\Phi, \Theta)$ and $P_2(\Phi, \Theta)$ are bilinear concomitants. By suitably choosing the boundary conditions so that P_1 and P_2 vanish at the boundaries, we state the adjoint problem as

$$\mathcal{L}^*\Theta + \lambda\mathcal{M}^*\Theta = 0 \ . \quad (3.23)$$

Boundary conditions for the adjoint problem turns out to be

the same as (3.20) and the adjoint operators are

$$\mathcal{L}^* = \mathcal{L} = d^4/dy^4 \quad ,$$

$$\mathcal{M}^* = 3/2(1 - y^2)\, d^2/dy^2 - 6y\, d/dy \quad . \tag{3.24}$$

If Φ_m and Θ_n are eigenfunctions of (3.19) and (3.23) respectively and the corresponding eigenvalues are λ_m and λ_n, it can be shown that

$$(\lambda_m - \lambda_n)(\mathcal{L}\Phi_m, \Theta_n) = 0 \quad .$$

When $m \neq n$, it then follows

$$(\mathcal{L}\Phi_m, \Theta_n) = (\Phi_m, \mathcal{L}\Theta_n) = 0$$

$$\text{or} \quad \int_{-1}^{1} \Phi_m'' \Theta_n''\, dy = 0 \quad , \quad m \neq n \tag{3.25}$$

We can define a new scalar product with respect to the operator $\mathcal{L}$, by the relation

$$[\Phi, \Theta] = (\mathcal{L}\Phi, \Theta) \quad , \tag{3.26a}$$

where Φ and Θ satisfy (3.20) and are sufficiently differentiable. Therefore,

$$[\Phi, \Theta] = (\Phi'', \Theta'') \quad . \tag{3.26b}$$

Equation (3.25) then becomes

$$[\Phi_m, \Theta_n] = 0 \quad , \quad m \neq n \quad . \tag{3.27}$$

Eigenfunctions of (3.19) and of its adjoint problem (3.23),

therefore, form a biorthogonal set, where the orthogonality relation is given by (3.27).

3.3.3 EIGENFUNCTION EXPANSION

We will require the expansion of functions satisfying suitable conditions into eigenfunctions of the equation (3.19). We shall assume that the required eigenfunction expansion converges in some sense.

Consider the expansion of a function f satisfying the boundary condition (3.20),

$$f = \sum_{m=1}^{\infty} b_m \Phi_m \quad . \tag{3.28}$$

The coefficient b_m can be obtained using the relation (3.27),

$$b_m = [f, \Theta_m] / [\Phi_m, \Theta_m] \tag{3.29}$$

3.3.4 SOLUTION OF THE LINEAR PROBLEM

The perturbation stream function ψ_1 is small sufficiently downstream, so that the nonlinear interaction of the modes in (3.3) can be neglected. The solution of the linear problem (3.4) can then be written as

$$\psi_1 = \sum_{m=1}^{\infty} A_m e^{-\lambda_m (x - x_o)} \phi_m(y) \quad . \tag{3.30}$$

The constant A_m in the expansion of ψ_1 can be found using the relation (3.29),

$$A_m = \left[\Psi_{10} , \theta_m\right] / \left[\Phi_m , \theta_m\right] , \tag{3.31}$$

where

$$\Psi_{10} = \Psi_1 \quad \text{at } x = x_o \tag{3.32}$$

3.4 METHOD OF CALCULATION

Let Ψ_1 in equation (3.2) be written as

$$\Psi_1 = \sum_{m=1}^{N} a_m(x)\, \Phi_m(y) , \tag{3.33}$$

where the coefficients a_m depend on x, and Φ_m are eigenfunctions of equation (3.6). In an N-term calculation summation index in (3.33) runs from one to N. The range of summation of indices will not be henceforth mentioned as it would be clear from the context. Substituting (3.33) in equation (3.3) followed by multiplication by θ_m , and integrating, we get

$$a_m' + \lambda_m a_m = \sum_p \sum_q C_{mpq}\, a_p' a_q , \tag{3.34}$$

where

$$C_{mpq} = \lambda_m I_{1mpq} / I_{2m} , \tag{3.35a}$$

$$I_{1mpq} = \left(\theta_m' , \Phi_p \Phi_q'' - \Phi_p' \Phi_q' \right) , \tag{3.35b}$$

$$I_{2m} = \left[\Phi_m , \Phi_m\right] . \tag{3.35c}$$

The differential equation (3.34) governing the coefficients of the eigenfunction in the expansion (3.33) is a set of

first order ordinary, quasi-linear, autonomous differential equations. The first term on the left in equation (3.34) represents the linearized part of the inertia term whereas the transverse viscous diffusion is represented by the second term. If the nonlinear interaction of the modes given by the term on the right side of (3.34) is negligible, a linear equation is obtained which has the solution (3.30). Equation (3.34) can also be written in the form

$$\sum_p \left(\delta_{mp} - \sum_q C_{mpq}\, a_q \right) a'_p = - \lambda_m\, a_m \ . \qquad (3.36)$$

The inertia terms have been collected on the left side in the above form. δ_{mn} is the Kronecker delta.

3.4.1 INITIAL CONDITION

The flow calculation is now reduced to solving equation (3.36) with appropriate initial conditions. Initial values of a_m can be obtained in a similar way from (3.33). At $x = 0$

$$\Psi_{10} = \sum a_m(0)\ \Phi_m(y) \ .$$

Therefore

$$a_{m0} = a_m(0) = (\Psi_{10} , \Theta_m^{iv}) \ / \ I_{2m} \ . \qquad (3.37)$$

If Ψ_0 prescribed in equation (2.6) is piecewise twice differentiable, so is Ψ_{10}. Equation (3.37) then leads to

$$a_{m0} = (\psi_0'' , \theta_m'') / I_{2m} \quad . \qquad (3.38)$$

3.4.2 LINEAR SUB-RANGE

As x goes to infinity, coefficients a_m go to zero. However, the computation need not be carried beyond a certain stage when the coefficients are small, in which case the solution of the linear problem can be utilised. Then

$$a_m = a_m (x_o) \exp \left[- \lambda_m (x - x_o) \right] \quad , \qquad (3.39)$$

where x_o is the streamwise coordinate beyond which the non-linear term in (3.34) are negligible.

3.4.3 SYMMETRIC PROBLEM

When dealing with a symmetric problem, only even eigenfunctions need to be considered. Index m in (3.33) then runs over the set of N even eigenfunctions. The range of integration with respect to y in any integral such as (3.22) can therefore be restricted to the upper half of the channel, $0 \leq y \leq 1$.

3.4.4 ONE-TERM SOLUTION

When only one term is used in the expansion (3.33) the resulting differential equation (3.36) can be integrated to give

$$\ln(a_1/a_{10}) - C_{111}(a_1 - a_{10}) = - \lambda_1 x \quad , \qquad (3.40)$$

where $a_{10} = a_1$ at $x = 0$. As $C_{111} = 0$ for a 1-term

asymmetric calculation, we obtain

$$a_1 = a_{10}\, e^{-\lambda_1 x} \quad .$$

3.5 ON EQUATION (3.36)

Equation (3.36) obtained for the calculation of flow development can be written in the form

$$C\, a' = -\Lambda\, a \quad , \tag{3.41}$$

where a is a vector whose elements are a_1, a_2, ... , Λ is the eigenvalue matrix, and C may be termed as an inertia matrix. C and Λ are N x N matrices and a is a N vector in a calculation based on N terms.

Equation (3.41) is a set of algebraic equations for a', which can be solved using any standard method. A typical integration scheme would then be as follows. At a given x, the derivative a' is obtained from the given a. Integration to the next point in x is then carried out using, say, the Euler method.

The derivative a' can be calculated provided C can be inverted, which is possible, only if the determinant of C is non-zero. The integration procedure, therefore, breaks down for the chosen value of N in the event the determinant of C becomes zero at any x. The singularity of the resulting equation (3.41), which arises when the

determinant of C is zero, is a general feature of the equations of the above type. Such a difficulty can occur when a moment method or an integral relations method is used to reduce partial differential equations to ordinary differential equations similar to (3.41). We take up a discussion of the phase space to examine further the nature of the singularity.

3.5.1 PHASE SPACE

An N-term solution can be represented by an integral curve in an N-dimensional phase space, whose coordinates are a_1, a_2, ...a_N. The equation governing such integral curves is

$$da_1/D_1 = da_2/D_2 = ... = da_N/D_N \quad , \qquad (3.42)$$

where D_m is the determinant of the matrix obtained by replacing the mth column of the matrix C by the vector on the right side of equation (3.41). As equation (3.36) is autonomous, D_m and D, the determinant of C, are functions of a_n. Furthermore, they are polynomials of degree N.

The origin of the phase space corresponds to the fully developed flow and therefore a 'meaningful' solution should approach this point. The given initial condition determines the integral curve in the phase space. The evolution of a_m with respect to x which can be regarded as

a parameter of the integral curve $a_m(x)$, can be obtained by solving one of the equations

$$a_m' = D_m/D \quad . \tag{3.43}$$

The condition D = 0 would normally represent a surface in the phase space. If an integral curve crosses the surface D = 0 (Figure 7), the direction of increasing x appears either 'sink' like or 'source' like and is physically unacceptable for describing a real flow. However, an integral curve could cross the surface D = 0 at certain singular points of the equation (3.42), if there are any. The phase space of symmetric calculation for N = 2 shows such a possibility, and is considered here as an illustration.

3.5.2 PHASE PLANE

The axes of the phase plane are a_1 and a_2, and the differential equation governing the integral curves is

$$da_1/da_2 = D_1/D_2 \quad . \tag{3.44}$$

Explicit forms of D_1, D_2, and D are given in Appendix 2. Conic sections that are associated with the quadratic expressions, D_1 and D_2, are ellipses and with D is a hyperbola. Figure 8 shows the ellipses $D_1 = 0$ and $D_2 = 0$. Evidently, when an integral curve crosses the ellipse $D_1 = 0$ or $D_2 = 0$, except at their intersection, it is

normal to the a_1 or the a_2 axis which is shown by vertical and horizontal arrows in Figure 8.

Both $D_1 = 0$ and $D_2 = 0$ pass through the origin 0 and are normal to a_1 and a_2 axes at 0. Therefore, 0 is a singular point of (3.44), and it can easily be shown that 0 is a stable two-tangent node with a_1 axis as the tangent.

Figure 8 shows another point of intersection of $D_1 = 0$ and $D_2 = 0$, which is denoted by P. Equation (3.44) therefore has another singular point P which is shown to be a saddle point in Appendix 3.

The curve $D = 0$ is also shown in Figure 8. The curve is seen to pass through P. This can also be shown from the differential equation. If $D_1 = 0$ and $D_2 = 0$ have a point of intersection other than 0, at which $D \neq 0$, then from (3.43) a_1' and a_2' are zero. The left side of (3.36) is therefore zero, whereas the right side is not. Therefore, we conclude that $D = 0$ at P.

Given an initial condition, the integral curve in the phase plane can be traced. A typical integral curve is shown in Figure 8. If the integral curve crosses $D = 0$, except at the second singular point P, the solution is physically unacceptable. However at P, as we shall see below, it is possible for an integral curve to cross from one side of the curve $D = 0$ to the other.

We consider a schematic of a saddle point singularity in Figure 9, where hollow arrows show the direction of x increasing if D were positive everywhere. Now let us draw a curve D = 0 passing through the saddle point. Let $D > 0$ above the curve D = 0, and $D < 0$ below it. The direction of x increasing is now shown by full arrows. We see that there is only one way of crossing from a given side of the curve D = 0 to the other that is physically acceptable. Figure 9 also shows the 'source' or 'sink' like behaviour of the integral curves at points other than P of the curve D = 0.

A point in the phase space which can be joined to the origin by an integral curve which is physically acceptable will be called accessible. The set of accessible points will be called the accessible domain.

It is therefore seen that all points of the phase plane are not accessible. If the given initial condition for equation (3.36) is such that the initial point is accessible, then no difficulty is encountered in the integration of equation (3.36).

3.5.3 CONCLUDING REMARKS

It is seen in the previous section that some of the points of the phase plane are not accessible due to the singularity of the differential equation. The occurrence of D = 0 and the presence of the singular points are the

features associated with the equation. They can therefore occur, in general, with any number of terms in a calculation. For example, in the case of 1-term symmetric calculations, the accessible domain is $a_{10} > 1/C_{111} - 2.5$.

3.6 THE INTEGRATION PROCEDURE

An integration procedure which proceeds in the phase space, is adopted with a view to have a simple control over the accuracy and the speed. Usual methods of integration with x as the independent variable will be applicable whenever the present method is successful. At each step of the integration of the differential equation (3.36), the derivatives

$$a'_m = E_m, \quad m = 1, 2, \ldots\ldots, N \quad , \tag{3.45}$$

are determined. Let n be such that

$$|E_n| \geq |E_m| \quad , \quad m = 1,2, \ldots\ldots, N \quad . \tag{3.46}$$

Then a_n is chosen to form the independent variable for the next step of integration. Equation (3.36) can then be written as

$$da_m/da_n = E_m/E_n \quad , \tag{3.47a}$$

$$dx/da_n = 1/E_n \quad . \tag{3.47b}$$

A simple predictor-corrector method is designed to

solve (3.47a). It maintains a uniform level of accuracy throughout the calculation. This is effected by incorporating a method of reducing the step length in a_n, to achieve the prescribed level of accuracy when the derivatives are large, and on the other hand, increase the step length to speed up the computation whenever possible. The method is self starting. It is described in Appendix 4 which also includes a brief description of the computer program.

As discussed in the previous section, equation (3.36) is singular at D = 0. Therefore, if during the integration, D vanishes at any stage, the integration is terminated.

The above integration procedure is used upto a point where the variables a_m are small enough for the solution of the linear problem to be applicable. If $|a_m| \leq \epsilon$ for all m, where ϵ is a prescribed small number, the integration is terminated, and equation (3.39) is used to extend the calculation upto downstream infinity.

3.7 RESULTS OF CALCULATION

The output of the calculation is primarily $a_m(x)$. One can then determine several flow variables. For instance, centreline velocity u_c, pressure gradient dp/dx and wall-vorticity ω can be determined by

$$u_c = 1.5 + \sum a_m \phi'_m(0) \quad , \tag{3.48a}$$

$$dp/dx = -3 + \sum a_m \phi'''_m(1) \quad , \tag{3.48b}$$

and $$\omega_{\pm} = \pm 3 - \sum a_m \phi''_m(\pm 1) \quad . \tag{3.48c}$$

The values of ω at the upper and the lower walls are denoted by suffix + and - respectively. Stream function is determined using equations (3.2) and (3.33).

Reattachment point on the wall is determined by the location where wall-vorticity changes sign. In the case where reattachment is on the centreline, the change of sign of u_c determines its location. The centre of the eddy is determined by finding the location of the extremum of stream function within the flow. This operation also yields the value of the recirculation.

In addition, two quantities which are of general interest are considered below.

3.7.1 DEVELOPMENT LENGTH

Development length is analogous to the entry length and it can be defined as the streamwise distance after which the centreline velocity is within a given fraction of the ultimate value. For example,

$$x_{99} : \left| u_c(x_{99}) - 1.5 \right| / 1.5 = 0.01 \quad , \tag{3.49a}$$

$$x_{999} : \left| u_c(x_{999}) - 1.5 \right| / 1.5 = 0.001 \quad . \tag{3.49b}$$

That is, x_{99} is the value of the streamwise coordinate at which centreline velocity u_c differs from its ultimate value 1.5 by 1%. Similarly x_{999} corresponds to a difference of 0.1%.

If x_o is a streamwise location after which the solution (3.39) is applicable, then the development length can be found from

$$\left| \sum a_m(x_o) \exp\left[- \lambda_m(x_{99} - x_o) \right] \phi_m'(0) \right| = 0.01 \times 1.5 .$$

The contribution of the modes higher than the first even mode, can usually be neglected, as they decay more rapidly. We then have

$$x_{99} = x_o - (1/\lambda_{e1}) \ln (0.01 \times 1.5 / |a_{e1}(x_o)|) \quad ,(3.50a)$$

where the subscript e1 denotes the first even mode. Similarly

$$x_{999} = x_o - (1/\lambda_{e1}) \ln (0.001 \times 1.5 / |a_{e1}(x_o)|) \quad .(3.50b)$$

3.7.2 PRESSURE RECOVERY COEFFICIENT

The non-dimensional pressure gradient is -3 in Poiseuille flow. We define $p_r(x)$ as

$$dp_r/dx = dp/dx + 3 . \qquad (3.51)$$

We take $p(0) = p_r(0) = 0$. The pressure recovery coefficient

is then defined by

$$P_r = p_r(\infty) \quad . \tag{3.52}$$

The asymptote to the curve p(x) is therefore given by

$$p = -3x + P_r \quad . \tag{3.53}$$

If the solution (3.39) is applicable beyond $x = x_o$, P_r is given by

$$P_r = P_{r1} + \sum a_m(x_o)\, \Phi_m''(1)/\lambda_m \quad , \tag{3.54}$$

where

$$P_{r1} = p_r(x_o) = p(x_o) + 3x_o \quad . \tag{3.55}$$

CHAPTER 4

ENTRY FLOW IN A CHANNEL : A TEST CASE

4.1 INTRODUCTION

We consider the entry flow in a straight channel as a first application of the calculation method developed in the previous chapter.

Although the problem is technically important, the attention it has attracted is considerably more than what might be expected. Its simple geometry provides a suitable testing ground for theories and methods. The present application is aimed at establishing the method by comparing its results with those obtained earlier by other methods. The comparison provides an indication not only of the accuracy of the method of integration but also the applicability of the limit equation and the initial condition hypothesis.

There are a large number of reported investigations on this problem. We, however, consider mainly those which are required for the comparison of the results. The first analytical work based on suitable approximations is due to Schlichting (1934, 1968). The flow near the inlet is assumed to consist of the wall boundary-layers together with an inviscid uniform central region which accelerates to satisfy the continuity requirement. A series method is

used to construct the boundary-layer solution in the initial portion. The solution for large downstream distances is obtained by perturbing the Poiseuille flow. The two solutions are patched at an intermediate location. This solution has been later improved by including additional terms in the perturbation series by Collins & Schowalter (1962, 1963) and by Roidt & Cess (1962). Bodoia & Osterle (1961) have obtained the solution of BLE using a finite-difference scheme. However, a large truncation error is unavoidable, and further, the scheme is unstable in the presence of reversed flow.

Wang & Longwell (1964) have considered two types of entry conditions in their solution of complete NSE obtained by a finite-diference method. The flow is assumed to be uniform at the channel entry in the first case and at the upstream infinity in the second. The solution for the first case is also obtained by Gillis & Brandt (1964) and by Morihara (1972). An off-centre maximum of streamwise velocity occurs after a short distance downstream of the inlet section, and it continues till it is eroded by the thickening of the boundary-layers. This apparently paradoxical situation has been clarified in an important paper by Van Dyke (1970), who also showed the singular perturbation nature of the entry flow problem. The problems considered by Schlichting (1934) and by Bodoia & Osterle (1961) are

essentially one-term downstream expansions. The first type of entry condition appears restricted and introduces fractional powers of Reynolds number in the expansion.

4.2 THE INITIAL CONDITION

The channel consists of two plane parallel plates located at $y = \pm 1$, $x > 0$ (Figure 10). As the flow is symmetrical in y, only the upper half of the channel is considered.

The flow calculation as formulated in Chapter 3 is reduced to solving equation (3.36) with an appropriate initial condition. At the inlet, flow is taken to be

$$\begin{aligned} u &= 1 \quad , \quad 0 \leq y < 1 \quad , \\ &= 0 \quad , \quad y = 1 \, . \end{aligned} \tag{4.1}$$

The initial condition for a_m is obtained from (3.37) as

$$a_{m0} = -\theta''(1) \Big/ \int_0^1 \varphi_m'' \, \theta_m'' \, dy \tag{4.2}$$

4.2.1 NUMBER OF TERMS

The number of terms N to be used in a calculation is to be chosen in the first place. The ability to predict to a good approximation with a few terms is a great advantage. We intend to use rather small number of terms in our calculation. A 1-term solution is given by (3.40).

Two, three and five terms have been used in the calculation whose results we discuss in the next section. Calculation with more terms is, in principle, straightforward.

4.3 RESULTS

The inlet velocity profile is approximated as shown in Figure 10. The given uniform velocity profile is approximated by functions which vanish at the wall. The region of significant error tends to get localised near the wall with increasing number of terms. This evidence can be regarded as a computational indication of the convergence of the approximating functions, although the nonuniformity in convergence near the wall is to be expected. A similar situation arises when a unit pulse is approximated by trigonometric functions. To balance the reduced mass flow near the wall, velocity elsewhere has to be greater than unity. Table 2 gives two indicators of the approximation, namely the centreline velocity u_{co} at $x = 0$ and the associated momentum flux M_o. The momentum flux is related to the integral of the square of the error in the streamwise velocity,

$$\int_0^1 (u - 1)^2 \, dy = \int_0^1 u^2 dy - 1 \quad .$$

It is seen from Table 2 that both the quantities approach the given value with increasing number of terms.

I.I.T. KANPUR
CENTRAL LIBRARY
Acc. No. A 51152

N	2	3	5	Given
u_{co}	1.206	1.122	1.090	1.0
M_o	1.088	1.071	1.051	1.0

TABLE 2 REPRESENTATION OF THE INITIAL PROFILE

Figure 11 shows the calculated centreline velocity. As mentioned above, u_c is initially different from unity. A convergent trend is clearly seen from the figure. In fact, all the three calculations give approximately the same $u_c(x)$, except for a small region near the inlet.

Pressure gradient is shown in Figure 12. The three calculations are markedly different near the inlet, but slightly away from it the three curves merge into a single curve and they approach a common asymptotic value. $|dp/dx|$ is expected to be large near the inlet. With increasing number of terms, values of $|dp/dx|$ predicted are indeed larger near the inlet, and show a sharper trend. The area under the dp/dx curve gives the pressure and is shown in Figure 12.

The results of Morihara (1972) for R = 1000 are also shown in Figure 12. The streamwise pressure gradient and as well the pressure are functions of both x and y coordinates in the above calculation. However, they are almost

independent of the transverse coordinate for large x. The points in Figure 12 are those corresponding to y = 0. The present results compare favourably with the pressure gradient obtained by Morihara. Rapid decay of $|dp/dx|$ near the inlet is approximately represented by the present calculation. The pressure distribution of Morihara is in good agreement with the 5-term calculation.

The asymptote to the curve p(x) is given by equation (3.53), where P_r is the pressure recovery coefficient and is the value of $(p + 3x)$ as $x \to \infty$. P_{r1} represents the value of $(p + 3x)$ at the point upto which the calculation is carried (see Equation (3.55)). P_r is obtained using Equation (3.54). Table 3a contains the values of P_{r1} and P_r. The difference between the values of any two calculations is the area between two respective dp/dx curves. With the increasing number of terms, the prediction of dp/dx is expected to converge near the inlet with an associated reduction of the differences in the numerical values of the pressure recovery coefficient.

N	$-P_{r1}$	$-P_r$
2	0.2187	0.2437
3	0.2645	0.2913
5	0.3245	0.3505

TABLE 3a PRESSURE RECOVERY COEFFICIENT

In Table 3b the pressure recovery coefficient is compared with that given by other investigators. Collins & Schowalter (1962, 1963) who had earlier obtained a value 0.338 have later reported 0.37. The calculation of Morihara (1972) at R = 1000, gives a value of 0.365. In the first case of Wang & Longwell (1964) there is a

Reference	$-P_r$
Schlichting (1934)	0.301
Bodoia & Osterle (1961)	0.338
Collins & Schowalter (1962)	0.338
" (1963)	0.37
Wang & Longwell (1964)[1]	0.370[2]
	0.352[3]
Morihara (1972)	0.365[4]
Present 5-term	0.351

TABLE 3b COMPARISON OF PRESSURE RECOVERY COEFFICIENTS

1. Values refer to case II, R=75, and are averages. See p.55.
2. Includes upstream contribution.
3. Excluding upstream contribution.
4. For R = 1000.

significant variation of pressure across a far-downstream section, which is attributed by the authors to the discontinuity at the inlet. Also, an error has been committed in the application of the boundary condition as vorticity is assumed to be zero at the inlet. In the second case, pressure is more or less constant across any section sufficiently away from the inlet. Three values of pressure given at y = 0.1, 0.5 and 0.9 are averaged. Also, these values are relative to pressure at $x = -\infty$. Therefore P_r includes a contribution from the upstream of the inlet. Thus, the value for excess pressure drop obtained with five terms is somewhere in the middle of the range of the values given by other workers. We, therefore, find that P_r given by the present calculation agrees quite well with that obtained from calculations based on NSE for large R.

The wall-vorticity $\omega_+ = - u_y$ at the upper wall is shown in Figure 13. It is also proportional to skin friction. Results due to Morihara for R = 1000 are also shown in the figure. The wall-vorticity is infinite at the inlet due to the form of the assumed initial velocity profile. The wall vorticity compares well with that obtained by Morihara except for a small distance near the inlet.

Velocity profiles at various x based on the 5-term calculation are shown in Figure 14. They show a small

waviness near the inlet due to the representation of the given velocity profile. The waviness rapidly smoothens out and the velocity profile appears like a growing wall boundary-layer together with a uniform central core, as assumed by Schlichting (1934), (Figure 14, see middle row). This comparison can be further checked by examining the growth of $(u_c - 1)^2$ for this intermediate range ($.004 < x < 0.02$), (Figure 15). The clear linear trend (cf. equation (9.69) of Schlichting, 1968) shows that the method brings out the qualitative features of the flow. The constant of proportionality obtained from the graph is 1.61 in comparison with the Blasius constant 1.72. The bottom row of Figure 14 shows how the velocity profiles evolve into Poiseuille flow at distances away from the inlet.

Development length x_{99} as defined in section 3.7.1 is given in Table 4 along with those obtained by other workers. The present values appear to be slightly less than those reported by others except that of Schlichting. Development length based on the 5-term calculation agrees with the value of Morihara (1972) within 1%.

Figure 16 compares the 5-term values of u_c with those of Bodoia & Osterle (1961), and of Wang and Longwell (1964) for R = 75, and those of Morihara (1972) for R = 1000. (Some of the points of Wang & Longwell shown in Figure 16 are taken from Figure 3 of Van Dyke, 1970). The results

Reference		x_{99}
Present	2-term	0.1642
	3-term	0.1662
	5-term	0.1679
Schlichting (1934)		0.160
Hwang & Fan (1964)		0.1688
Morihara (1972)		0.1692
Bodoia & Osterele (1961)		0.176
Gillis & Brandt (1964)		0.1768
Roidt & Cess (1962)		0.1816

TABLE 4 DEVELOPMENT LENGTH

of Wang and Longwell and of Morihara agree well with that of Bodoia and Osterle near the inlet. However, away from the inlet they agree more closely with the present calculation. As mentioned earlier, the difference near the inlet could be due to the very small number of terms. Possibly agreement there could be improved by including more terms. Incidentally the limit process used to obtain the governing equation corresponds to the downstream limit. Therefore the present calculation could be at slight variance, near the inlet, with the results obtained for some large value of R. A similar agrument also holds for the calculation of

Bodoia & Osterle. But however one finds that the agreement of their calculation with that based on NSE for large R is better near the inlet than away from it. This difference could be due to the accumulation of error as pointed out earlier.

It should be noted that the criterion of determining the initial condition leads to a good agreement slightly away from the inlet, although the predictions are not as accurate near the inlet. That is to say in some integral sense the initial condition in the present calculation represents the flow well enough for even a few terms to give quite accurate predictions slightly away from the inlet. Inclusion of more terms may hardly affect the calculation away from the inlet (Figure 11), however, we expect improvement in predictions near the inlet.

As the basic equations in the present work are the same as those of Bodoia & Osterle (1961), comparison with their work can be regarded as a check on the accuracy of the present method of integration. Also it might be argued that a systematic difference in two curves shown in Figure 16 might be due to a shift in the initial condition. The forward-difference formulation of Bodoia & Osterle could lead to significant accumulation of error. We therefore regard the solution of the complete equations at large Reynolds number to be a reliable guide in establishing our

method. Then the large x behaviour can be said to be well predicted. Since the prediction near the inlet can be improved using more terms in the calculation, a good agreement for all x with calculations based on NSE at large R is possible in principle.

It has been demonstrated in this charter that the method predicts the entry flow in a straight channel quite well, although the maximum number of terms used in the calculation is limited to five. Not only the quantitative comparison of the centreline velocity, the pressure, the wall-vorticity etc. are favourable, but also the calculated flow shows qualitative features like a wall boundary-layer and a uniform centralcore over a certain intermediate range of x. Of course, the real test comes in the next chapter when we apply the method to flows having recirculation.

CHAPTER 5

APPLICATION TO SEPARATED FLOW PROBLEMS

5.1 INTRODUCTION

Having tested the method of calculation for the entry flow problem in the previous chapter, we give results in this chapter for separated flow problems where many earlier methods of calculation would not be normally applicable.

Flow problems in three types of geometrical configurations are considered (Figure 1). The first type (Figure 1a) is the flow in a channel having symmetric sudden expansion. The second type of problem (Figure 1b) is flow in an asymmetric sudden expansion, which can also be regarded as a backward-facing step with a top wall, or a base with a long splitter plate in a channel. The third type of problem (Figure 1c) deals with a base placed symmetrically between two parallel flat walls.

We further consider two types of entry condition in each of these problems. A parabolic velocity profile corresponds to a fully developed entry condition. A short inlet leads to a uniform velocity profile. It is possible to consider intermediate cases having a non-zero boundary-layer thickness a little upstream of, say, the base. It is also possible to consider other geometrically different problems. However, we restrict ourselves to what seems to

be a representative sample of the above three types of problems with one geometrical parameter h and with two simple but extreme entry conditions.

The number of terms N in (3.33) has to be determined for each calculation. We can increase N till any further increase does not affect the results significantly. Alternatively, we can fix N and find the range of the geometrical parameter in which results are acceptable.

Consider now the flow in a symmetric sudden expansion with h = 0.5 when the entry profile is parabolic. NS solution for values of R upto 160 is given by Macagno and Hung (1966). Their Figure 7 shows that an asymptotic trend has been attained and therefore their results can be used for comparison with the present calculation. Morihara (1972) has also obtained NS solution for this problem for values of R upto 20 (see Figure 5). The present calculation is started with a few terms and later more terms are included. We shall see that five terms are sufficient to indicate convergence. Therefore, the number of terms in subsequent calculations is restricted to five.

At this stage it may be appropriate to briefly summarise the important steps in the development of the present work. A limit equation is obtained for large R for a class of problems which may have recirculating regions.

A method of flow calculation is then developed which leads to a set of ordinary differential equations. The upstream condition is used directly to obtain the required initial condition. The concern of the present chapter is to test the consequences of the basic inputs, that is the calculation method in its final form when the flows have recirculating regions. It is applied to a variety of situations and comparison with available results is made wherever possible. Also some of the results are believed to be new.

5.2 CHANNEL WITH A SYMMETRIC SUDDEN EXPANSION

Consider the flow in a channel having a symmetric sudden expansion (Figure 1a). The expansion ratio, which is defined as the ratio of the downstream channel width to that upstream, is given by 1/h.

5.2.1 INITIAL CONDITION

In the case of the parabolic velocity profile at the entry, the initial flow is given by:

$$u_o = 3/(2h)(1 - (y/h)^2) \quad , \quad 0 \leq y \leq h \ ,$$
$$= 0 \quad , \quad h \leq |y| \leq 1. \qquad (5.1)$$

The initial condition a_{mO} is then obtained to be

$$a_{mO} = -3 \left[h \theta'_m - \theta_m \right]_{y=h} / (G_m h^3) \quad , \qquad (5.2)$$

where

$$G_m = \int_0^1 \phi_m'' \theta_m'' \, dy = \tfrac{1}{2} I_{2m} \quad . \tag{5.3}$$

When the inlet velocity profile is uniform, that is

$$\begin{aligned} u_o &= 1/h \ , \quad 0 \leq |y| < h \ , \\ &= 0 \ , \quad h \leq |y| \leq 1 \ . \end{aligned} \tag{5.4}$$

the initial condition for a_m is found to be

$$a_{m0} = - \theta_m'' (h) \ / \ (G_m \, h) \quad . \tag{5.5}$$

We first discuss the case for which NS solution has been obtained by Hung and Macagno (1966). Other cases are discussed later.

5.2.2 RESULTS FOR h = 0.5 WITH PARABOLIC ENTRY PROFILE

The assumed parabolic entry profile given by (5.1), is shown in Figure 17 with its approximation using 2, 3 and 5 terms. Clearly, the given velocity profile is better approximated with increasing number of terms. 3- and 5-term representations are closer to each other.

Streamlines based on the 3-term calculation are shown in Figure 18. Also streamlines obtained by Hung and Macagno (1966) for R = 46.6 are replotted with the present variables in the same figure. It is seen that the streamline pattern obtained by the present method is in excellent

qualitative agreement with that obtained by Hung and Macagno. The numerical details of the flow are compared in Table 5. Values given in the first row are obtained from the graphs given by Hung and Macagno.

	Reattachment point x_r	Centre of eddy x_e	Recirculating mass flow ψ_{e-1}
Hung and Macagno	0.066	0.013	0.052
Present 3-term	0.064	0.014	0.045

TABLE 5 SYMMETRIC SUDDEN EXPANSION, h = 0.5

This favourable comparison of the present calculation with that of Hung and Macagno (1966) which is based on NSE, supports the following views. Equation (2.5) is appropriate as the limit equation for large R for the 'far' region, and the streamwise length scale is of order R. The method devised to solve equation (2.5) is applicable even in the presence of recirculating flow. Also the hypothesis used to obtain the initial condition to integrate the equation appears to give acceptable results.

The centreline velocity u_c is shown in Figure 19. 3-term and 5-term calculations give almost the same u_c except very close to the expansion. Although a very small

number of terms are used, the results can be said to be indicative of a convergent trend. Velocity profiles at various streamwise locations based on the 3-term calculation are shown in Figure 20. The velocity profile at $x = 0.06$ is approximately that at the reattachment point.

Figure 21 shows the pressure distribution obtained using 2, 3 and 5 terms. The point of reattachment x_r is marked on each of the curves. At first the pressure increases followed by a continual decrease as required by the Poiseuille flow. It is seen that the maximum pressure occurs after the reattachment. The numerical values of P_r, x_{99} and x_r are given later in Table 8a with those for other values of h.

5.2.3 RESULTS FOR OTHER VALUES OF h

Numerical calculation with two types of entry profiles, the parabolic and the uniform, are carried out for various values of h given in Table 6. A zero indicates the occurrence of the singularity and the termination of the calculation (Sections 3.5 and 3.6). $h = 1$ corresponds to the entry flow problem. 2-term calculations are also carried out for some intermediate values of h in addition to those given in Table 6. Table 7 gives some typical initial values of a_m.

N	h = 1	0.95	0.9	0.75	0.5	0.25	0.1
			Parabolic entry profile				
2		1	1	1	1	1	1
3		1	1	1	1	0	0
5		1	1	1	1	0	0
			Uniform entry profile				
2	1	1	1	1	1	1	1
3	1	1	1	1	1	1	0
5	1	1	1	1	1	0	0

TABLE 6 CALCULATIONS PERFORMED FOR SYMMETRIC SUDDEN EXPANSION

1 : $D \neq 0$

0 : $D = 0$ for some x (see Section 3.5).

h	a_{10}	a_{20}	a_{30}	a_{40}	a_{50}
			Parabolic entry profile		
0.9	.1322	-.0160	.0330	-.0073	.0141
0.5	1.1668	-.0200	-.2516	.0228	.0650
0.1	3.8088	1.0040	3.1894	.9347	2.3766
			Uniform entry profile		
0.9	-.3751	.0443	-.0865	.0176	.0348
0.5	.6744	-.1758	.0059	.1124	-.1807
0.1	3.7262	.9442	2.7992	.7358	1.5681

TABLE 7 INITIAL CONDITION FOR SYMMETRIC SUDDEN EXPANSION

For small values of h the initial flow is like a strong jet, and therefore the higher modes are expected to be significant. On the other hand, for h close to one the details of the flow will not be brought out accurately unless higher modes are included in the calculation. For h = 0.1, the order of magnitude of a_{m0} (see Table 7) suggests that more terms should be considered in the expansion. On the other hand for h = 0.9, the order of magnitude of a_{m0} suggests that inclusion of more terms may not be necessary. However, it turns out that the small 'back-step' requires higher modes to be included for the calculation of flow details like recirculation. In the case of h = 0.5, which is in the middle of the range of h, the inclusion of the fourth and the fifth modes affect the calculation only slightly.

For h = 0.5 the assumed uniform entry velocity profile (5.4) with its approximations is shown in Figure 22. The assumed velocity profile has a discontinuity at h = 0.5. The approximation is considerably improved when higher modes are included. Another example where the assumed velocity profile is discontinuous is the entry flow in a channel considered in the previous chapter. However, there the discontinuity is at the wall, whereas in the present case it is located within the interval (0,1). In both cases the approximation is improved with the inclusion of higher modes (see also Figure 10). This suggests that discontinuous

velocity profiles can be expanded into eigenfunctions of (3.6). Figure 22 also shows u_c obtained with 2, 3 and 5 terms. The three calculations show a consistent trend.

Figure 23 shows u_c for three values of h based on 5-term calculations with both types of entry conditions. For the parabolic entry profile the figure shows a monotonic decrease of u_c to the Poiseuille flow value. An interesting behaviour is observed for h = 0.75 with uniform entry profile. First u_c decreases and then increases to attain the Poiseuille flow value. The incoming flow, due to its mixing with the 'dead' fluid, first decelerates. Later as the flow develops, u_c increases as $u_c(0) < u_c(\infty)$. The above qualitative trend is not shown by the 2-term calculation. We therefore see that the inclusing of higher modes in the calculation helps in realising the flow picture more accurately and thus a better quantitative prediction can be obtained. For h = 0.9 the 'dip' in u_c is however absent. Possibly the 'dip' is small and may require more terms in the calculation. Figure 24 shows the pressure distribution based on 5-term calculations for the above values of h. While each of the curve for the parabolic entry profile show a positive pressure recovery coefficient P_r, positive as well as negative P_r occur for uniform entry profile (see Tables 8a, b). Points of reattachment x_r have been marked in the figure. Following x_r a maximum

h	N	P_r	x_{99}	x_r
0.95	2	.0445	.0712	-
	3	.0521	.0784	-
	5	.0585	.0706	-
0.9	2	.1033	.1157	-
	3	.1199	.1148	-
	5	.1360	.1140	-
0.75	2	.3892	.1876	.0030
	3	.4292	.1862	.0080
	5	.4622	.1860	.0090
0.5	2	1.320	.2839	.0659
	3	1.234	.2779	.0638
	5	1.390	.2775	.0656
0.25	2	2.022	.3594	.1431
0.1	2	1.838	.3715	.1558

TABLE 8a SUMMARY OF RESULTS WITH PARABOLIC ENTRY PROFILE

h	N	P_r	x_{99}	x_r
1	2	-.2437	.1642	-
(Entry flow)	3	-.2913	.1662	-
	5	-.3505	.1679	-
0.95	2	-.2604	.1673	-
	3	-.3147	.1693	-
	5	-.3699	.1711	-
0.9	2	-.2700	.1696	-
	3	-.3179	.1714	-
	5	-.3570	.1726	-
0.75	2	-.1590	.1559	-
	3	-.1096	.1571	-
	5	-.0955	.1673	.0007
0.5	2	.6397	.1495	.0219
	3	.6889	.1438	.0234
	5	.4970	.1386	.0220
0.25	2	2.028	.3432	.1265
	3	2.285	.3406	.1253
0.1	2	1.884	.3708	.1551

TABLE 8b SUMMARY OF RESULTS WITH UNIFORM ENTRY PROFILE

occurs, as though there is a region of approximately uniform pressure after the reattachment. A similar trend is observed in other calculations to be described later. Tables 8a and 8b give the values of P_r, x_{99} and x_r for parabolic and uniform entry profiles respectively.

5.2.4 PRESSURE RECOVERY COEFFICIENT

It would be of interest to see how the calculated value of P_r compares with an approximate integral calculation. One such approximation is given here. Flow at a downstream section is given by Poiseuille flow, and at x = 0 it is a known flow. The constant pressure gradient of -3 of the fully developed flow and any direct viscous effect are disregarded. Pressure P_r acting on the downstream section is therefore due to the change in momentum flux.

We now calculate P_r with the above approximation. When the entering flow is parabolic (5.1), momentum balance between the sections at the expansion and at some distance downstream gives

$$P_r = 6/5\ (1/h - 1) \quad . \tag{5.6}$$

When the entering flow is uniform (5.3), we get

$$P_r = 1/h - 6/5 \quad . \tag{5.7}$$

Approximate calculations have been earlier based on

uniform velocity profiles which give

$$P_r = 1/h - 1 \quad . \tag{5.8}$$

It should be noted that P_r in (5.7) could be positive or negative depending on the value of h, whereas (5.8) always predicts a positive value for P_r.

The approximations on which the above formulae are based become increasingly inaccurate as h becomes very small or the expansion ratio becomes very large. They can be expected to provide an estimate for moderate expansions.

The calculated values of P_r are compared with the approximate values given by equations (5.6,7) in Figure 25. To avoid overlapping some of the points in Figure 25 (and also in Figure 26) have been staggered. For a small 'back-step' i.e. h close to one, with the uniform entry profile, P_r is approximately equal to that for the entry flow problem (h = 1). For the parabolic entry velocity profile P_r goes to zero as h goes to one. It is seen that for the expansion ratio upto about two, equations (5.6, 7), shown by solid lines, predict P_r rather well. As h goes to zero these equations are singular and therefore cannot be expected to be valid for large expansion ratios. 2-term calculation predicts an approximately uniform level of P_r for large expansion ratios. P_r is expected to be reduced considerably as the losses due to the expansion will be

significant for large expansion ratios. It is suggested that for the range of the expansion ratio greater than, say, three, P_r may be approximately taken to be a constant and equal to two irrespective of the entry condition.

5.2.5 REATTACHMENT AND DEVELOPMENT LENGTHS

The reattachment points x_r and the development length x_{99} are shown in Figure 26. For h = 0.9 and 0.95 the reattachment is not obtained with upto five terms. As noted earlier, more terms will be needed for smaller 'back-step', to predict accurately the details such as reattachment. For the ratio of expansion equal to three, Durst et. al. (1974) have calculated the flow using NSE. Although the upstream condition used in their calculation is derived from the experiment, it is believed that the entry velocity profile is approximately parabolic. The point of reattachment as read from their Figure 6 is shown. Although R in their calculation is only moderately large, x_r obtained by them compares well with the present result. Generally x_r with the uniform entry profile is smaller compared to that with the parabolic entry profile. It is to be expected that the flow reattaches earlier in the former case as the mixing layer is stronger than in the latter case. x_{99} obviously approaches zero with parabolic entry profile as h goes to one. However with the uniform entry profile the above limit corresponds to the entry flow problem.

5.3 CHANNEL WITH AN ASYMMETRIC SUDDEN EXPANSION

The flow in a one-sided expansion of a channel shown in Figure 1b is now considered. The primary aim of this application is to demonstrate the use of antisymmetric eigenfunctions.

5.3.1 INITIAL CONDITION

The downstream channel width is two. The step height is denoted by h. When the entry velocity profile is parabolic the initial condition for a_m becomes

$$a_{m0} = - \frac{1.5 \times (-1)^m}{(1 - h/2)^3 G_m} \left[(1 - h/2)\, \theta_m' - \theta_m \right]_{\substack{y = 1 - h, \\ 0 \leq h \leq 1,}} \qquad (5.9)$$

where G_m is given by (5.3). In the case of a uniform entry profile, the initial condition for a_m is obtained to be

$$a_{m0} = - \frac{(\theta_m''(1) + (-1)^m \theta_m''(1 - h))}{(2 - h)\, G_m} \quad , \; 0 \leq h \leq 1 \; . \qquad (5.10)$$

Equations (5.9) and (5.10) can be modified when $1 < h < 2$.

5.3.2 RESULTS

Table 9 gives various values of h for which the calculations are carried out. With parabolic entry profile, the given flow for small h differs only slightly from the fully developed flow (see Table 10). The small perturbation results given in Section 3.3.4 can be used. For h = 0,

N	h =	0.05	0.1	0.25	0.5	0.75	1.0
				Parabolic entry profile			
2		1	1	1	1	0	1
3		1	1	1	1	1	1
5		1	1	1	1	1	0
				Uniform entry profile			
2		1	1	1	1	1	1
3		1	1	1	1	1	0
5		1	1	1	1	1	0

TABLE 9 CALCULATIONS PERFORMED FOR ASYMMETRIC SUDDEN EXPANSION

1, 0 : refer to Table 6.

h	a_{10}	a_{20}	a_{30}	a_{40}	a_{50}
		Parabolic entry profile			
1.0	-.8595	-1.0544	-.0256	-.0727	-.0595
0.5	-.3877	.3129	-.1066	.0080	.0035
0.1	-.0108	.0591	-.0067	-.0071	-.0069
		Uniform entry profile			
1.0	-.6062	-.3340	.3203	.0401	-.3017
0.5	.1670	.0021	-.1056	-.0319	-.1524
0.1	.0659	-.3535	.0404	.0421	.0405

TABLE 10 INITIAL CONDITIONS FOR ASYMMETRIC SUDDEN EXPANSION

the problem is trivial. In the case of uniform entry profile, h = 0 corresponds to the entry flow problem. Initial conditions obtained for some typical values of h are given in Table 10.

The given parabolic entry profile with its approximations is shown in Figure 27 for two values of h. With increasing number of terms the approximation is seen to improve. In the figure instead of showing each of the three approximations (2, 3 and 5 terms), only two have been shown. The omitted one lies close to the next higher approximation.

When the entry profile is uniform, its approximations are shown in Figure 28. Even 5 terms provide a poor approximation in this case. In fact for some values of h it appears that the total flow is less in the upper half of the channel than in the lower half, whereas the opposite is true for the given profile. However, a convergence of the oscillatory type cannot be ruled out. Here, the numerical results for only the parabolic entry profile are discussed.

The asymmetry of the flow is shown in a simple way by considering the skin friction at the two walls. The values at the upper and the lower walls are denoted by suffix + and - respectively. The skin friction coefficient c_f is also related to the wall-vorticity ω by

$$\tfrac{1}{2} c_{f_{\pm}} R = \pm\omega_{\pm} \quad .$$

$\frac{1}{2} c_f R$ at the two walls are shown in Figure 29 for h=1. As the flow develops the asymmetry of the flow reduces and vanishes ultimately. Compared to the 2-term calculation, the 3-term calculation shows more asymmetry.* A small recirculating region is obtained on the lower wall with three terms. The point of reattachment is taken to be the point where the skinfriction curve meets the x axis going upward (see also Figure 30).

Velocity profiles at various streamwise locations based on the 3-term calculation are shown in Figure 30. The gradual evolution of the flow into a Poiseuille flow is seen from the figure. Pressure distribution is shown in Figure 31. Predictions by the 2-term and the 3-term calculations are qualitatively similar. At the beginning the pressure drop is large followed by a region over which the pressure is approximately uniform, and then the pressure decreases further to its asymptotic trend. It is interesting to note that the reattachment as predicted by the 3-term calculation marked by x_r in the figure, is followed by a region of approximately uniform pressure. Pressure distribution is shown in Figure 32 for some typical values of h. Numerical results are summarised in Table 11 which gives P_r, x_{99} and x_r for various values of h.

---

* It should be noted that the eigenvalues are numbered in the increasing order, and the first and the third eigenfunctions are antisymmetric.

h	N	P_r	x_{99}	x_r
0.05	2	.0147	.0318	-
	3	.0147	.0318	-
	5	.0209	.0318	-
0.1	2	.0333	.0751	-
	3	.0321	.0732	-
	5	.0455	.0726	-
0.25	2	.1078	.1428	-
	3	.1017	.1361	-
	5	.1388	.1319	-
0.5	2	.3114	.2101	-
	3	.2553	.1892	.0094
	5	.3437	.1883	.0145
0.75	3	.4104	.2463	.0409
	5	.4252	.2365	.0421
1.0	2	.1617	.2857	-
	3	.1016	.2799	.0617

TABLE 11 ASYMMETRIC SUDDEN EXPANSION

5.4 BASE IN A CHANNEL

Consider a base having thickness 2h, placed symmetrically in a channel as shown in Figure 1c. The flow behind a thick long flat plate with a bluff end placed in a wind-tunnel can be idealized to lead to the present problem, although it is recognised that only a few features of the base flow are modelled in the present problem.

5.4.1 INITIAL CONDITION

Two types of entry conditions are chosen as before. For the parabolic velocity profile at the entry, the initial condition for a_m is obtained to be

$$a_{m0} = - \frac{6}{(1 - h^2)G_m} \left[\theta_m' + 2/(1 - h)\, \theta_m\right]_{y = h} . \quad (5.11)$$

In the case of the uniform entry profile the initial condition for a_m turns out to be

$$a_{m0} = \frac{1}{(1 - h)G_m} \left[\theta_m''(h) - \theta_m''(1)\right] . \quad (5.12)$$

5.4.2 RESULTS

Table 12 shows the range of the calculations. Table 13 gives initial conditions for some typical cases. It should be noted here that as $h \to 0$ the base shrinks to a thin plate. For the parabolic entry profile the problem

N	h = .05	.1	.25	.5	.75
	Parabolic entry profile				
2	1	1	1	1	1
3	1	1	1	0	1
5	1	1	1	0	0
	Uniform entry profile				
2	1	1	1	1	1
3	1	1	1	1	1
5	1	0	1	1	0

TABLE 12 CALCULATIONS PERFORMED FOR THE BASE IN A CHANNEL

1, 0 : Refer to Table 6.

h	a_{10}	a_{20}	a_{30}	a_{40}	a_{50}
		Parabolic entry profile			
.1	-1.4384	-.0690	-.0769	.0016	.0250
.25	-1.7555	.0738	.2185	.0296	-.0377
.5	-1.3457	.3270	-.5916	.0205	.1490
		Uniform entry profile			
.1	-.7851	.0604	-.4038	-.0603	-.2316
.25	-1.3608	-.0630	-.0646	.1101	.1305
.5	-1.3424	.2559	-.1729	-.0737	.0774

TABLE 13 INITIAL CONDITION FOR THE BASE IN A CHANNEL

considered is then like a flow behind a trailing edge of a flat plate having finite, equal and opposite vorticity on the two sides. When the entering flow is uniform, there are two vortex sheets of equal and opposite strength. The eigenfunctions which are used in the approximation have zero vorticity at the centreline. Therefore for $h = 0$, the present approximation is non-uniform in a neighbourhood of $y = 0$. We observe that as $h \to 0$, expression (5.12) reduces to (4.2) which corresponds to the entry flow problem. However for $h \neq 0$, the approximation is expected to have the desired features of the given entry profile such as $u = 0$ at $y = 0$.

Figure 33 shows the entry condition as approximated by 2, 3 and 5 terms for $h = 0.25$ with the parabolic entry profile. Table 14 compares the centreline velocity at the entry u_{co} and the associated momentum flux M_o given by the three approximations with the actual value. Once again we see that the approximation is improved with the inclusion of

	2-term	3-term	5-term	Actual
u_{co}	-.1817	.0368	.0287	0
M_o	1.6139	1.5978	1.5984	1.6

TABLE 14 REPRESENTATION OF THE INITIAL PROFILE FOR THE BASE IN A CHANNEL

higher modes.

The approximations to uniform entry condition for $h = 0.1$ and 0.5 are shown in Figure 34. Although any marked improvement in the approximation with the inclusion of higher modes is not evident for $h = 0.5$, it is clearly seen for $h = 0.1$.

The streamline pattern based on the 5-term calculation is shown in Figure 35 for $h = 0.25$ with parabolic entry profile. A closed bubble behind the base is obtained. Near the base the streamline pattern shows slight waviness which is possibly due to the representation of the initial condition. This waviness decays rapidly. The development of streamwise velocity profiles based on the 5-term calculation is shown in Figure 36. The centreline velocity is shown in Figure 37. The initially decreasing u_c due to entrainment is absent in the 2-term calculation, whereas 3- and 5-term calculations give a better picture of the recirculating flow behind the base. Entrainment of the 'dead' fluid followed by detrainment is seen from the figure. Although the size of the recirculating region is approximately the same for 3- and 5-term calculations, the eddy is stronger and its centre lies closer to the base in the 5-term calculation. Table 15 compares the three calculations. As the 2-term calculation does not lead to closed streamlines, some of the entries in Table 15 are indicated by -.

	2-term	3-term	5-term
Point of reattachment, x_r	.0086	.0086	.007
Maximum half-width of the recirculating region	.263	.205	.264
Location of the centre of the eddy,			
x_e	-	.0042	.0024
y_e	-	.108	.146
Total recirculation, $-\psi_e$	-	.007	.021
Maximum reversed flow velocity at the centreline	-.1817	-.0918	-.2198
Development length, x_{99}	.213	.206	.201
Pressure recovery coefficient, P_r	-.492	-.214	-.116

TABLE 15 BASE IN A CHANNEL (h = 0.25)
WITH PARABOLIC ENTRY PROFILE

The pressure distribution is shown in Figure 38. The point of reattachment x_r is also marked on the figure. The figure suggests that there is a tendency to form a region of approximately uniform pressure following the point of reattachment.

Figure 39 and 40 show centreline velocity and pressure distributions respectively when the entering flow is uniform. For h = 0.5 and 0.25, u_c decreases initially, however, no reversed flow is obtained. This evidently is due to the error in the approximation of the entry profile. It is interesting to note that for h = 0.5 the calculation shows a region of uniform pressure which in the fewer terms calculation is absent. Tables 16a and 16b give P_r, x_{99} and x_r for parabolic and uniform entry profiles respectively.

h	N	P_r	x_{99}	x_r
.75	2	-.4835	.1846	-
	3	-.9255	.2117	-
.5	2	-.9233	.2248	.0216
.25	2	-.4921	.2130	.0086
	3	-.2138	.2057	.0086
	5	-.1155	.2007	.0070
.1	2	-.1621	.1955	.0001
	3	-.2262	.1947	.0005
	5	-.1229	.1948	.0006
.05	2	-.1596	.1944	-
	3	-.2561	.1914	-
	5	-.1729	.1916	-

TABLE 16a BASE IN A CHANNEL WITH PARABOLIC ENTRY PROFILE

h	N	P_r	x_{99}	x_r
.75	2	-.5190	.1899	-
	3	-.9782	.2157	-
.5	2	-.8727	.2253	-
	3	-.9321	.2264	.0173
	5	-.3219	.2244	-
.25	2	-.1971	.1970	-
	3	-.2360	.1960	-
	5	-.2731	.1901	-
.1	2	-.1789	.1872	-
	3	-.4337	.1822	-
.05	2	-.2176	.1795	-
	3	-.3854	.1792	-
	5	-.4331	.1766	-

TABLE 16b BASE IN A CHANNEL WITH UNIFORM ENTRY PROFILE

EPILOGUE

EXTERNAL SEPARATED FLOW

The internal separated flow provides a suitable ground for the testing of limit equations for $L_y \sim 1$. We then find that for $\Psi \sim 1$, two principal limits are possible and they correspond to $L_x \sim 1$ and $L_x \sim R$. While we are familiar with the first limit process which leads to the Euler equation, the second limit process which is rather new is examined in this thesis.

The limit equation (2.4) corresponding to the limit $L_x \sim R$ is wellknown and is associated with the classical boundary-layer. We test the applicability of this equation to a class of separated flows. Good comparison with solutions using complete NSE supports its validity.

External separated flows differ in one important respect from the internal separated flows. The interaction between the outer irrotational flow and the separated region is an essential characteristic of the external separated flow and poses considerable difficulty in the analysis. As it stands, it is difficult to ascertain apriori the transverse length scale of the separated wake. In fact some drastically different models of the limit flow have been proposed. However, if we assume that the transverse length scale of the separated wake is of order one,

some of the conclusions of this work such as the appropriateness of the limit equation (2.4) would be applicable.

The experimental results given by Acrivos and his colleagues (1964, 1965, 1968) for flow past a circular cylinder suggest $L_y \sim 1$ and $L_x \sim R$. The limit equation (2.4) therefore should be applicable. In this limit the viscous and the inertial forces are of same order. This nature of the flow is different from the other shear driven recirculating regions where the limiting flow is expected to be governed by the Euler equation.

The present work may give an insight into one element of the external separated flow at large Reynolds number whose global picture continues to fascinate many.

REFERENCES

Acrivos, A., Snowden, D.D., Grove, A.S. & Petersen, E.E. (1965) The steady separated flow past a circular cylinder at large Reynolds number, J. Fluid Mech. 21, 737-760.

Acrivos, A., Leal, L.G., Snowden, D.D. & Pan, F. (1968) Further experiments on steady separated flows past bluff objects, J. Fluid Mech. 34, 25-48.

Ban, S.D. & Kuerti, G. (1969) The interaction region in the boundary layer of a shock tube, J. Fluid Mech. 38 109-125.

Bodoia, J.R. & Osterle, J.F. (1961) Finite difference analysis of plane Poiseuille and Couette flow developments, Apl. Sci. Res. 10, 265-276.

Briley, W.R. (1971) A numerical study of laminar separation bubbles using the Navier-Stokes equations, J. Fluid Mech. 47, 713-736.

Brown, S.N. & Stewartson, K. (1969) Laminar separation, Ann. Rev. Fluid Mech. 1, 45-72.

Catherall, D. & Mangler, K.W. (1966) The integration of the two-dimensional laminar boundary-layer equations past the point of vanishing skin friction, J. Fluid Mech. 26, 162-182.

Collins, M. & Schowalter, W.R. (1962) Laminar flow in the inlet region of a straight channel, Phys. Fluid 5, 1122-1124.

Collins, M. & Schowalter, W.R. (1963) Behaviour of non-Newtonian fluids in the inlet region of a channel, AIChE J.9, 98-

Dorodnitsyn, A.A. & Meller, N.A. (1970) Application of the small parameter method to the solution of Navier-Stokes equations, Fluid Dyn. Trans. 5, pt. II, 67-82.

Durst, F., Melling, A. & Whitelaw, J.H. (1974) Low Reynolds number flow over a plane symmetric sudden expansion, J. Fluid Mech. 64, 111-128.

Gillis, J. & Brandt, A. (1964) The numerical integration of the equations of motion of a viscous fluid, Weizmann Institute, AF EOAR SR-1.

Goldstein, S. (1948) On laminar boundary-layer flow near a position of separation, Q.J. Mech. & Apl. Math. 1, 43-69.

Grove, A.S., Shair, F.H., Petersen, E.E. & Acrivos, A. (1964) An experimental investigation of the steady separated flow past a circular cylinder, J. Fluid Mech. 19, 60-80.

Hung, T.K. & Macagno, E.O. (1966) Laminar eddies in a two-dimensional conduit expansion, La Houille Blanche 21, 391-401.

Hwang, C.L. & Fan, L.T. (1964) Finite difference analysis of forced convection heat transfer in entrance region of a flat rectangular duct, Apl. Sci. Res. A13, 401-422.

Klemp, J.B. & Acrivos, A. (1972) A method for integrating the boundary-layer equations through a region of reverse flow, J. Fluid Mech. 53, 177-191.

Morihara, H. (1972) Numerical integration of the Navier-Stokes equations, Ph.D. Thesis, State U. of New York at Buffalo.

Roidt, M. & Cess, R.D. (1962) An approximate analysis of laminar magnetohydrodynamic flow in the entrance region of a flat duct, J. Apl. Mech., Trans. ASME 29, Ser E 171-

Schlichting, H. (1934) Laminare Kanaleinlaufstromung, Z.A.M.M. 14, 368-373.

Schlichting, H. (1968) Boundary-Layer Theory, 6th ed., McGraw-Hill Book Company, 176-178.

Van Dyke, M. (1970) Entry flow in a channel, J. Fluid Mech. 44, 813-823.

Wang, Y.L. & Longwell, P.A. (1964) Laminar flow in the inlet section of parallel plates, AIChE J. 10, 323-329.

Wilson, S. (1969) The development of Poiseuille flow, J. Fluid Mech. 38, 793-806.

APPENDIX 1

SOLUTION OF THE EIGENVALUE PROBLEM

1. The eigenvalue problem obtained in Chapter 3 is

$$\Phi^{iv} + \lambda\left[3/2(1 - y^2)\Phi'' + 3\Phi\right] = 0 \quad , \tag{A1.1}$$

$$\Phi = \Phi' = 0 \quad \text{at} \quad y = \pm 1 \quad . \tag{A1.2}$$

Calculation of odd and even eigenvalues proceed separately. The region of integration is restricted to $0 \leq y \leq 1$. The boundary condition imposed at $y = 0$ is therefore as follows

$$\text{Odd} : \quad \Phi' = \Phi''' = 0 \qquad \text{at } y = 0 \quad , \tag{A1.3}$$

$$\text{Even} : \quad \Phi = \Phi'' = 0 \qquad \text{at } y = 0 \quad . \tag{A1.4}$$

For a given λ two linearly independent odd solutions of (A1.1) can be obtained. One such solution is

$$\Phi_1 = (1 - y^2). \tag{A1.5}$$

Another solution is obtained on integrating (A1.1) with the initial conditions

$$\Phi_2 = 1, \quad \Phi_2' = \Phi_2'' = \Phi_2''' = 0 \quad \text{at } y = 0 \quad . \tag{A1.6}$$

A general solution which is odd can then be written as

$$\Phi_o = A\,\Phi_1 + B\,\Phi_2 \quad . \tag{A1.7}$$

If a non-trivial Φ_o satisfies (A1.2), we get

$$\Phi_2(1\ ;\lambda) = 0 \quad . \tag{A1.8}$$

Thus the zeros of the function $\Phi_2(1\ ;\lambda)$ gives the odd eigenvalues.

Similarly for determining even eigenvalues, we consider two linearly independent even solutions of (A1.1). A pair of such solutions is obtained on integrating (A1.1) with the initial conditions

$$\Phi_3 = 0\ ,\ \Phi_3' = 1\ ,\ \Phi_3'' = \Phi_3''' = 0 \text{ at } y = 0\ , \tag{A1.9}$$

$$\Phi_4 = \Phi_4' = \Phi_4'' = 0\ ,\ \Phi_4''' = 1 \qquad \text{at } y = 0\ . \tag{A1.10}$$

If a non-trivial linear combination of Φ_3 and Φ_4 satisfies (A1.2), then

$$(\Phi_3 \Phi_4' - \Phi_3' \Phi_4)_{y=1} = 0\ . \tag{A1.11}$$

The left side of (A1.11) is a function of λ. Its zero, therefore, gives the even eigenvalues.

The values of the functions on the left side of (A1.8) and (A1.11) can easily be obtained for a given λ. In the integration of the equation (A1.1) the fourth order Runge-Kutta-Gills method with a step length of 0.05 is used. Using the Newton-Raphson method zeros of the above functions are obtained.

The eigenfunctions are scaled in the following way

Odd : $\Phi = 1$ at $y = 0$, (A1.12)

Even : $\Phi' = 1$ at $y = 0$. (A1.13)

Solution of the adjoint problem is obtained in a similar way. Note that Θ = constant is a solution of the adjoint equation (3.23). The scaling used is similar to (A1.12, 13).

Odd : $\Theta = 1$ at $y = 0$, (A1.14)

Even : $\Theta' = 1$ at $y = 0$. (A1.15)

Engeinvalues are given in Tables A1 and A2. Each time a calculation is to be performed, it is not necessary to go through the process of recalculating the eigenvalues. They can be given as data in the program and the eigenfunctions can be generated as solutions of an initial value problem. Three of the required four conditions at $y = 0$ are given by (A1.3, 12) or (A1.4, 13). The fourth condition which can go as data in the program, is also given in Tables A1 and A2.

m	λ_m	$\Phi_m''(0)$	$\Theta_m''(0)$
1	14.4535	-5.82126	-8.45962
2	48.8857	5.70202	150.811
3	104.572	-10.3516	-60.7067

TABLE A1 ODD EIGENVALUES

m	λ_m	$\Phi_m'''(0)$	$\Theta_m''(0)$
1	18.8146	-18.0682	-22.4208
2	57.5463	-194.425	-90.9318
3	117.486	-116.047	-167.001
4	199.103	-592.211	-305.759
5	303.073	-312.985	-441.431

TABLE A2 EVEN EIGENVALUES

2. The orthogonality relation satisfied by the eigenfunctions is given by equation (3.27). We therefore have the relation

$$[\Phi_m, \Theta_n] \Big/ \sqrt{[\Phi_m, \Theta_m]\,[\Phi_n, \Theta_n]} = \delta_{mn} \qquad \text{(A1.16)}$$

As a check we compute the right side of (A1.16) for even eigenfunctions which are given in Table A3. Terms on the diagonal in the table are by definition one. The off-diagonal terms in comparison are very small. If we take the first two terms, the off-diagonal terms are less than .001. Similarly if we take the first three, four and five terms the off-diagonal terms are respectively less than .006, .02, .062. We thus see that with higher modes the error increases. This behaviour is to be expected as the step size used in the integration of (A1.1) and the

	n= 1	2	3	4	5
m = 1	1	.0003	.0010	.0014	.0029
2	.0009	1	.0058	.0034	.0129
3	.0009	.0018	1	.0076	.0086
4	.0030	.0038	.0193	1	.0614
5	.0030	.0036	.0116	.0192	1

TABLE A3 A CHECK ON BIORTHOGONALITY

adjoint problem becomes rather large compared with distance over which significant variations occur when higher modes are considered. If we decrease the step size, we can expect this error to reduce significantly. However we accept these calculated eigenfunctions and efforts to obtain them more accurately were not made. Incidentally this exercise confirms the development of the biorthogonal set.

APPENDIX 2

ON THE PHASE PLANE

1. The differential equation (3.36) is written as

$$(1 - C_{111}a_1 - C_{112}a_2)a_1' - (C_{121}a_1 + C_{122}a_2)a_2' = -\lambda_1 a_1, \quad (A2.1)$$

$$-(C_{211}a_1 + C_{212}a_2)a_1' + (1 - C_{221}a_1 - C_{222}a_2)a_2' = -\lambda_2 a_2. \quad (A2.2)$$

The above equations can be solved for a_1' and a_2' to give

$$a_1' = D_1/D \quad , \quad a_2' = D_2/D \quad , \quad (A2.3)$$

where D, D_1 and D_2 are functions of a_1 and a_2 given below

$$D = (C_{111}C_{221} - C_{121}C_{211})a_1^2 + (C_{111}C_{222} + C_{112}C_{221} - C_{121}C_{212} - C_{122}C_{211})a_1a_2 + (C_{112}C_{222} - C_{122}C_{211})a_2^2 - (C_{111} + C_{221})a_1 - (C_{112} + C_{222})a_2 + 1 \quad , \quad (A2.4)$$

$$D_1 = \lambda_1 C_{221}a_1^2 + (\lambda_1 C_{222} - \lambda_2 C_{121})a_1a_2 - \lambda_2 C_{122}a_2^2 - \lambda_1 a_1, \quad (A2.5)$$

$$D_2 = -\lambda_1 C_{211}a_1^2 + (\lambda_2 C_{111} - \lambda_1 C_{212})a_1a_2 + \lambda_2 C_{112}a_2^2 - \lambda_2 a_2 . \quad (A2.6)$$

The above expressions are qudaratic, that is they are of the form

$$Q = \beta_1 a_1^2 + \beta_2 a_1 a_2 + \beta_3 a_2^2 + \beta_4 a_1 + \beta_5 a_2 + \beta_6 \quad . \qquad (A2.7)$$

The numerical values of the coefficients, β's of D, D_1 and D_2 are given in Table A4

	D	D_1	D_2
β_1	.1796	-5.546	-1.267
β_2	-.1793	74.79	-22.23
β_3	-3.702	-611.3	-203.6
β_4	.6947	-18.81	0
β_5	2.366	0	-57.55
β_6	1	0	0

TABLE A4 COEFFICIENTS IN THE EXPRESSION (A2.7)

The location of the origin and the inclination of the conic section associated with quadratic expressions D, D_1 and D_2 are given in Table A5.

	D	D_1	D_2
Origin of the conic section (a_1 , a_2)	-1.753, .3620	-2.887, -.1766	2.382, -.2715
Inclination in degrees	-1.322	3.519	-3.136

TABLE A5 DETAILS OF THE CONIC SECTIONS

In the transformed coordinates that is the principal coordinates of the conic section, D is given as

$$D = 0.1817\,\xi^2 - 3.704\,\eta^2 + 0.8191 \quad . \qquad \text{(A2.8)}$$

It is seen from (A2.8) that $D = 0$ represents a hyperbola. Similarly D_1 and D_2 are written as

$$D_1 = -3.246\,\xi^2 - 613.6\,\eta^2 + 27.16 \quad , \qquad \text{(A2.9)}$$

$$D_2 = -.6576\,\xi^2 - 204.2\,\eta^2 + 7.811 \quad , \qquad \text{(A2.10)}$$

where ξ, η are their respective principal coordinates. $D_1 = 0$ and $D_2 = 0$ therefore represent ellipses, and are shown on Figure 8.

2. A short version of the program for the symmetric 2-term calculation based on (A2.3) and the coefficients given in Table A4, can be written. This is suitable for a quick calculation of quantities such as pressure, skin friction and centreline velocity.

APPENDIX 3

THE SECOND SINGULAR POINT OF (3.44)

D_1 and D_2 in equation (3.44) are given by (A2.5, 6). We consider the behaviour in the neighbourhood of the second singular point P. The coordinates of point P are

$$a_{1P} = -.7309 \ , \quad a_{2P} = -.1849 \ . \tag{A3.1}$$

We define

$$\xi_1 = a_1 - a_{1P} \ , \quad \xi_2 = a_2 - a_{2P} \ . \tag{A3.2}$$

For the analysis in the neighbourhood of P, the linear terms in ξ_1 and ξ_2 are considered. We can then write

$$\frac{da_2}{da_1} = \frac{(\partial D_2/\partial a_1)_P \xi_1 + (\partial D_2/\partial a_2)_P \xi_2}{(\partial D_1/\partial a_1)_P \xi_1 + (\partial D_1/\partial a_2)_P \xi_2} \ . \tag{A3.3}$$

Therefore,

$$\xi_1' = (\partial D_1/\partial a_1)_P \xi_1 + (\partial D_1/\partial a_2)_P \xi_2 \ , \tag{A3.4a}$$

$$\xi_2' = (\partial D_2/\partial a_1)_P \xi_1 + (\partial D_2/\partial a_2)_P \xi_2 \ . \tag{A3.4b}$$

Here dash does not denote differentiation with respect to x, but with respect to some other parameter. Inserting the numerical values in the above expressions we get

$$\xi_1' = -24.52\,\xi_1 + 171.4\,\xi_2 \quad , \tag{A3.5a}$$

$$\xi_2' = 5.96\,\xi_1 + 33.89\,\xi_2 \quad . \tag{A3.5b}$$

The above can also be written as

$$\begin{bmatrix} \xi_1' \\ \xi_2' \end{bmatrix} = \begin{bmatrix} -24.52 & 171.4 \\ 5.96 & 33.89 \end{bmatrix} \begin{bmatrix} \xi_1 \\ \xi_2 \end{bmatrix} \tag{A3.6}$$

Therefore trace T and the determinant Ω of the matrix on the right side of (A3.6) are

$$T = 9.37 \quad , \quad \Omega = -1852 \quad . \tag{A3.7}$$

As $\Omega < 0$, P is a saddle point. The eigenvalues of the above matrix equation are found to be 47.93 and -38.56. The principal directions then are,

$$\eta_1 = \xi_1 - 2.36\,\xi_2 \quad , \tag{A3.8a}$$

$$\eta_2 = 0.082\,\xi_1 + \xi_2 \quad . \tag{A3.8b}$$

In the coordinate system (η_1, η_2), equation (A3.6) is written as

$$\eta_1' = -38.56\,\eta_1 \tag{A3.9a}$$

$$\eta_2' = 47.93\,\eta_2 \tag{A3.9b}$$

APPENDIX 4

ON THE COMPUTER PROGRAM

1. The predictor-corrector method used to integrate equation (3.47a) is as follows. The predictor used is the Euler's method,

$$b_m - a_m = (a'_m / a'_n)\, H \quad , \tag{A4.1}$$

where b_m is the predicted value of a_m at the next point of integration, and H is the step length in a_n. The corrector used is the Euler's modified method,

$$c_m - a_m = H/2 \left[(a'_m/a'_n) + (b'_m/b'_n) \right] \quad , \tag{A4.2}$$

where c_m is the corrected value. The maximum difference between the predicted and the corrected values is given as

$$e = \underset{m}{\text{maxm.}} \left| c_m - b_m \right| \quad . \tag{A4.3}$$

In general more than one use of the corrector is necessary to get e within a prescribed level of accuracy ACY. However the repeated use of the corrector is permitted only upto a prescribed number of time MAXCOR within which if e does not fall below ACY the step length is halved, H = H/2, and the procedure is started again from (A4.1). However in halving the step length if H falls below a prescribed minimum HLOW, the integration is terminated as the roundoff error will be significant.

At the end of the integration over the step, equation (3.47b) is integrated as

$$\Delta x = H/2\ (1/a_n' + 1/b_n') \quad , \qquad (A4.4)$$

where Δx is the increment in x. Since the error of the corrector (A4.2) is of order H^3, the step length is doubled, $H = 2H$, if $e \leq ACY/10 = ACYLOW$, at the end of the integration over the step.

A schematic layout of the above predictor-corrector method which incorporates the adjustment of the step length, is shown on the next page. At the beginning of the integration a_m and a_m' are known. Equation (3.46) is used to determine the independent variable a_n. The diagram explains the integration over one step.

Rectangular boxes in the diagram show mathematical operations and the logical operations are shown by diamonds. Print statements are deleted to keep the diagram simple. Arrows show the flow of operation. The mathematical operations are stated within boxes either explicitly or inside brackets. Few steps of the diagram are explained. The first box contains b_m(A4.1) which means that b_m are calculated using equation (A4.1). To obtain the derivative b_m', a subroutine YPRIME is used, which is shown in another box. The remaining operations are clear from the diagram.

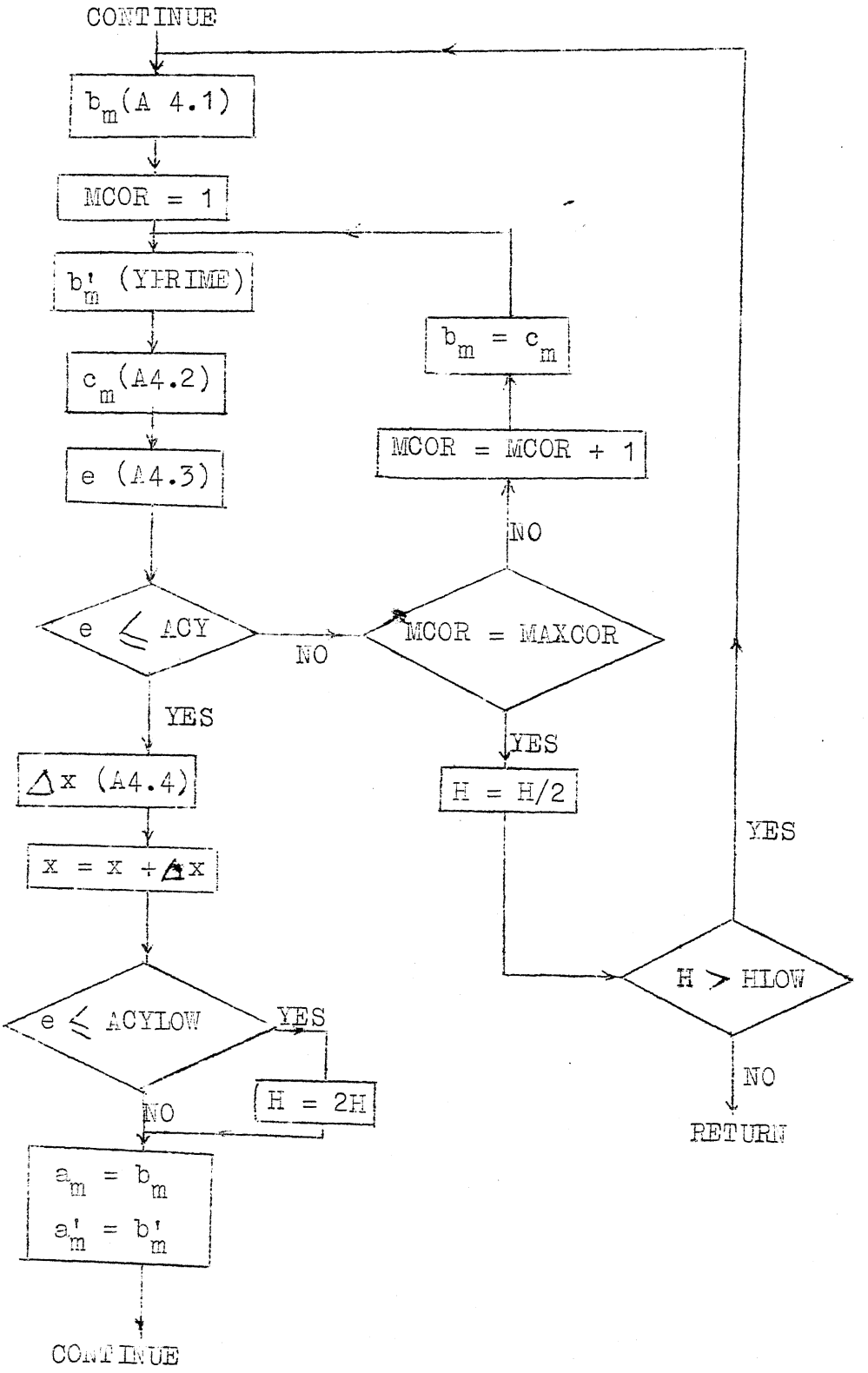
CONTINUE
b_m(A 4.1)
MCOR = 1
b'_m (YPRIME)
c_m(A4.2)
e (A4.3)
e ≤ ACY
NO
YES
MCOR = MAXCOR
NO
YES
$b_m = c_m$
MCOR = MCOR + 1
Δx (A4.4)
x = x + Δx
e ≤ ACYLOW
YES
H = 2H
NO
H = H/2
H > HLOW
YES
NO
RETURN
$a_m = b_m$
$a'_m = b'_m$
CONTINUE

2. The sequence of operations in a calculation is as follows.

Information in the form of whether the calculation is symmetric or asymmetric, is required to determine the expansion set. N is the number of terms in (3.33). In case of symmetric calculation N is the number of even eigenfunctions included in the calculation.

The required eigenfunctions and its adjoint functions are generated. Coefficients C_{1mn} and I_{2m} given by (3.35) are calculated.

The initial condition for a_m given by (3.37) is calculated next.

The integration of the equation (3.36) forms the heart of the program, and is carried out in a separate subroutine 'PHASEN'. This requires a subroutine YPRIME to solve the set of equations (3.36) for the derivatives a'_m. The predictor-corrector method used for the integration has been described above. In addition following features have been incorporated.

i) If the initial condition is such that D <0, RETURN is executed with a message.

ii) If at any stage of the computation D changes sign, RETURN is executed with a message.

iii) If $\max_m |a_m|$ is less than or equal to a prescribed small number ϵ, RETURN is executed (linear subrange, see Section 3.4.2).

iv) If the computation proceeds longer than a prescribed number of steps, RETURN is executed.

After the successful execution of PHASEN, the desired results are printed out.

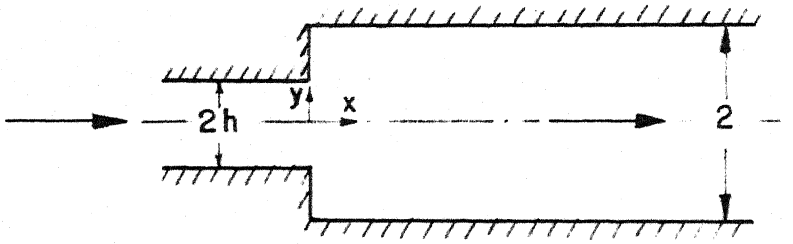

a. SYMMETRIC SUDDEN EXPANSION

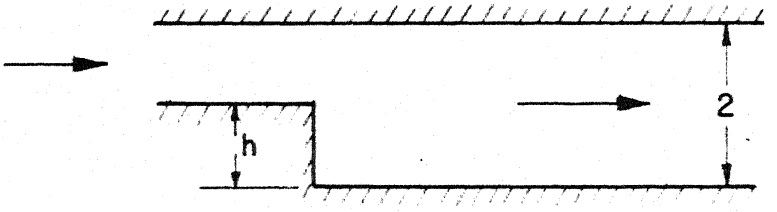

b. ASYMMETRIC SUDDEN EXPANSION

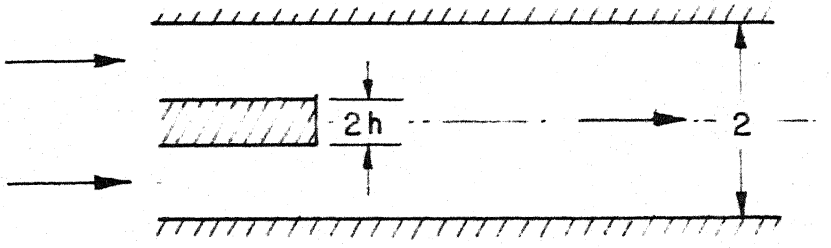

c. BASE IN A CHANNEL

FIG. 1 TYPES OF SEPARATED FLOW PROBLEMS CONSIDERED

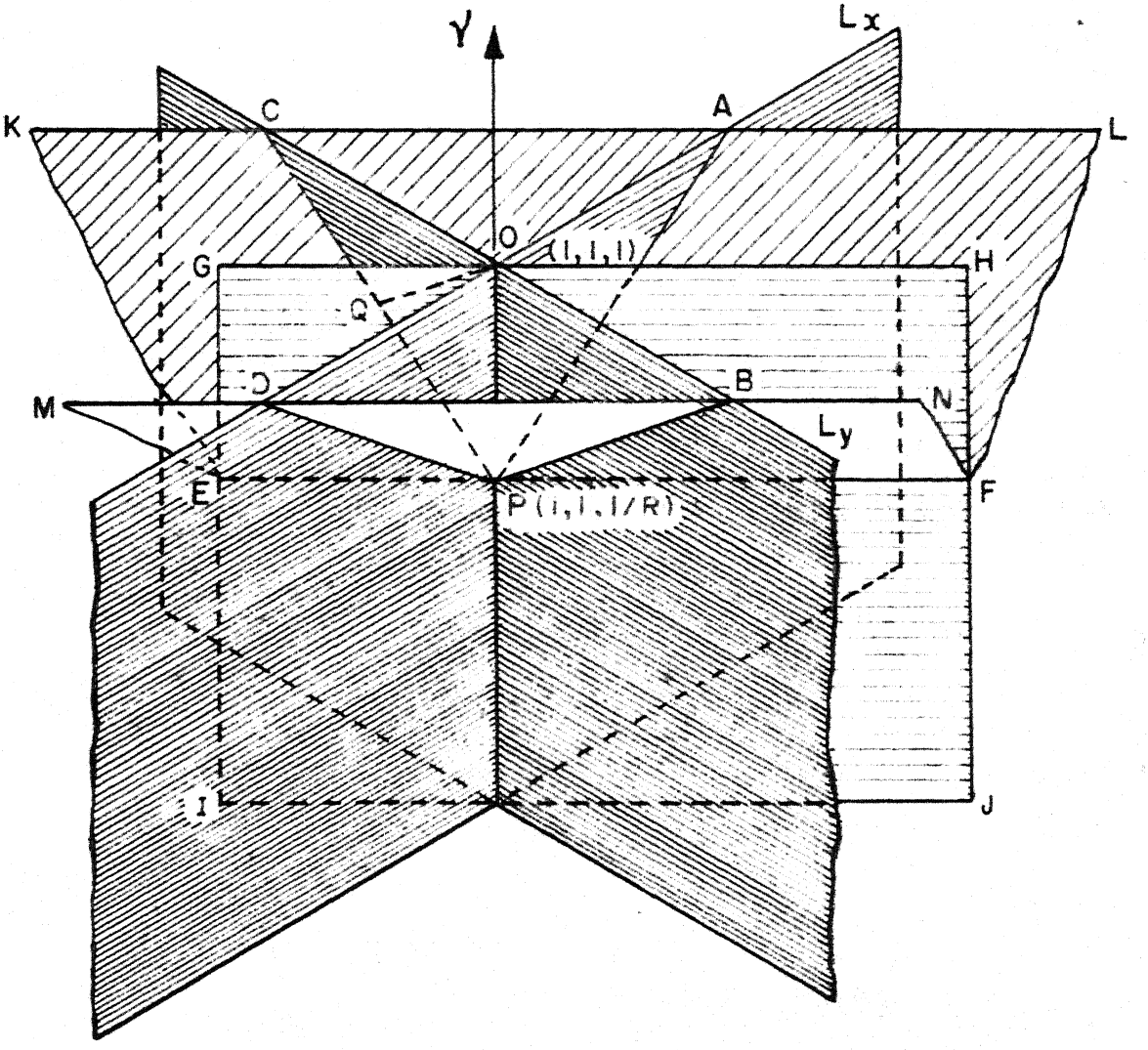

FIG. 2 ORDER SPACE REPRESENTATION OF LARGE REYNOLDS NUMBER LIMITS OF NSE

(Log SCALE FOR L_x, L_y & γ AXES)

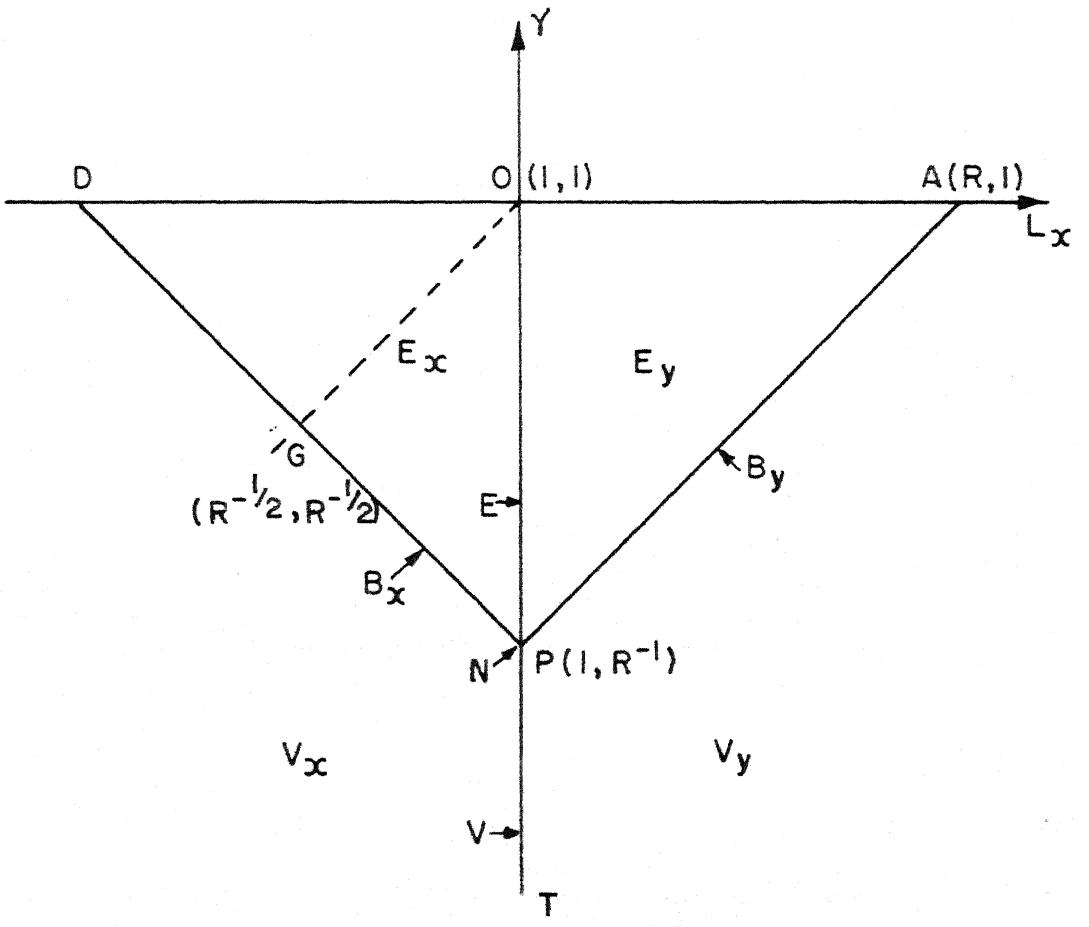

FOR N, E, V, B_y, B_x, E_y, E_x, V_y & V_x SEE EQN. (2.2)

FIG.3 DOMAIN OF VALIDITY FOR LIMIT EQUATIONS WHEN $L_y \sim 1$

(Log SCALE FOR L_x AND Y AXES)

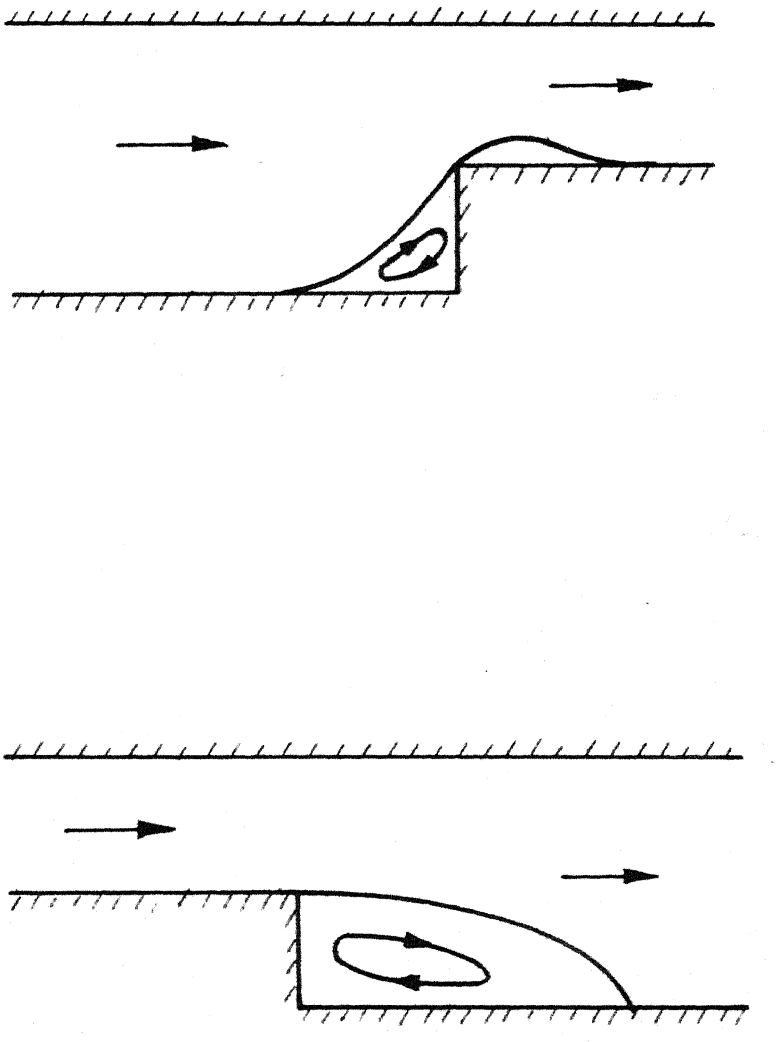

FIG.4 SCHEMATIC OF TWO TYPES OF INTERNAL SEPARATED FLOWS

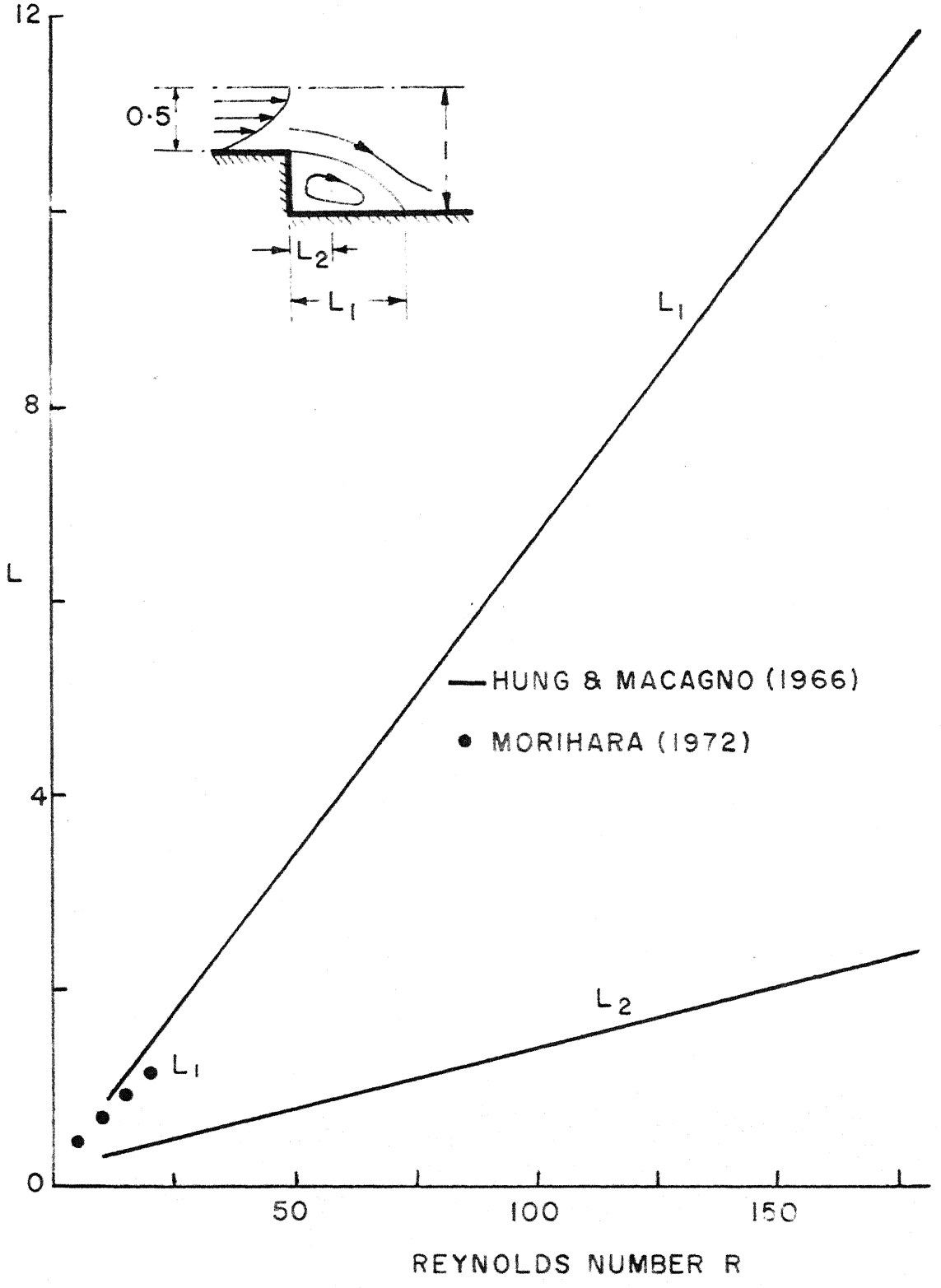

FIG.5 DEPENDANCE OF STREAMWISE LENGTH SCALE ON REYNOLDS NUMBER

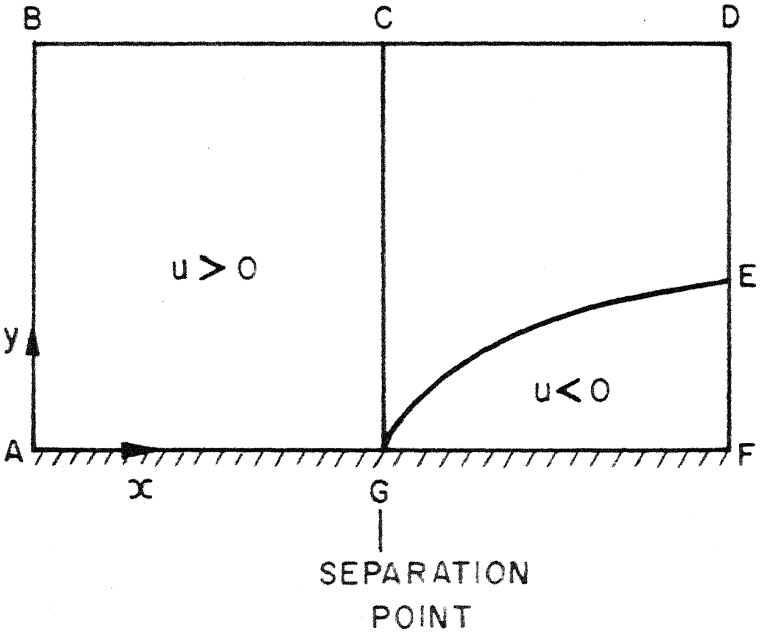

FIG.6 SCHEMATIC OF FORWARD AND REVERSED FLOW REGIONS

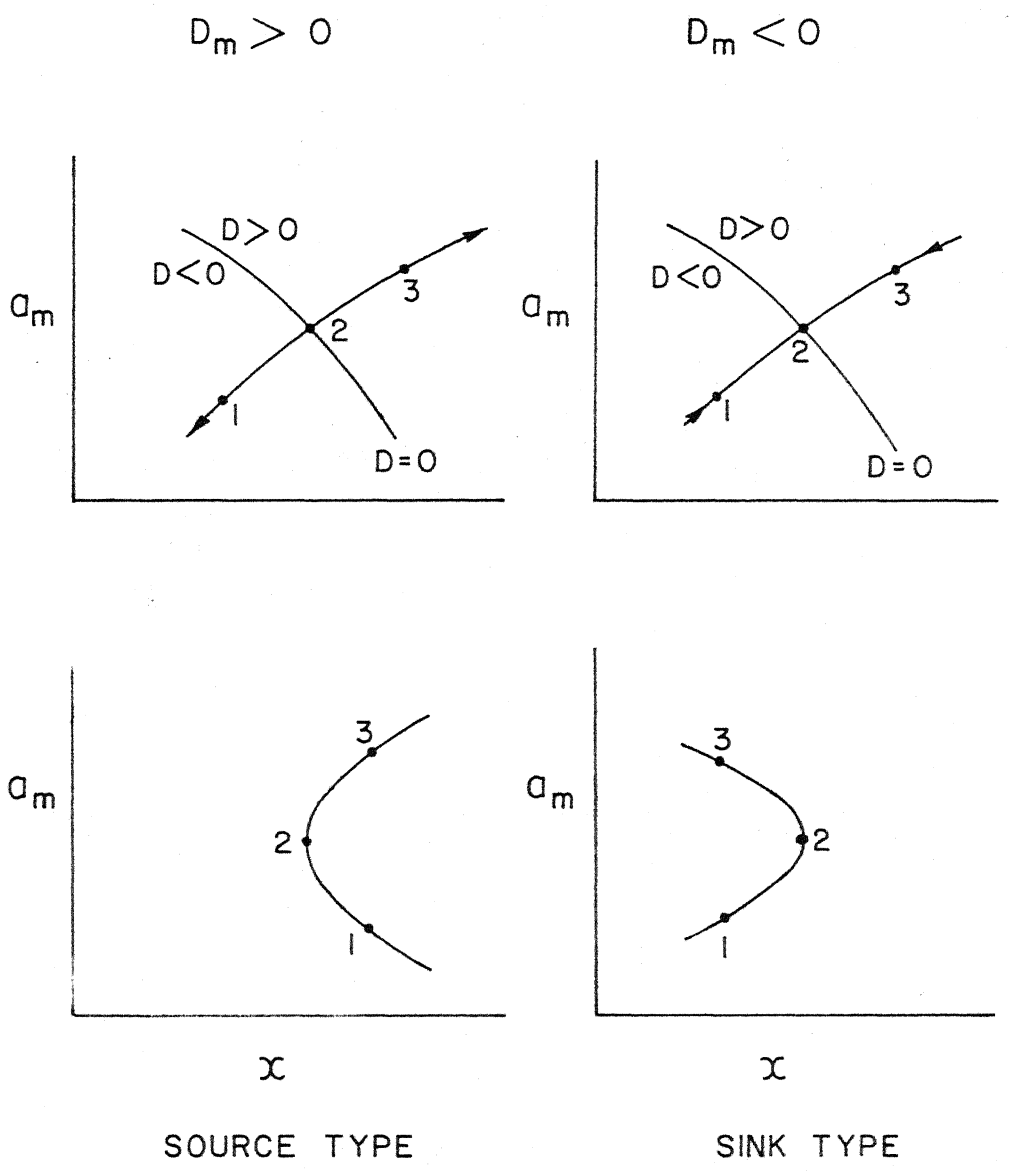

FIG. 7 PHASE SPACE REPRESENTATION

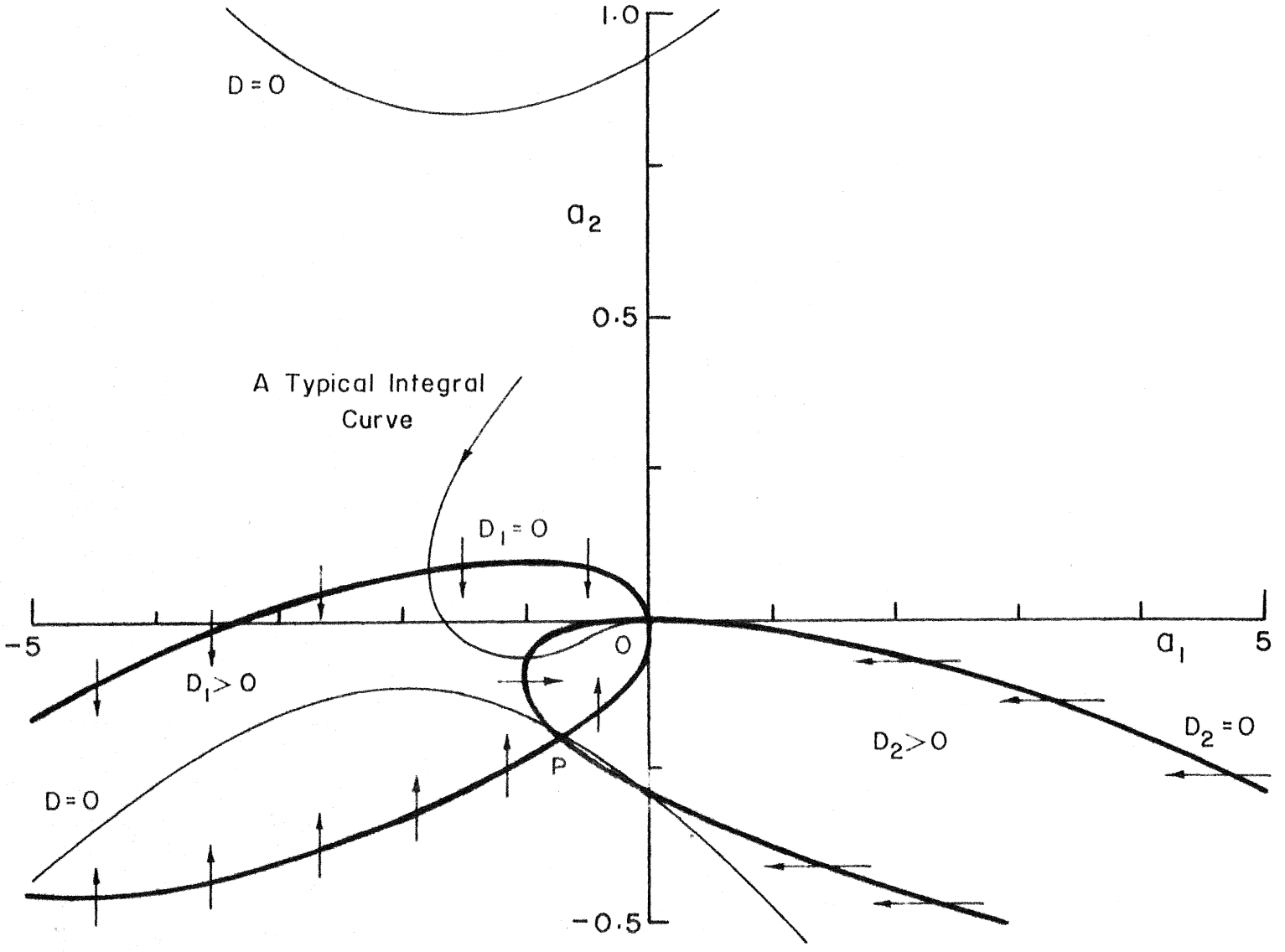

FIG. 8 PHASE PLANE

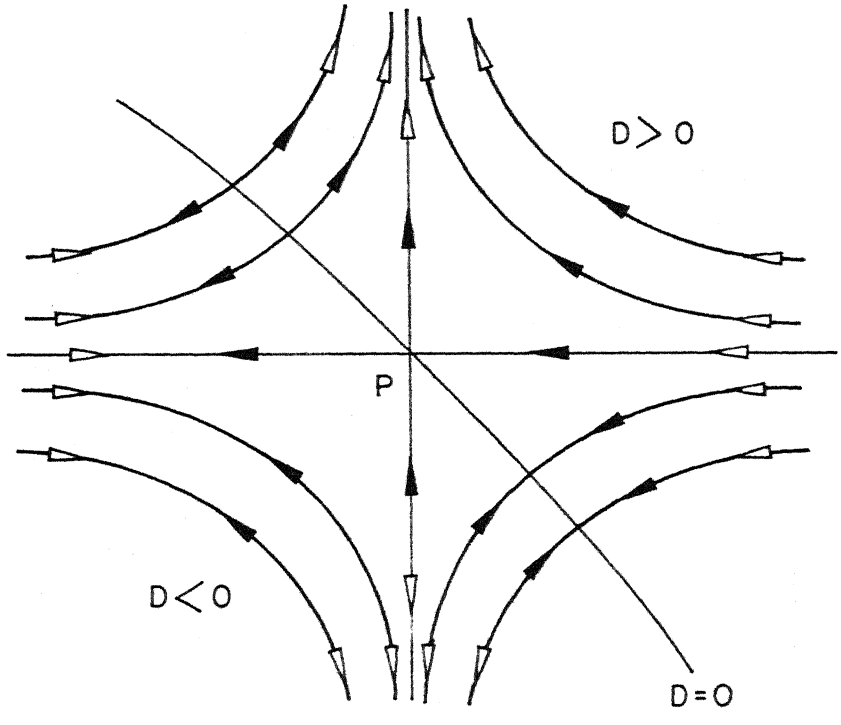

FIG 9 SCHEMATIC OF A SADDLE POINT SINGULARITY IN PHASE PLANE WITH D=0

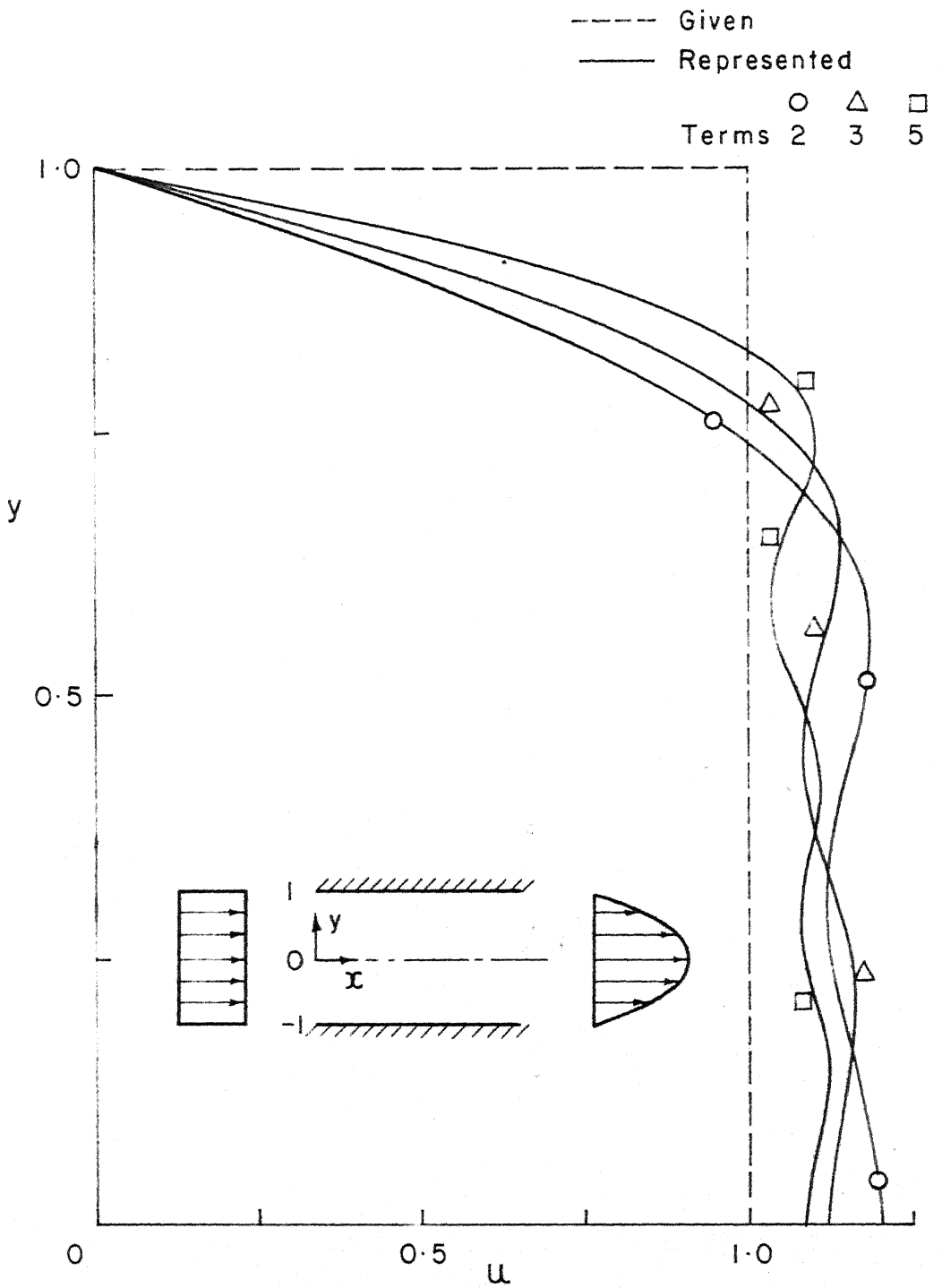

FIG. 10 REPRESENTATION OF THE INITIAL PROFILE FOR ENTRY FLOW

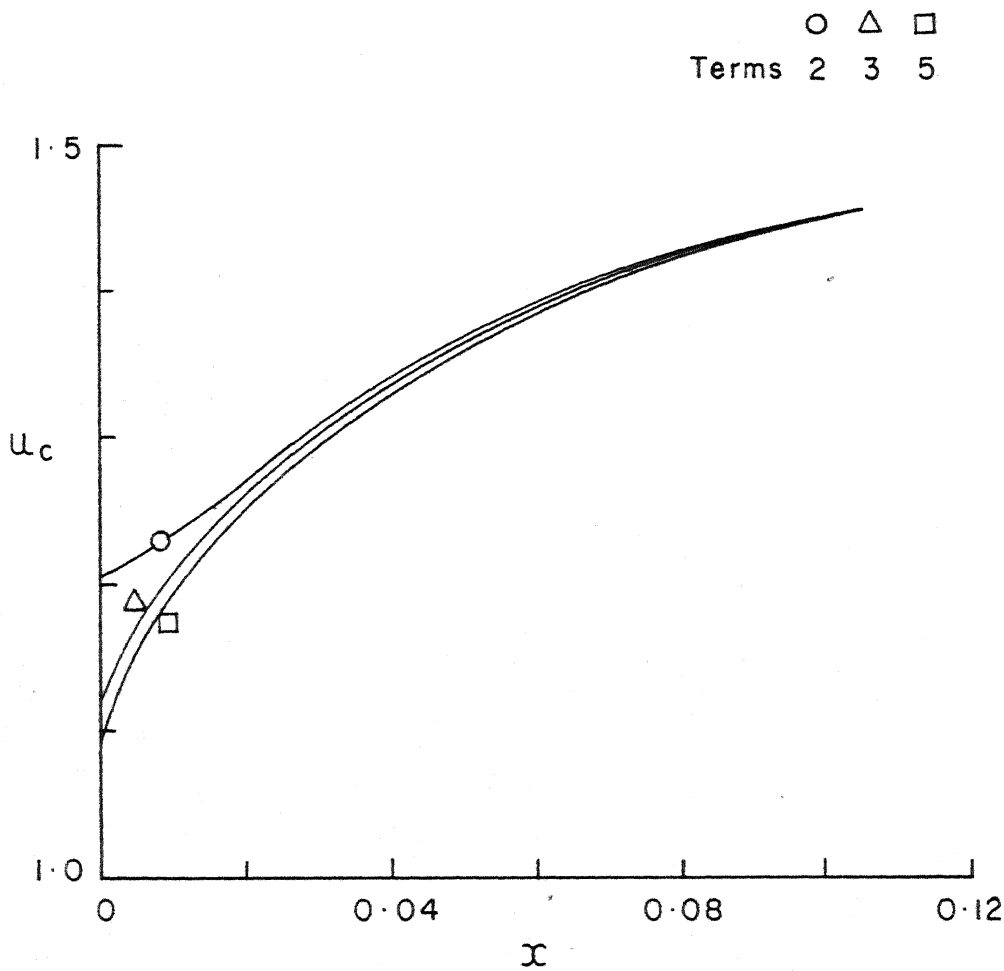

FIG. 11 CENTRELINE VELOCITY DISTRIBUTION FOR ENTRY FLOW

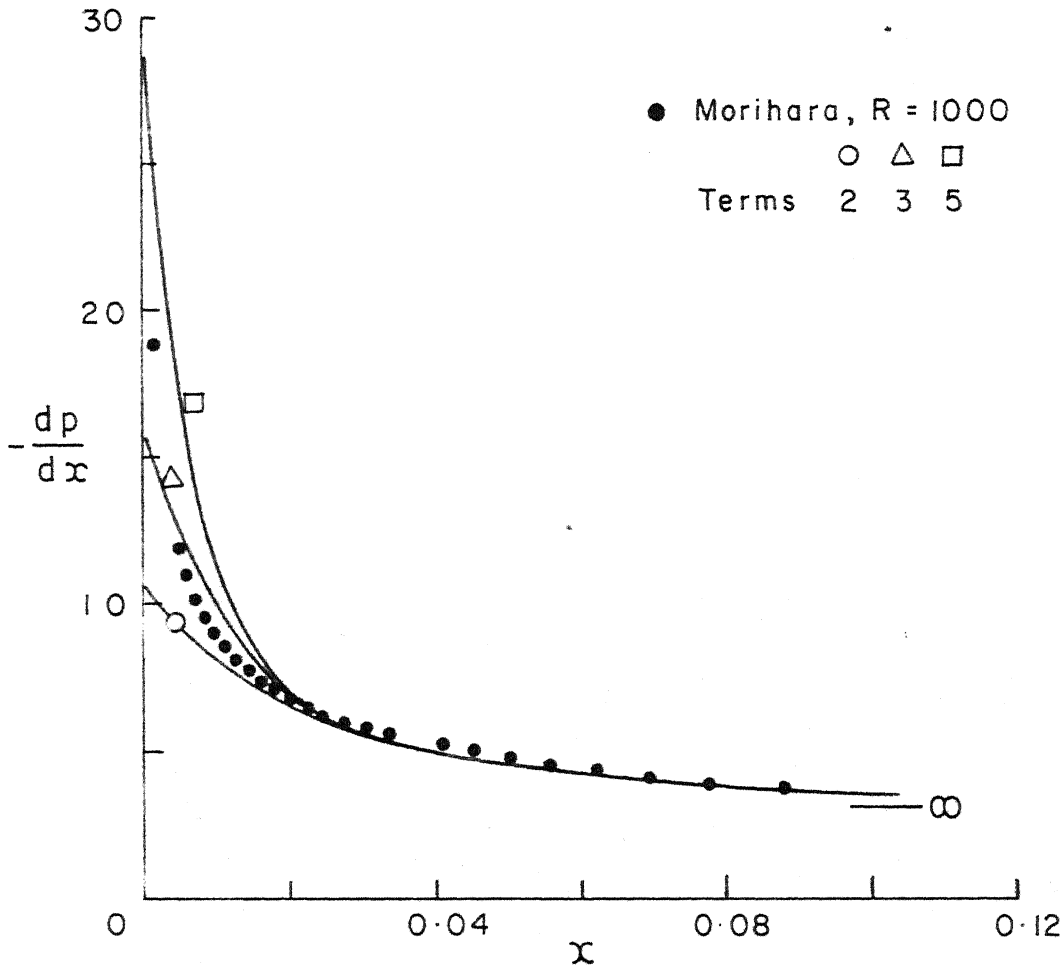

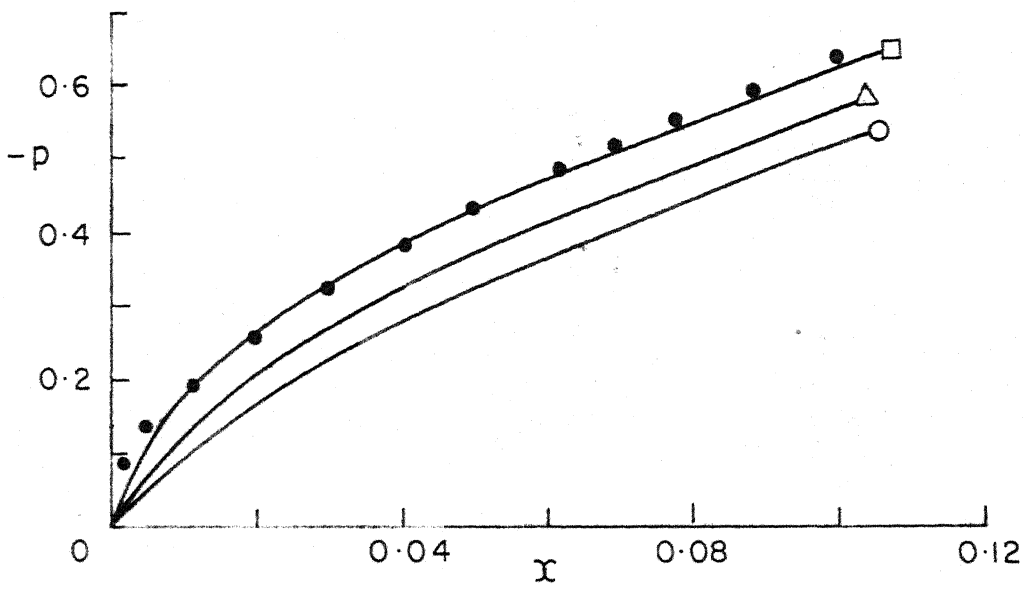

FIG. 12 PRESSURE GRADIENT & PRESSURE

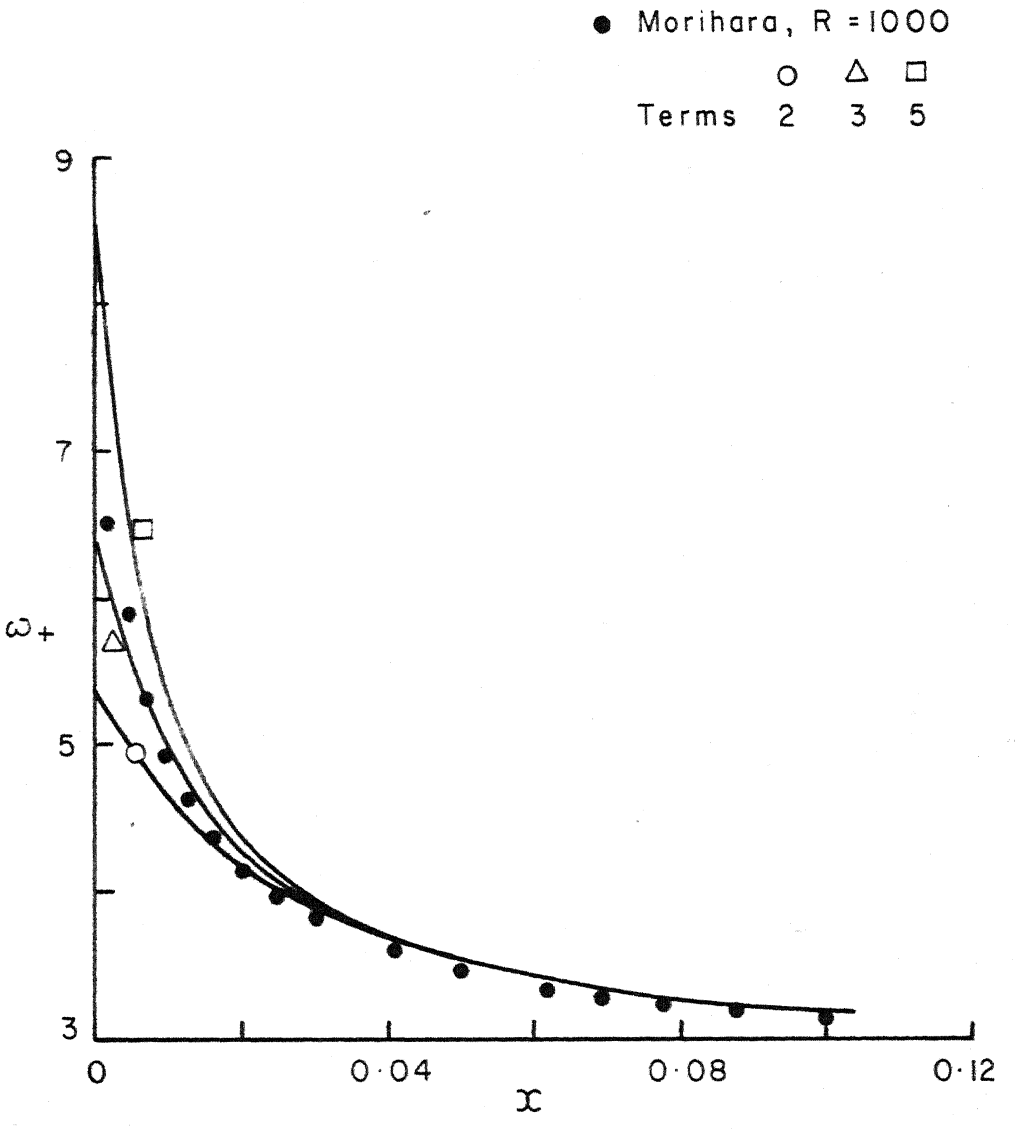

FIG. 13 WALL - VORTICITY FOR ENTRY FLOW

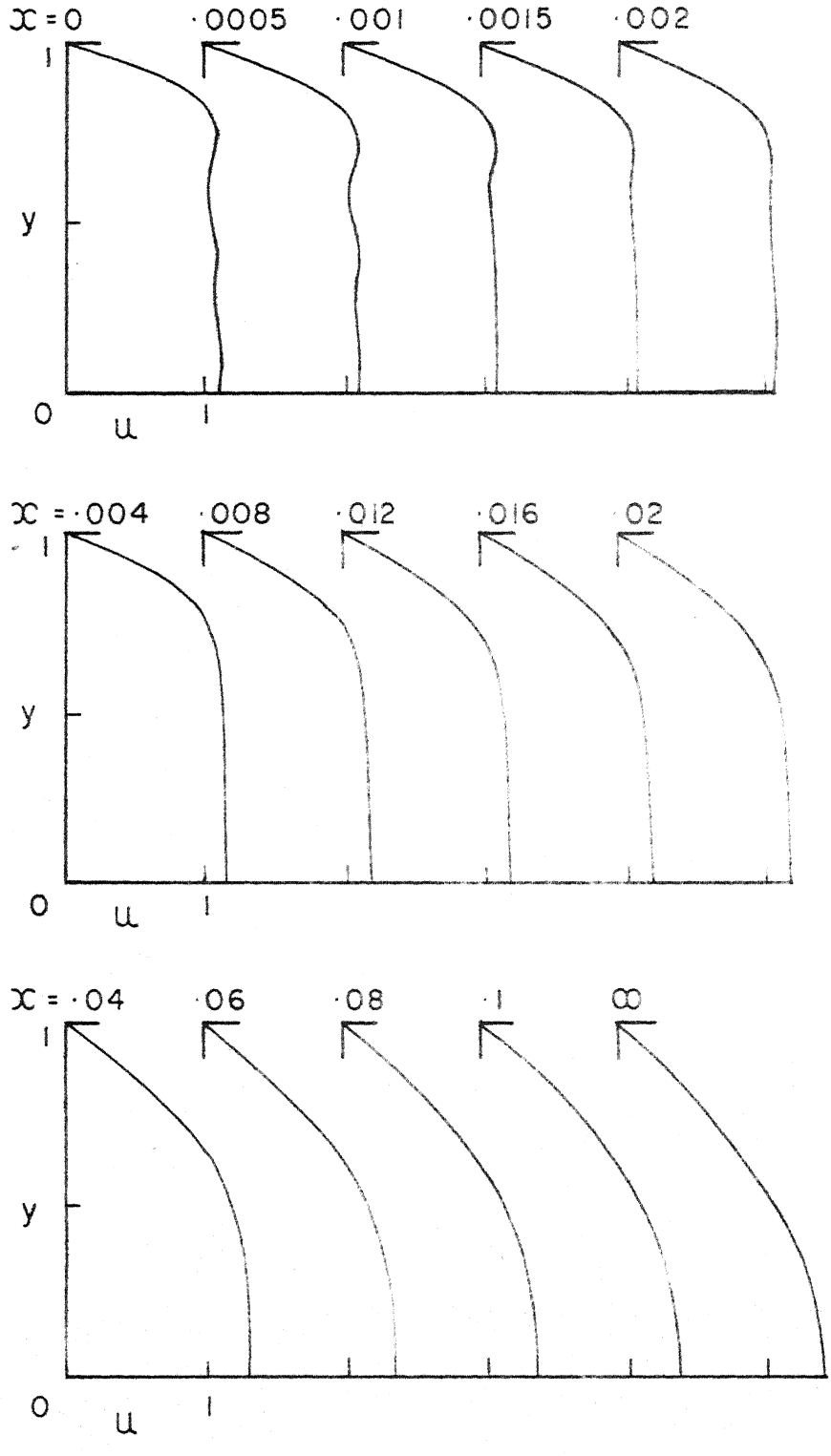

FIG. 14 FLOW DEVELOPMENT

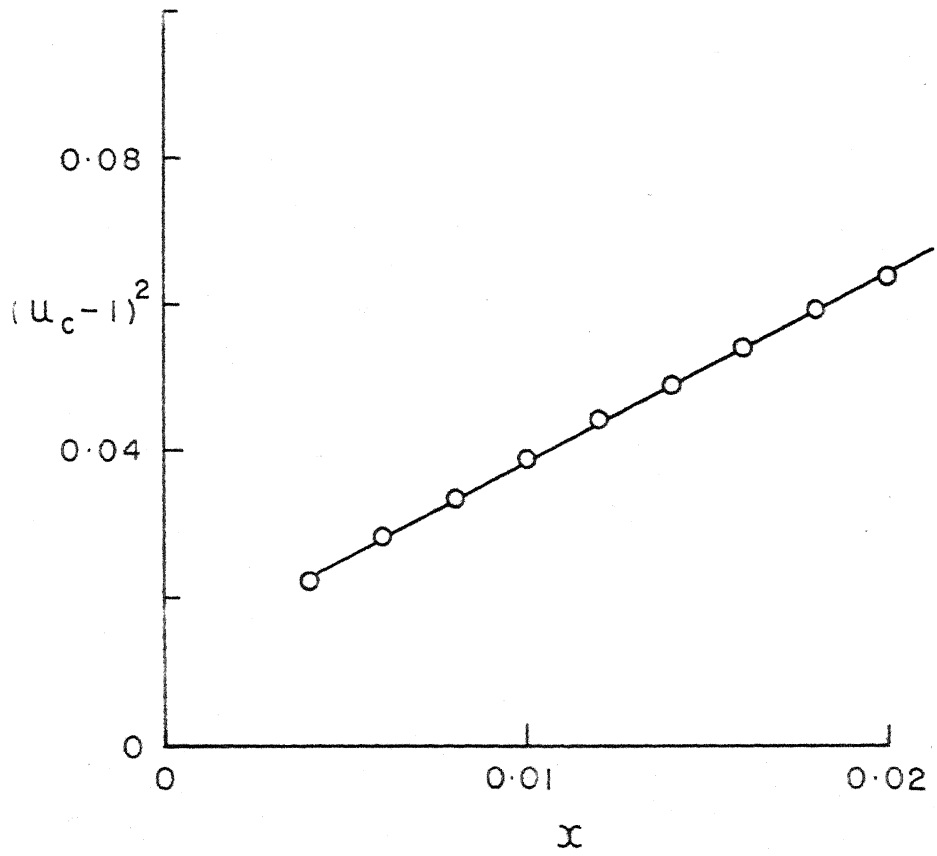

FIG. 15 $(u_c-1)^2$ IN AN INTERMEDIATE RANGE OF x

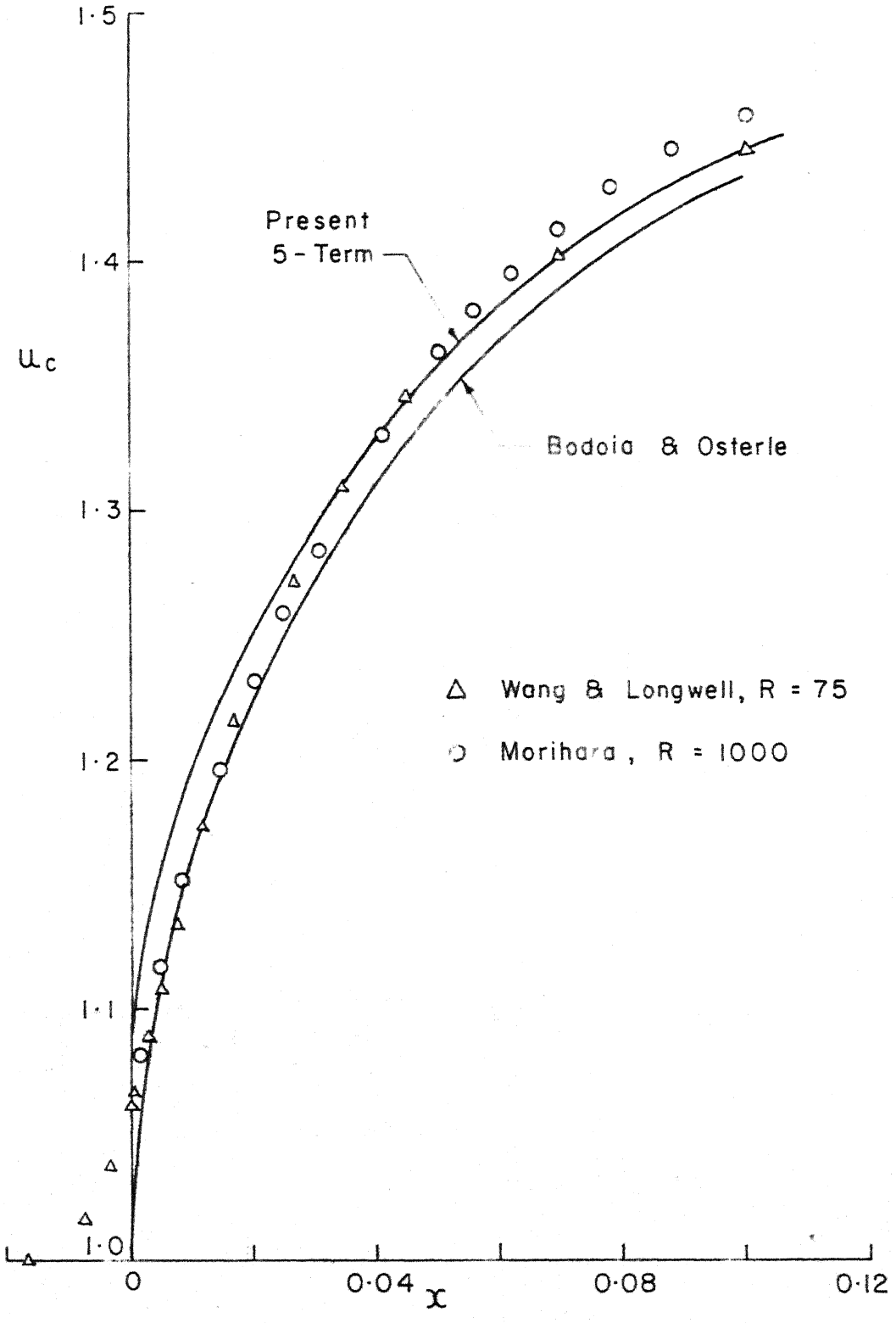

FIG. 16 CENTRELINE VELOCITY DISTRIBUTION

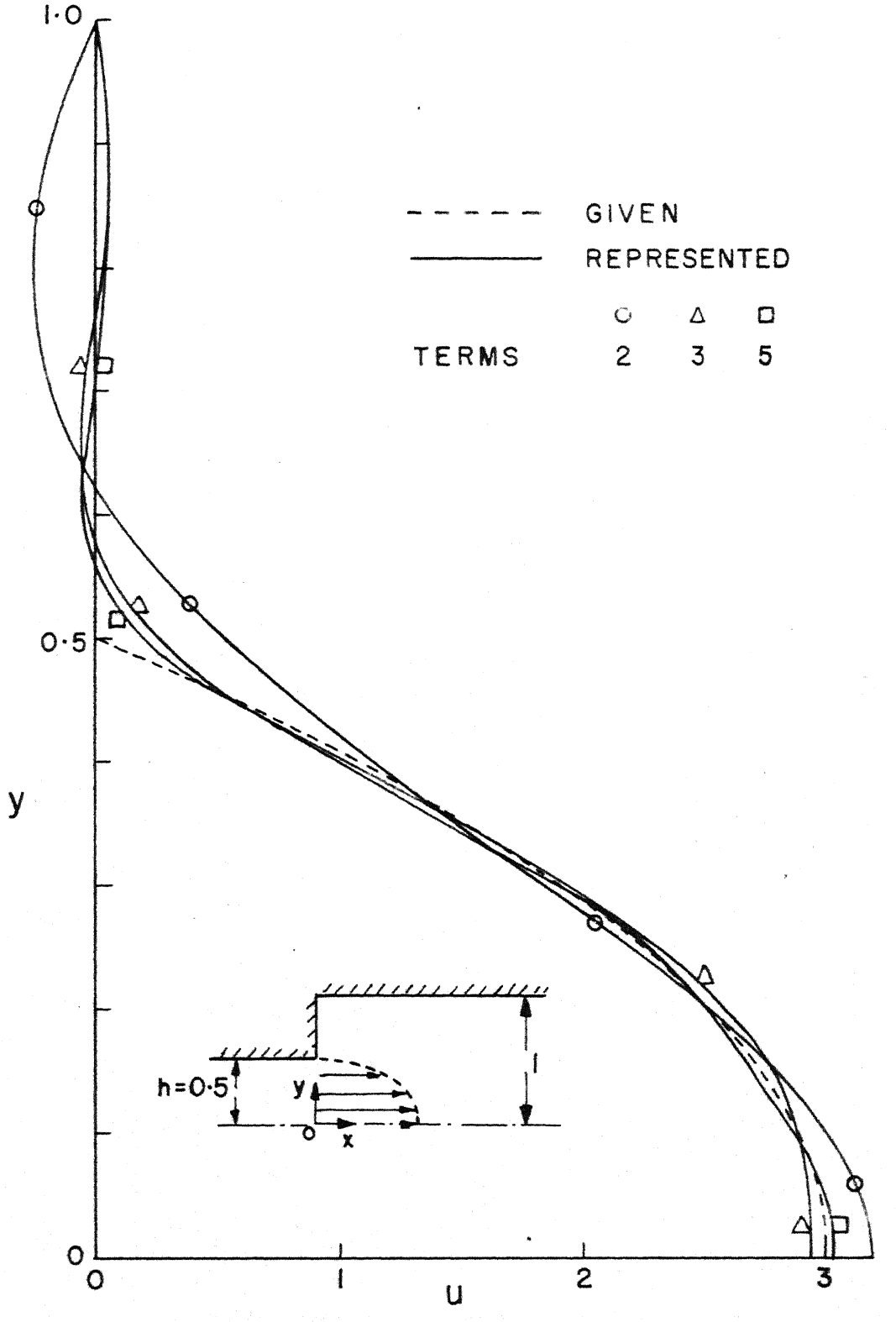

FIG·17 REPRESENTATION OF THE ENTRY ONDITION FOR SYMMETRIC SUDDEN EXPANSION

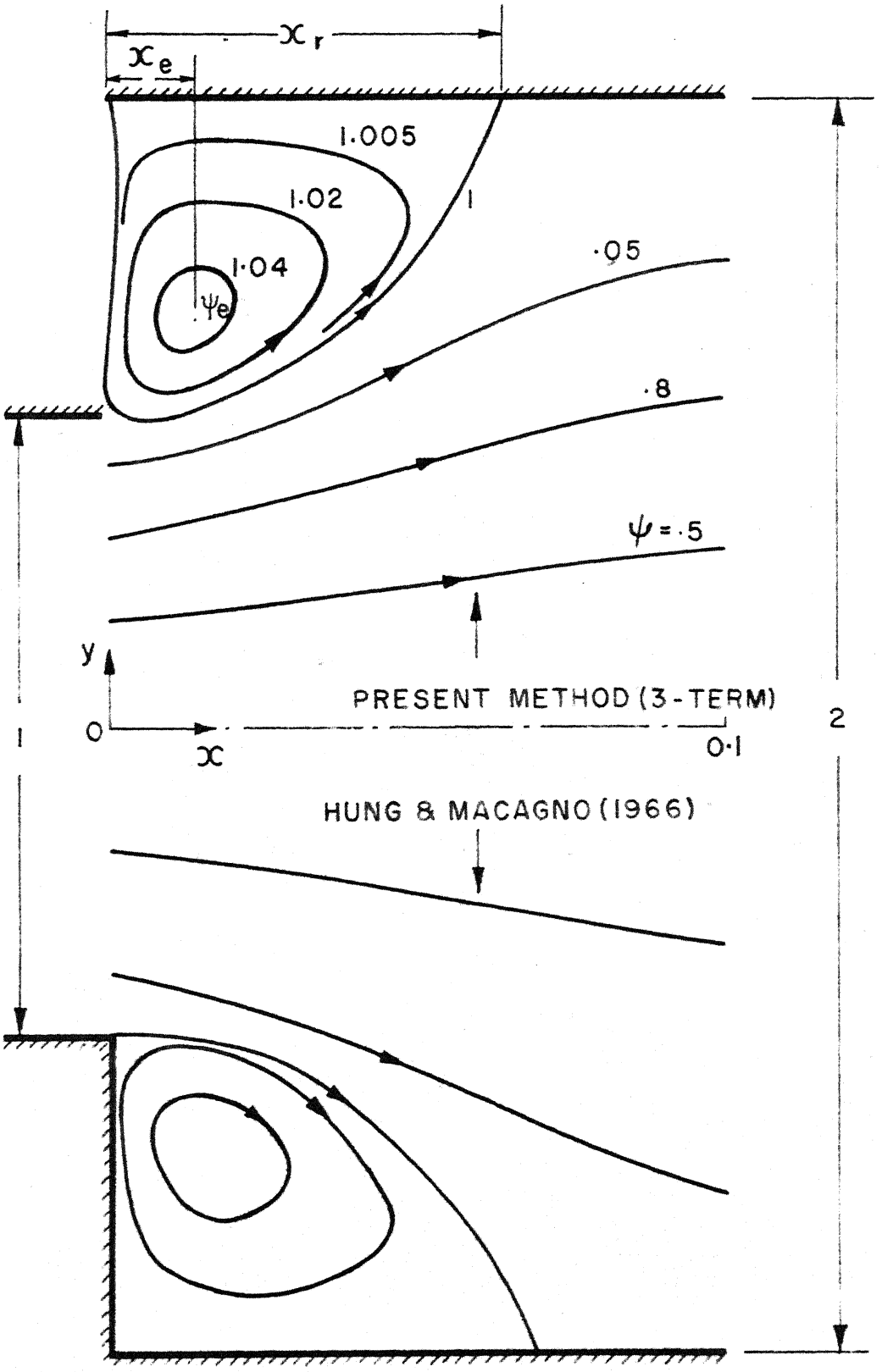

FIG. 18 STREAMLINES FOR SYMMETRIC SUDDEN EXPANSION

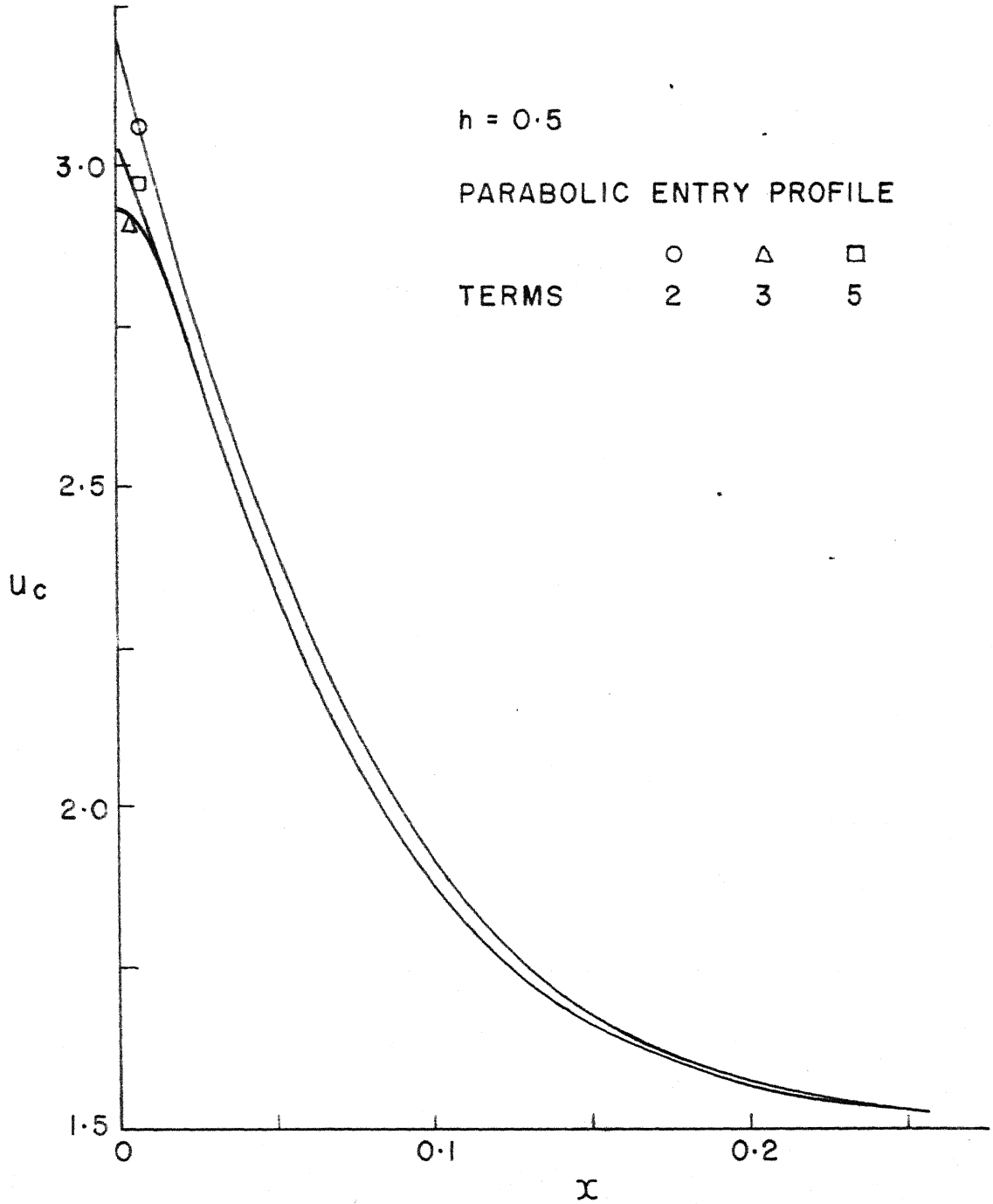

FIG·19 CENTRELINE VELOCITY DISTRIBUTION FOR SYMMETRIC SUDDEN EXPANSION

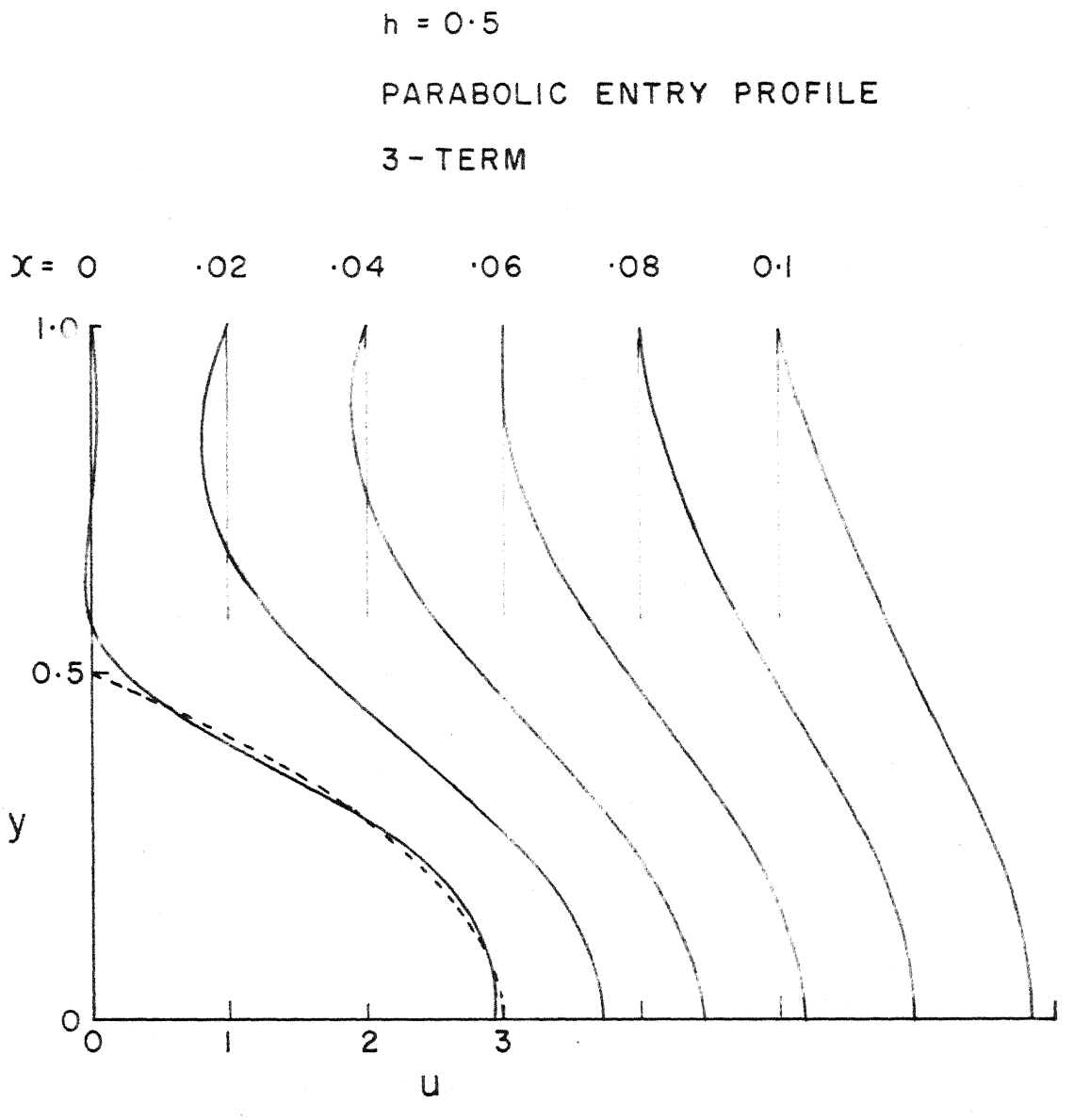

FIG.20 FLOW DEVELOPMENT IN SYMMETRIC SUDDEN EXPANSION

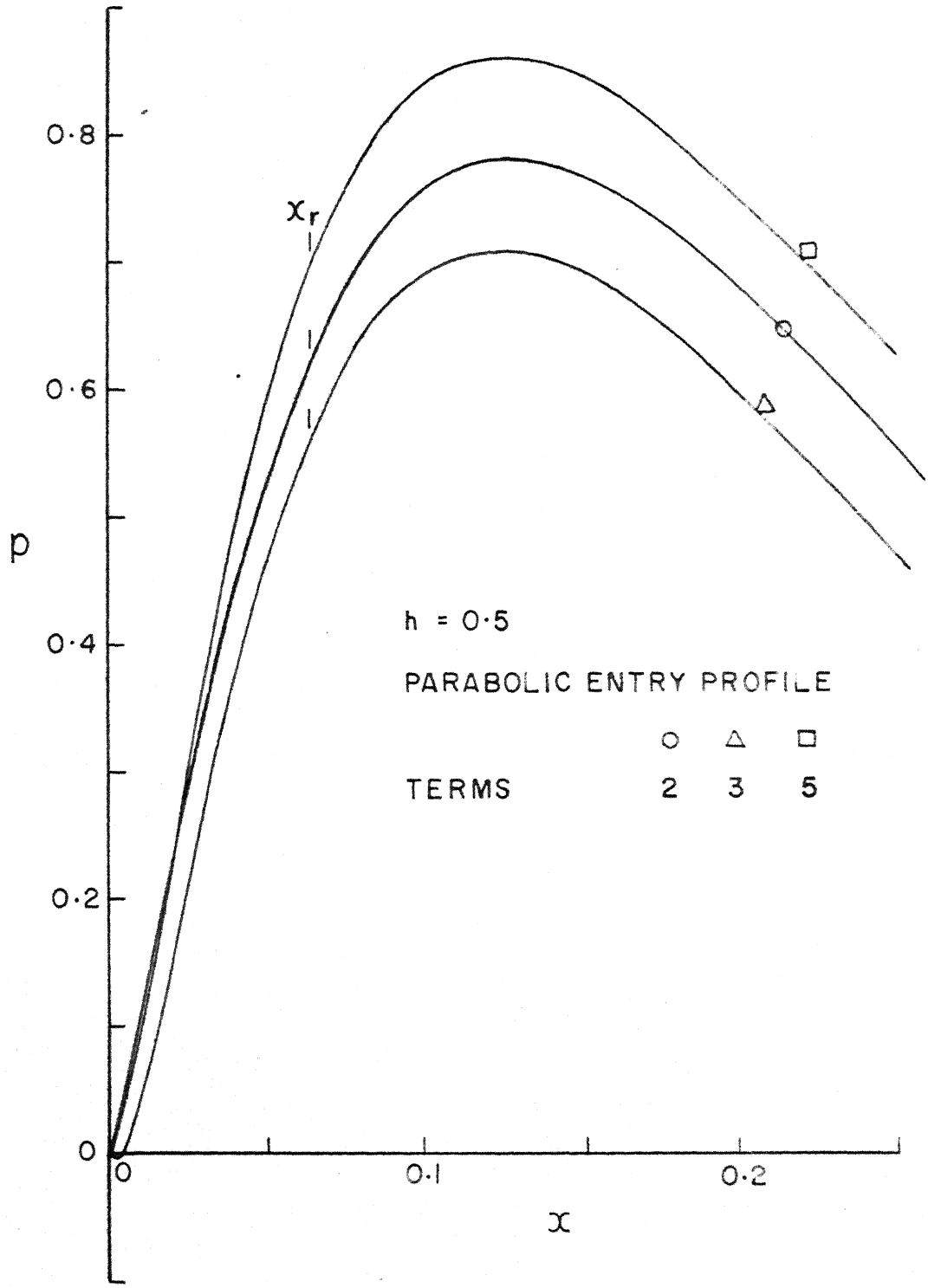

FIG·21 PRESSURE DISTRIBUTION FOR SYMMETRIC SUDDEN EXPANSION

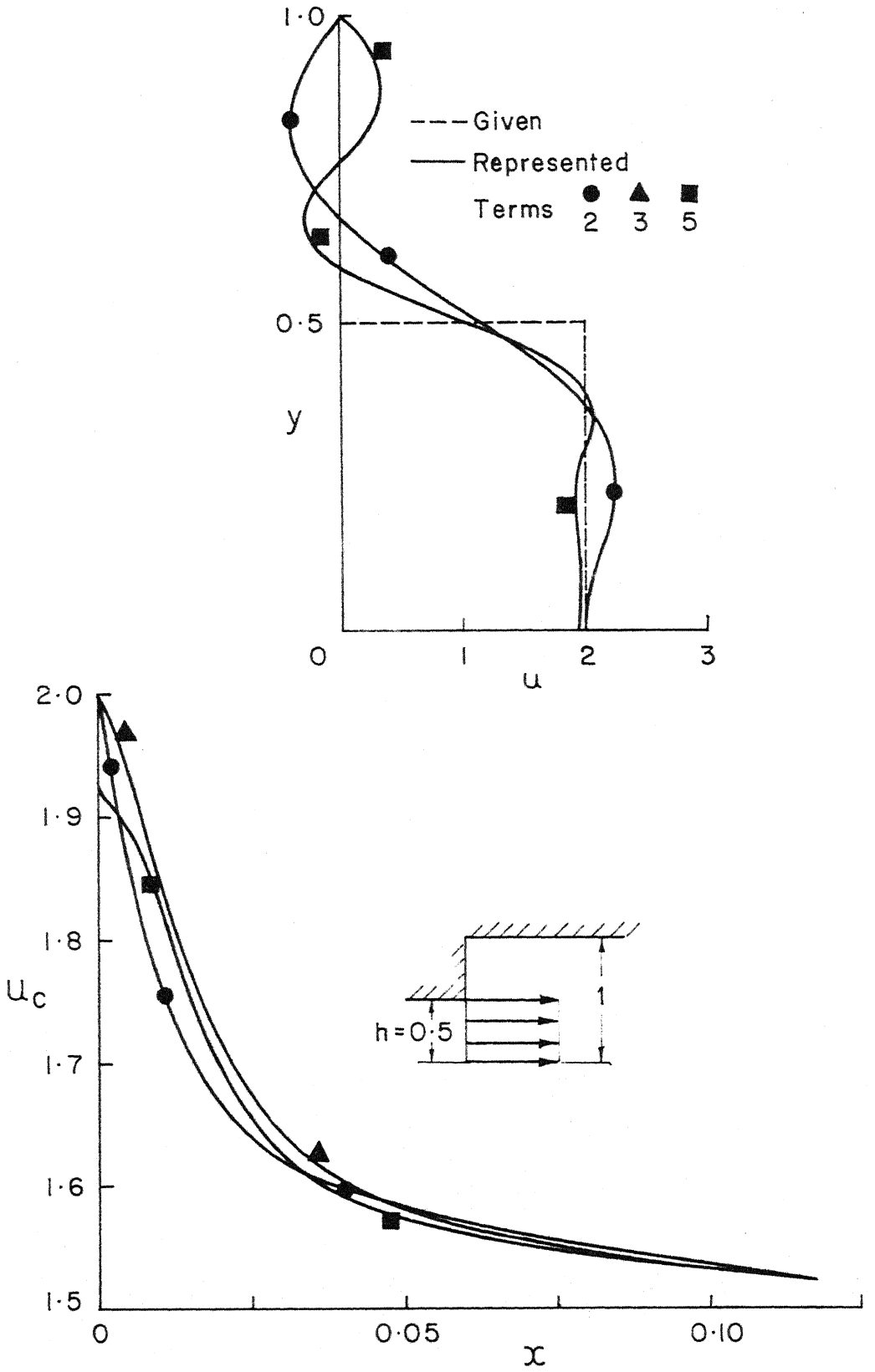

FIG 22 REPRESENTATION OF THE ENTRY PROFILE, AND CENTRELINE VELOCITY DISTRIBUTION

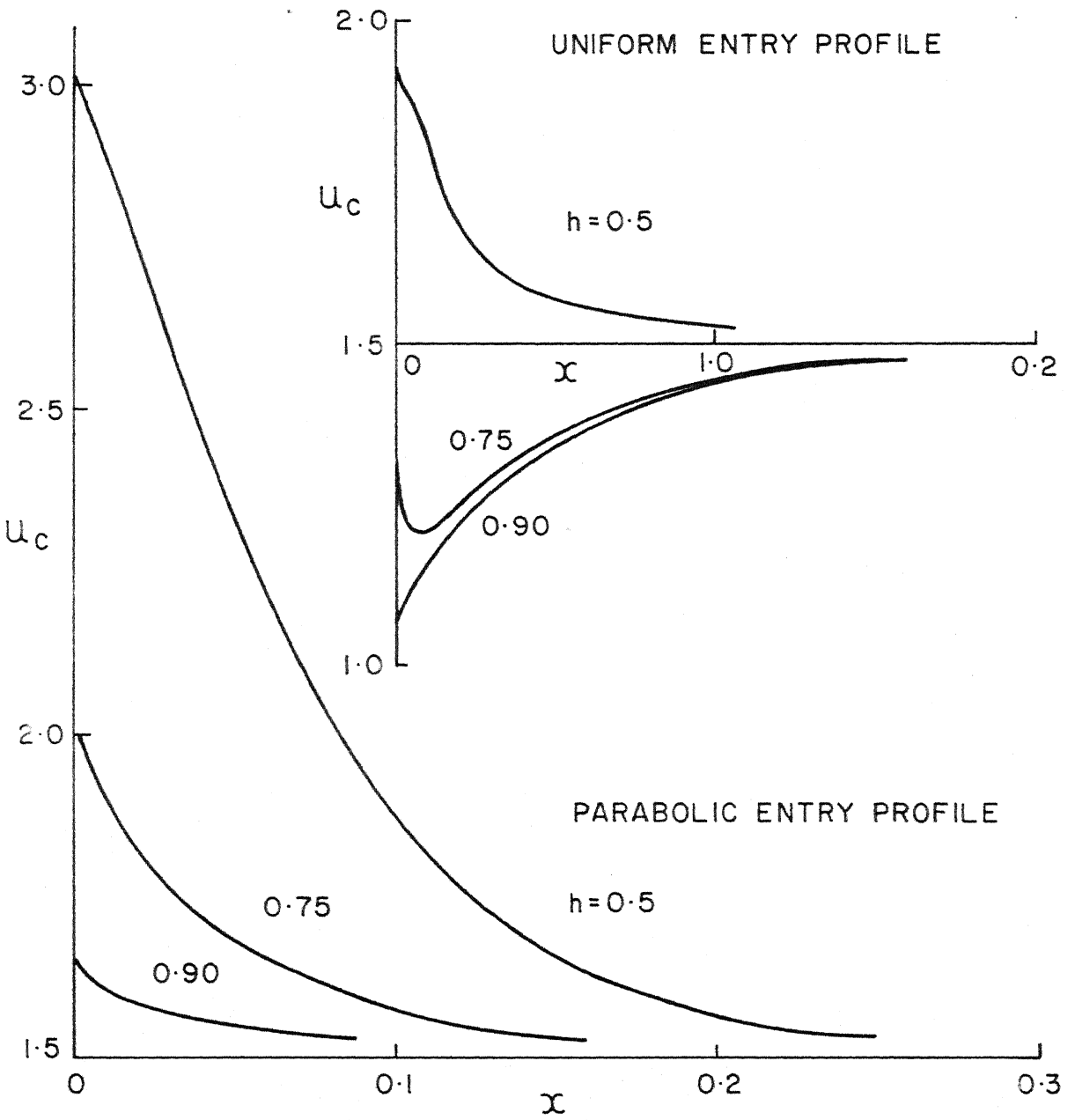

FIG. 23 CENTRELINE VELOCITY DISTRIBUTION FOR SYMMETRIC SUDDEN EXPANSION

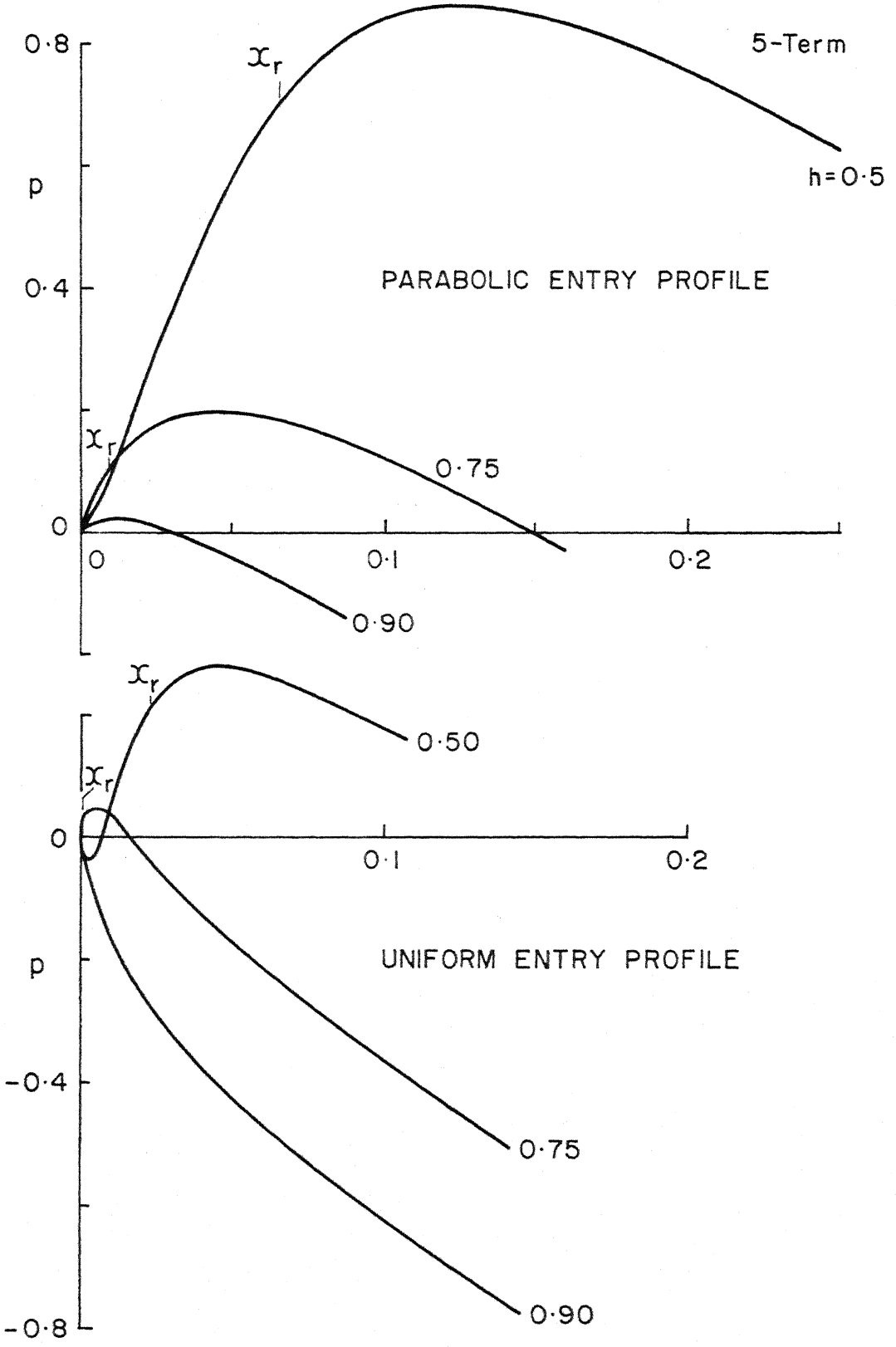

FIG. 24 PRESSURE DISTRIBUTION

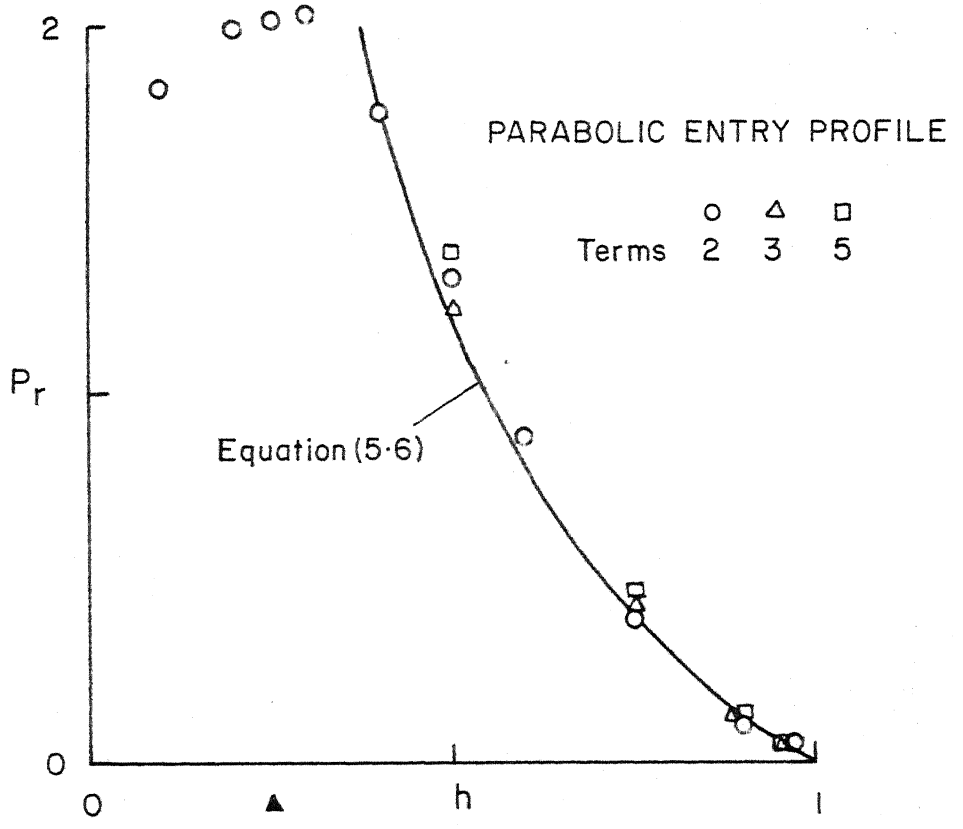

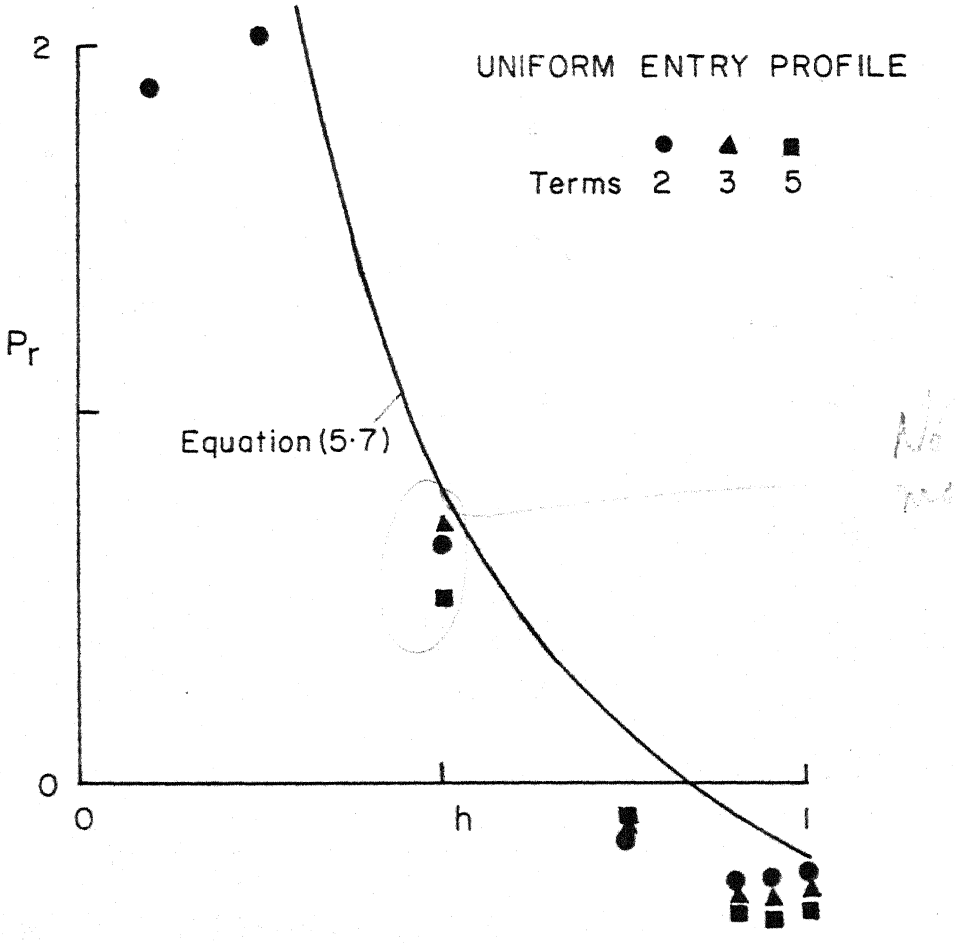

FIG. 25 PRESSURE RECOVERY COEFFICIENT

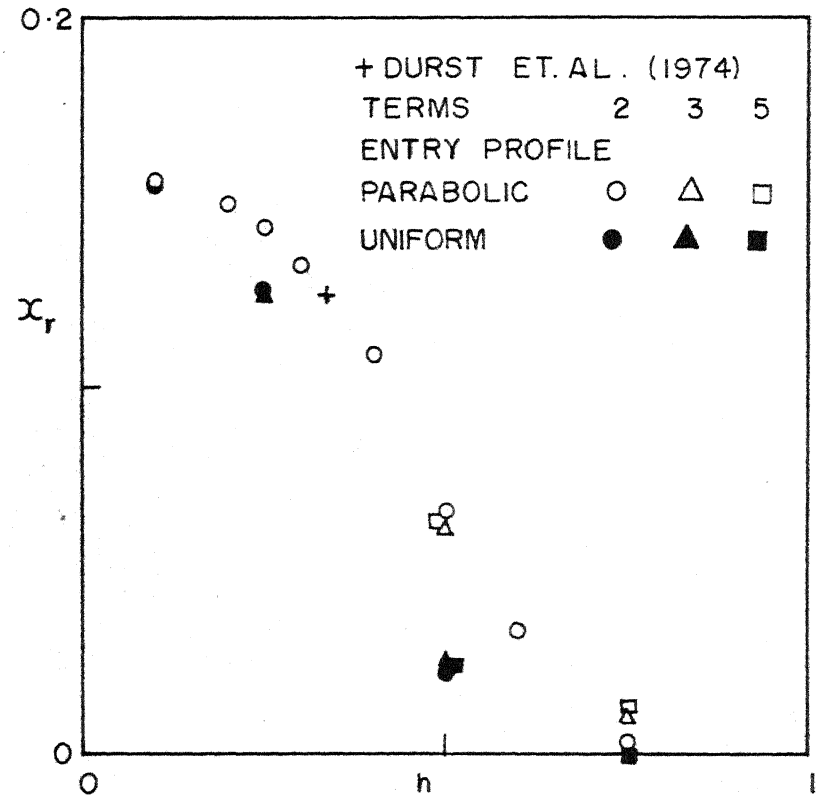

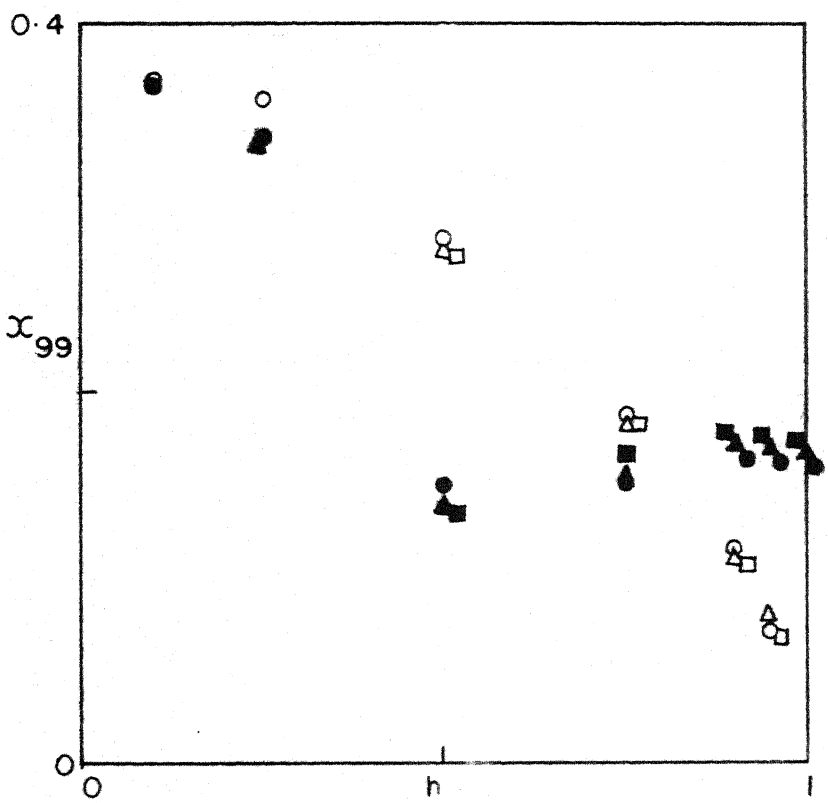

FIG. 26 REATTACHMENT AND DEVELOPMENT LENGTHS

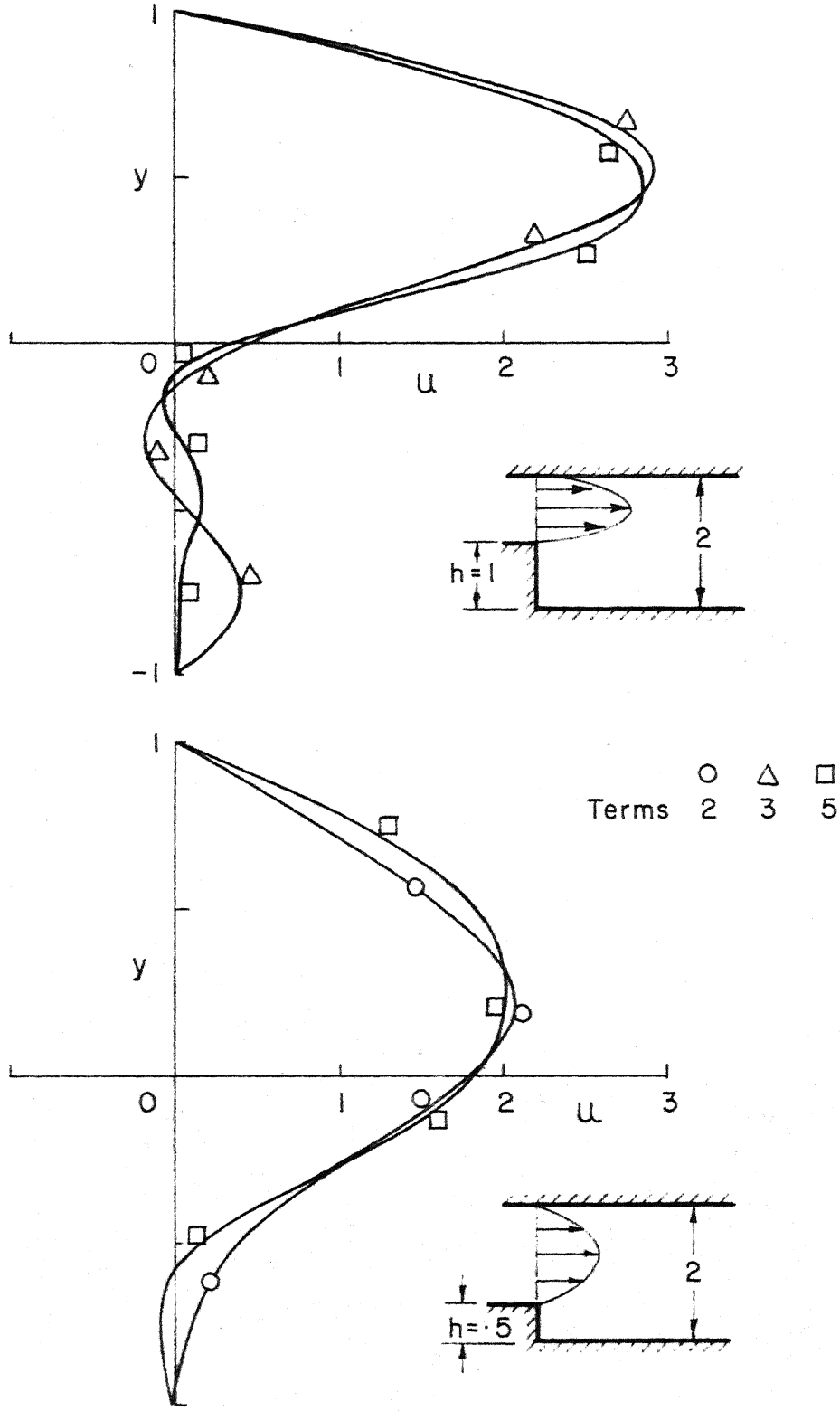

FIG. 27 REPRESENTATION OF THE ENTRY PROFILE

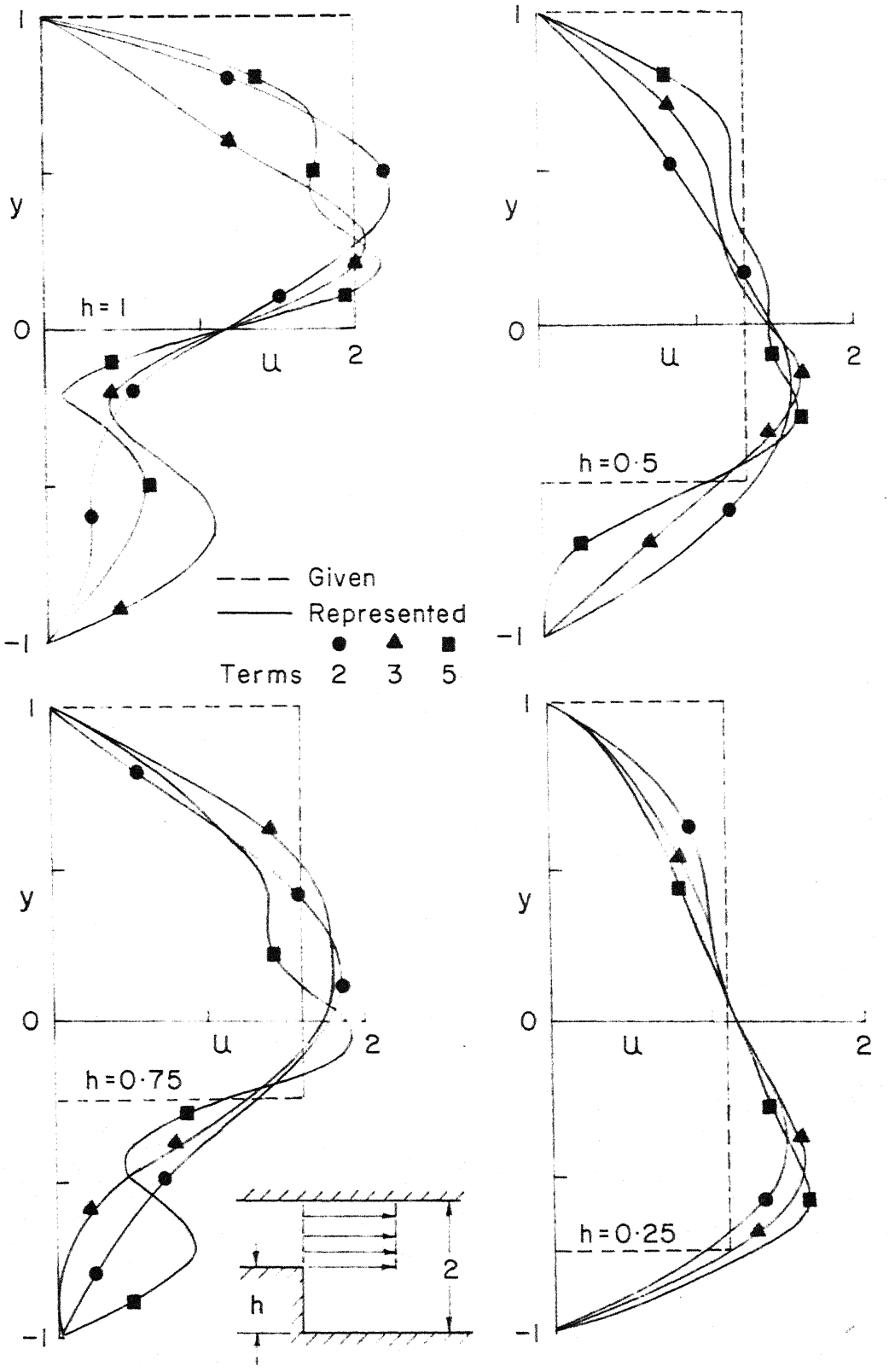

FIG. 28 REPRESENTATION OF THE ENTRY PROFILE

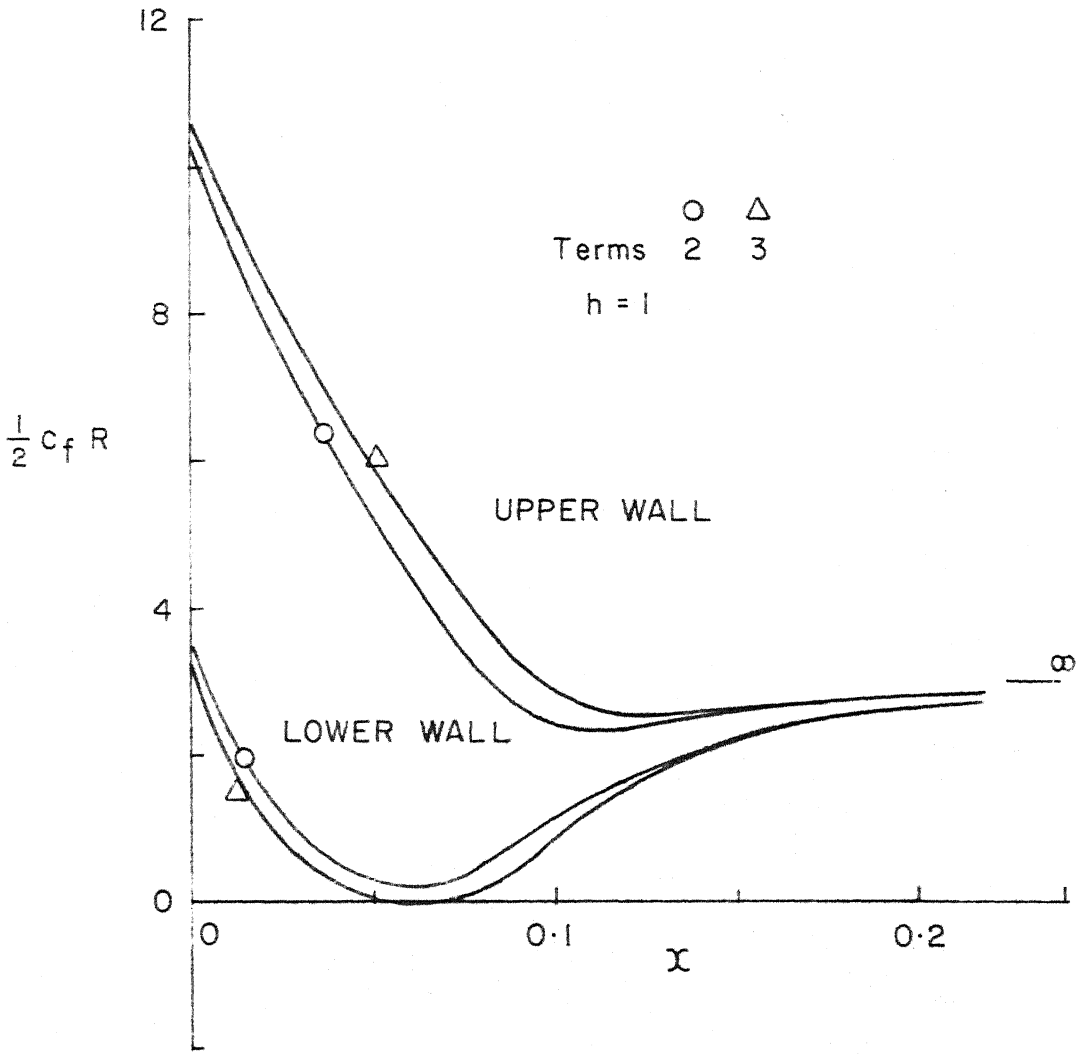

FIG. 29 SKIN FRICTION FOR ASYMMETRIC SUDDEN EXPANSION

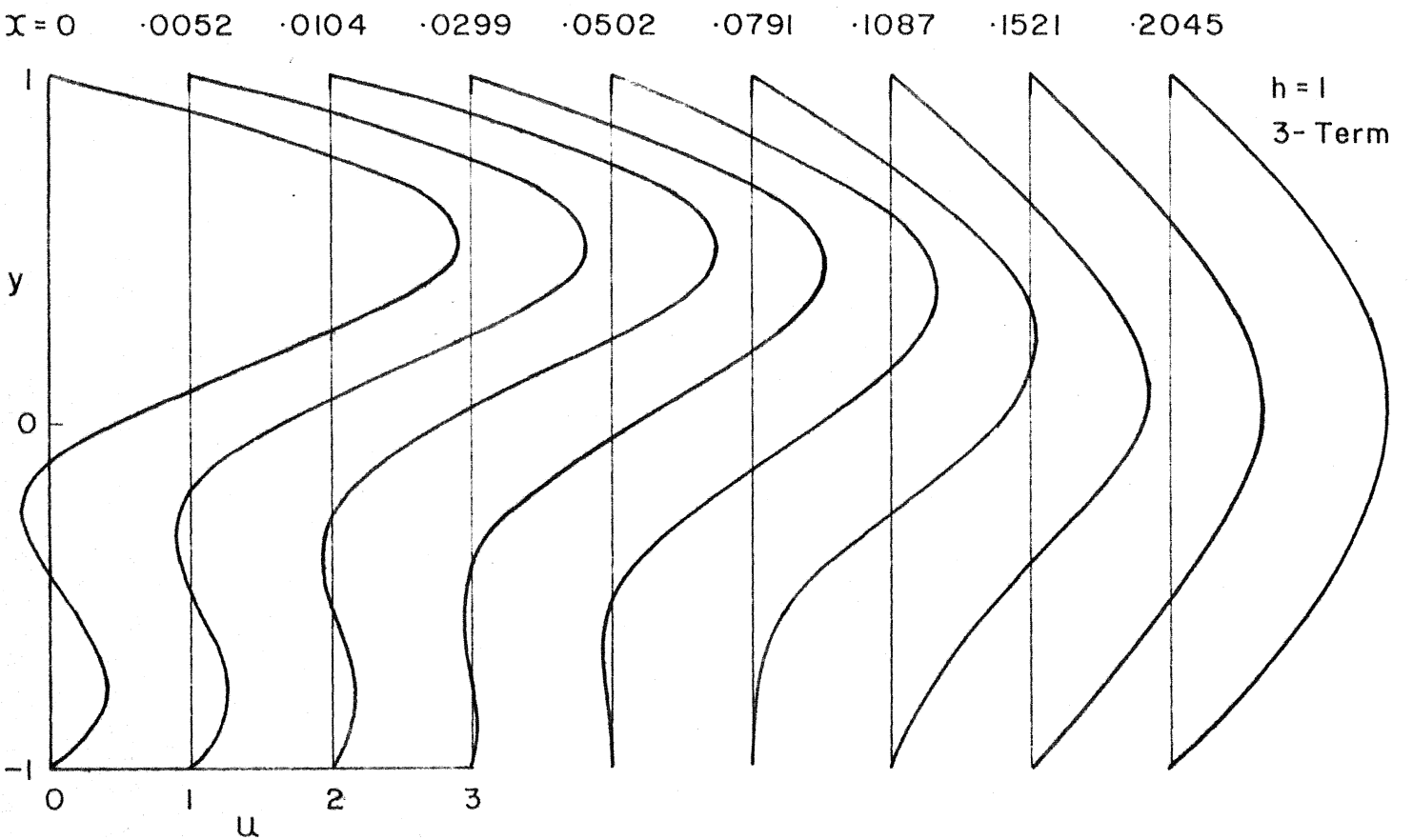

FIG. 30 FLOW DEVELOPMENT IN ASYMMETRIC SUDDEN EXPANSION

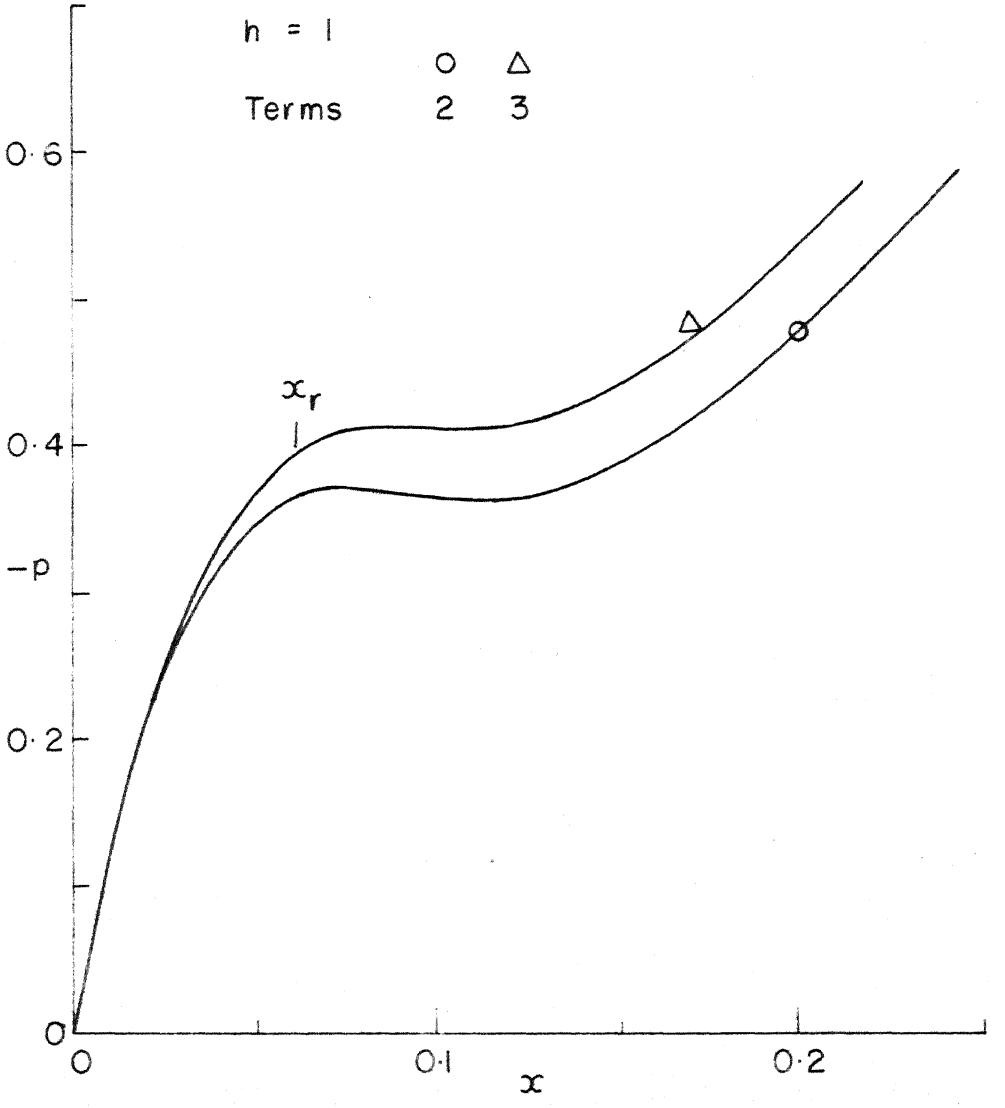

FIG. 31 PRESSURE DISTRIBUTION FOR ASYMMETRIC SUDDEN EXPANSION

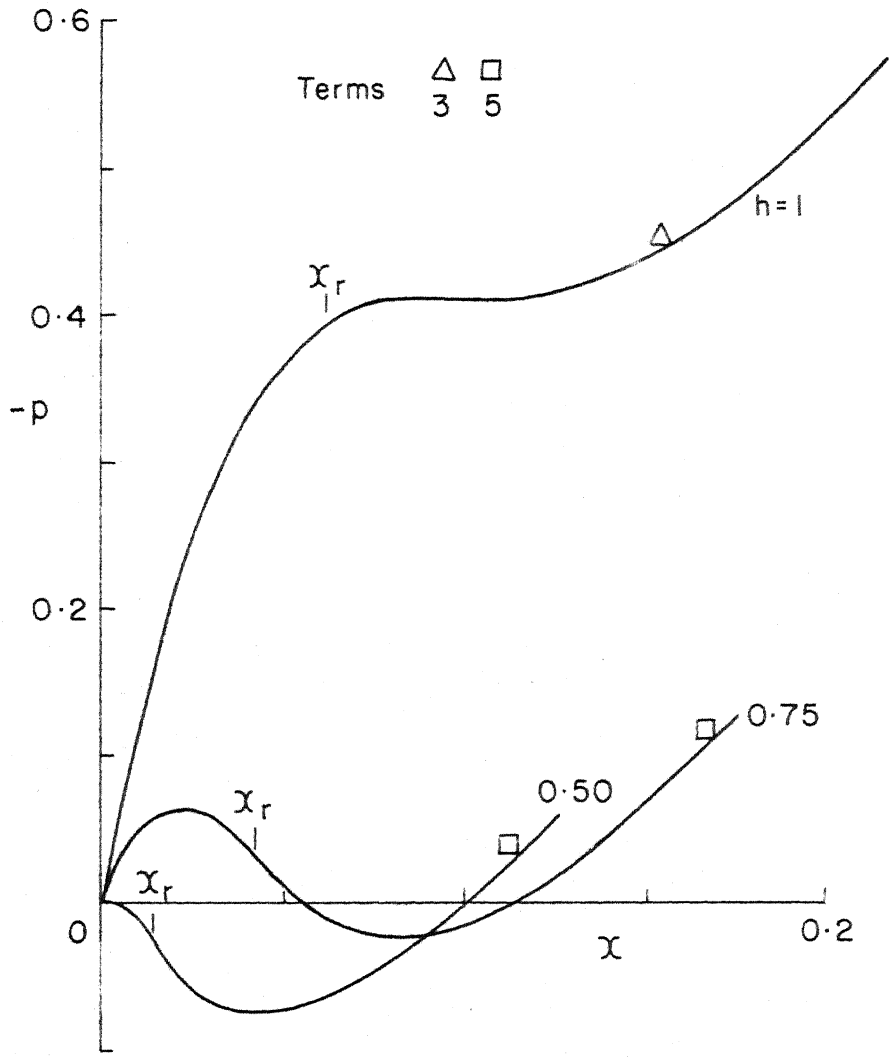

FIG. 32 PRESSURE DISTRIBUTION FOR ASYMMETRIC SUDDEN EXPANSION

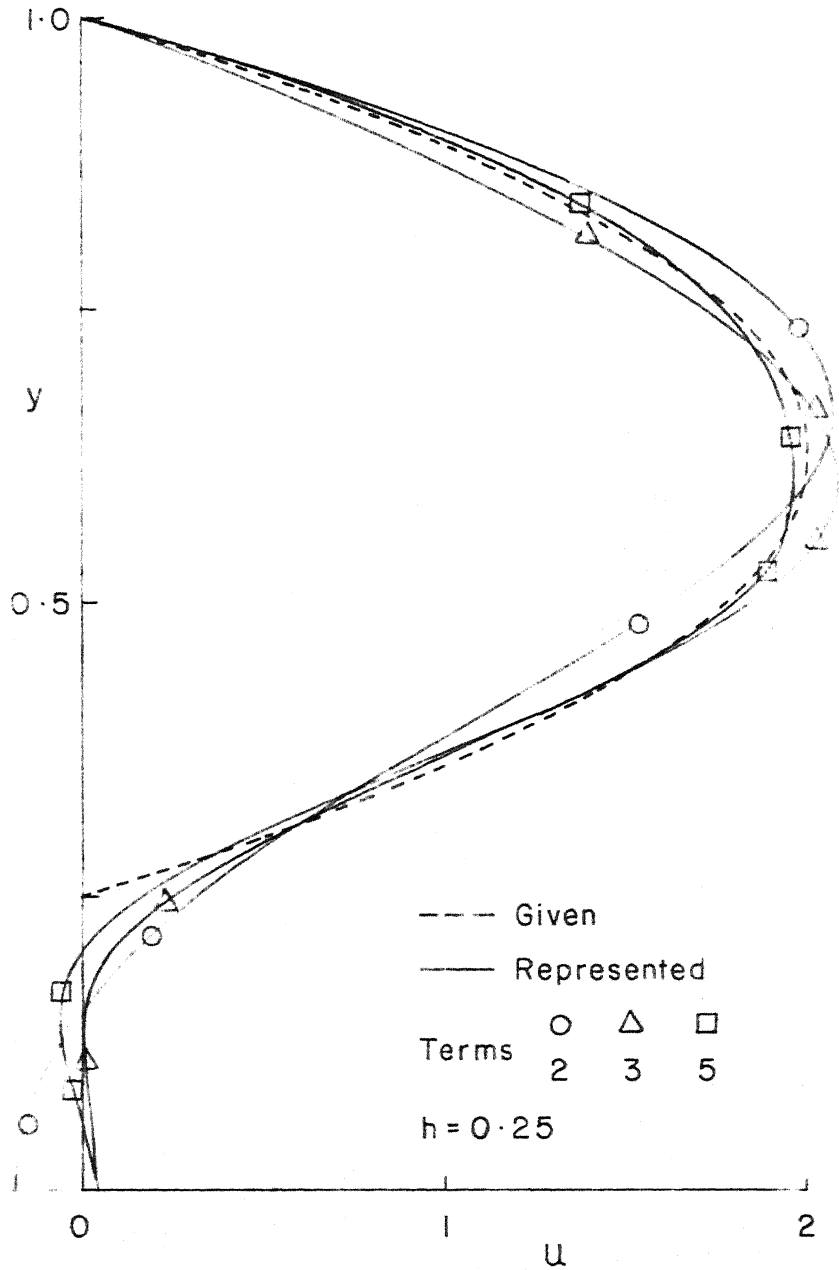

FIG. 33 REPRESENTATION OF THE ENTRY PROFILE FOR THE BASE IN A CHANNEL

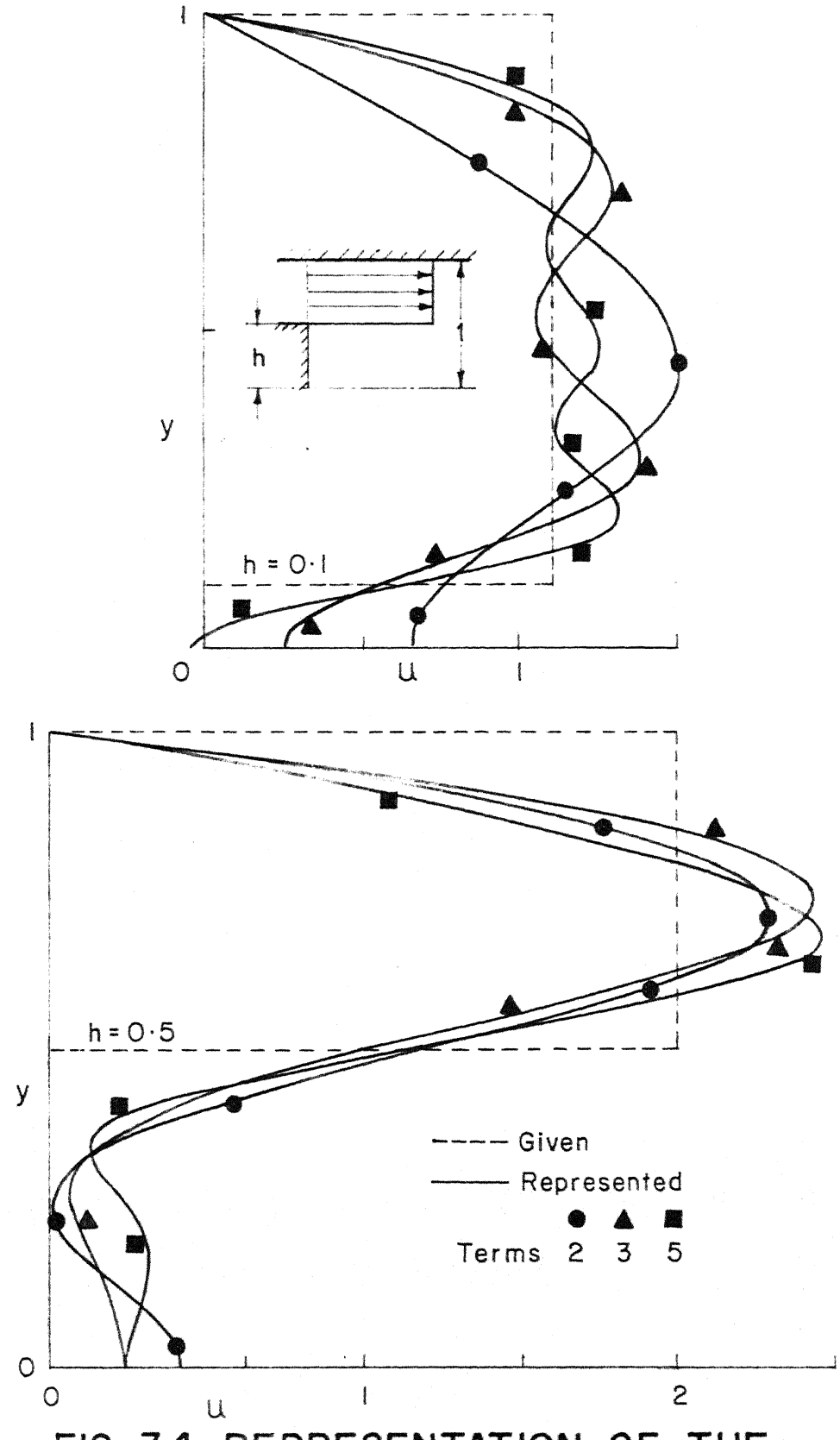

FIG. 34 REPRESENTATION OF THE ENTRY PROFILE

h = 0·25
PARABOLIC ENTRY PROFILE
5 – TERM

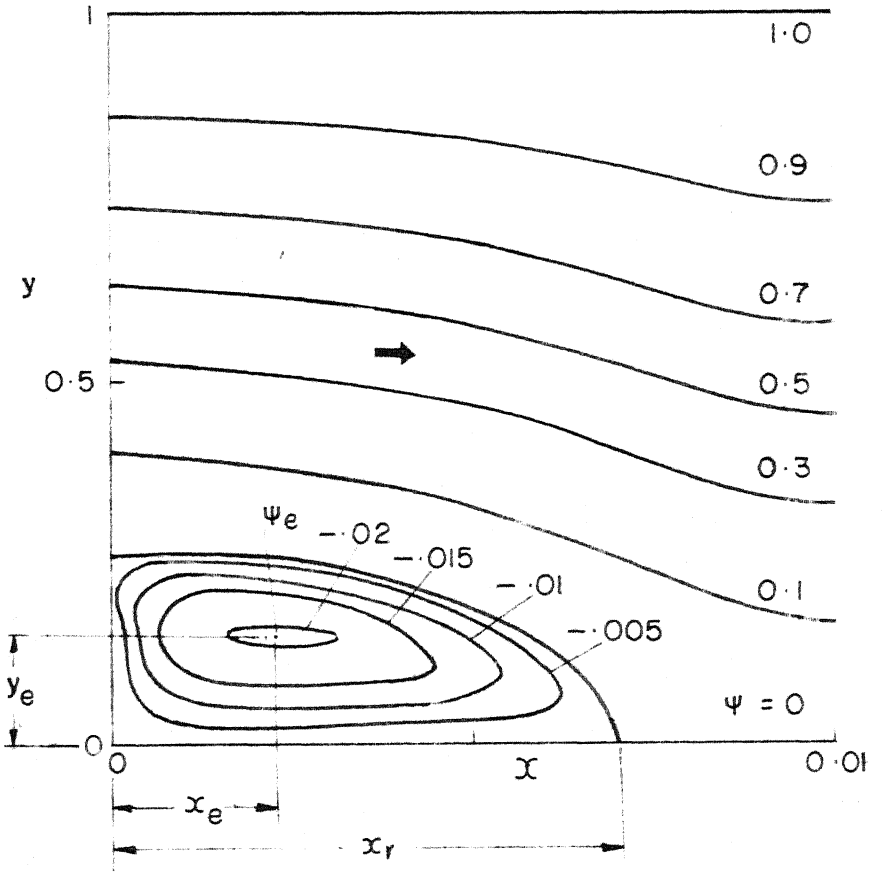

FIG. 35 STREAMLINES FOR THE BASE IN A CHANNEL

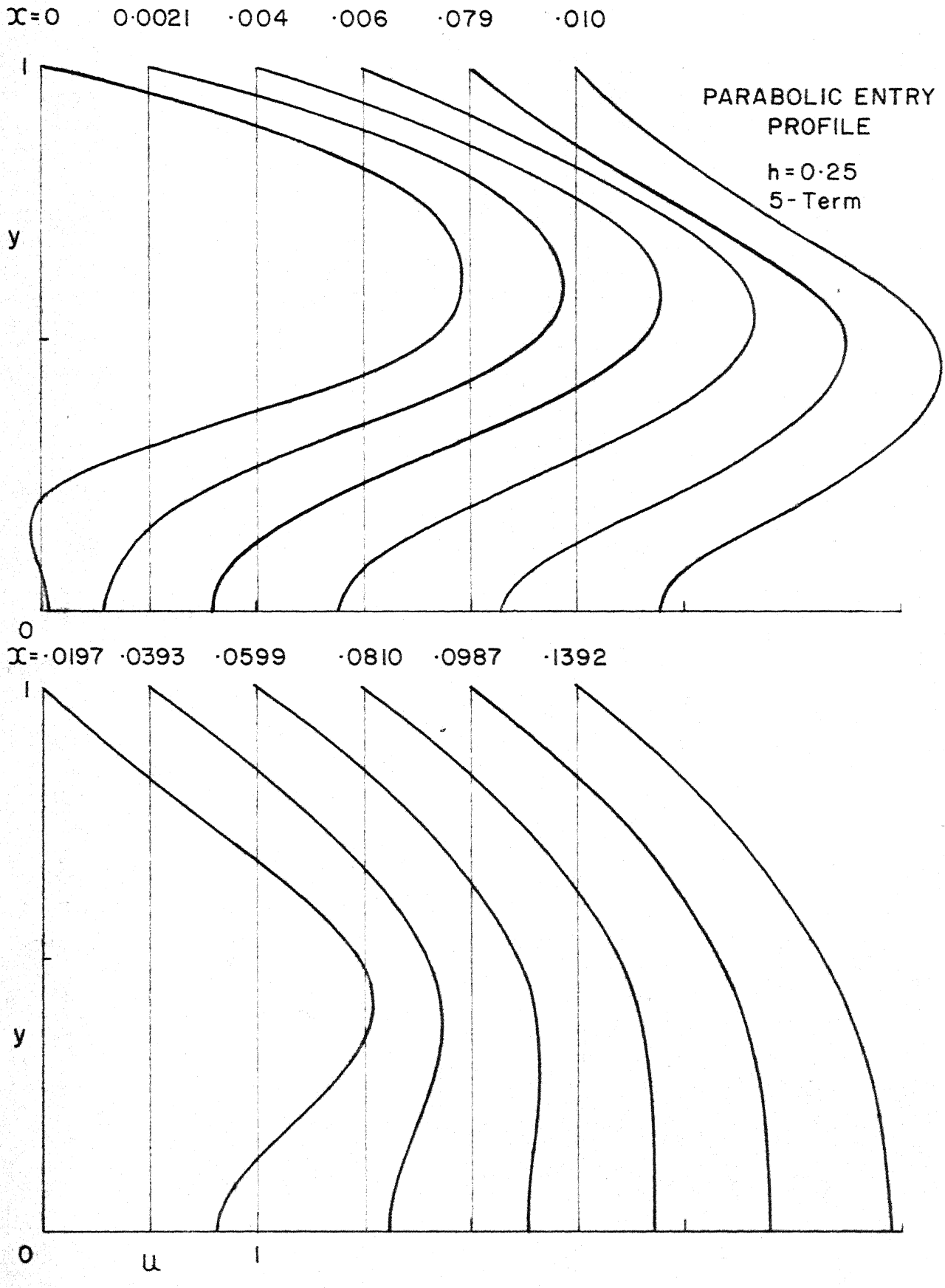

FIG. 36 FLOW DEVELOPMENT FOR THE BASE IN A CHANNEL

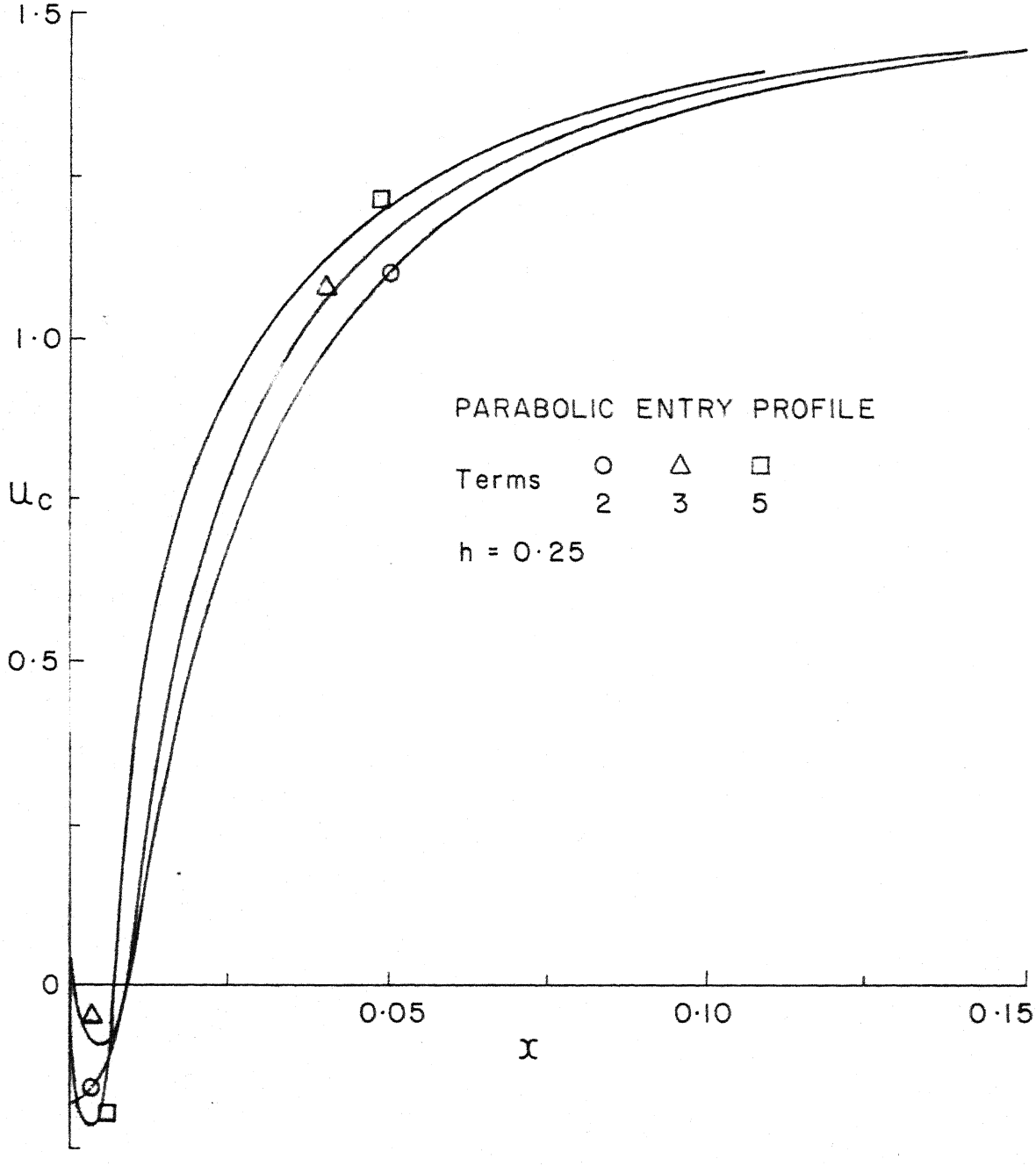

FIG. 37 CENTRELINE VELOCITY DISTRIBUTION FOR THE BASE IN A CHANNEL

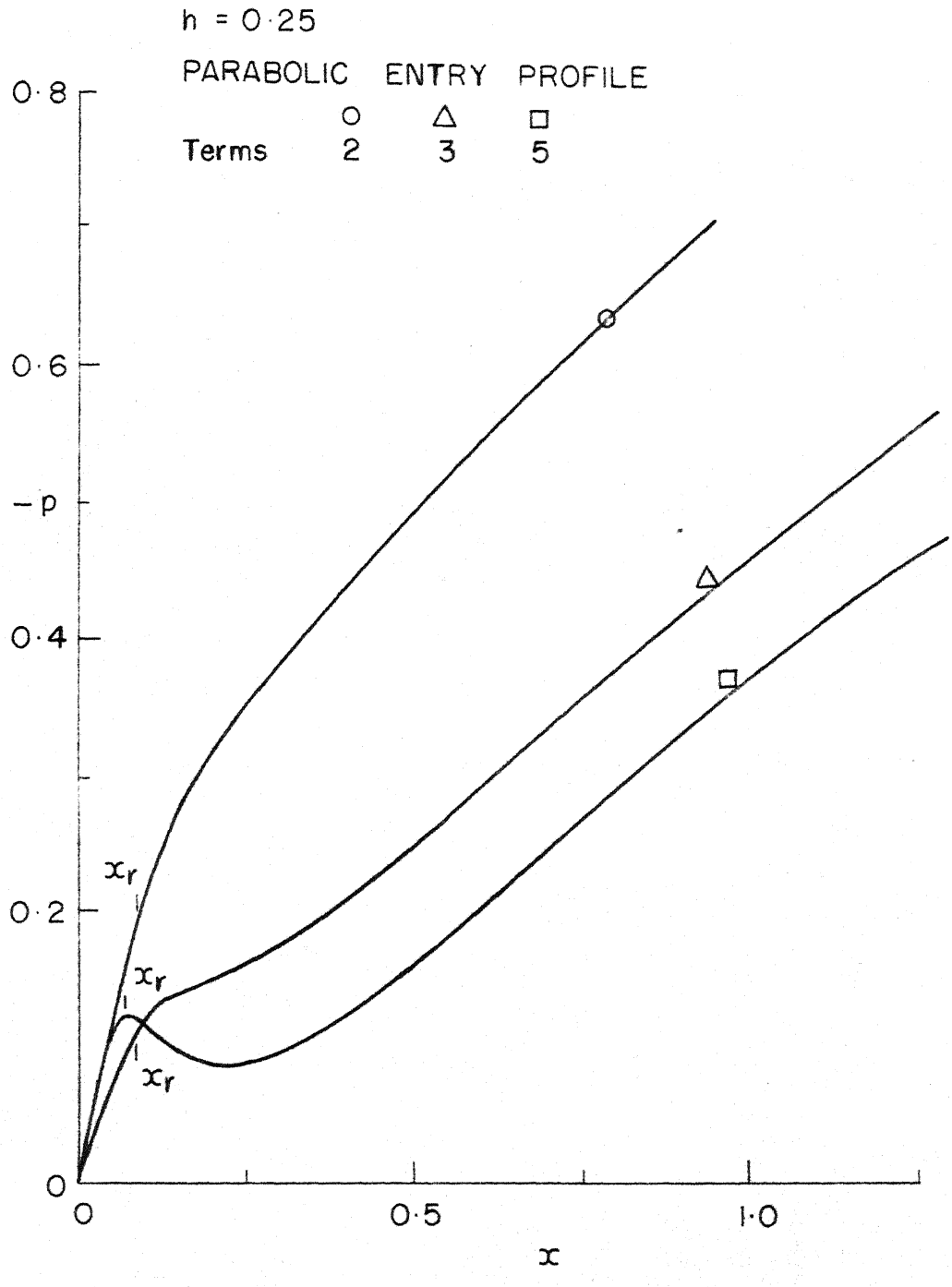

FIG. 38 PRESSURE DISTRIBUTION FOR THE BASE IN A CHANNEL

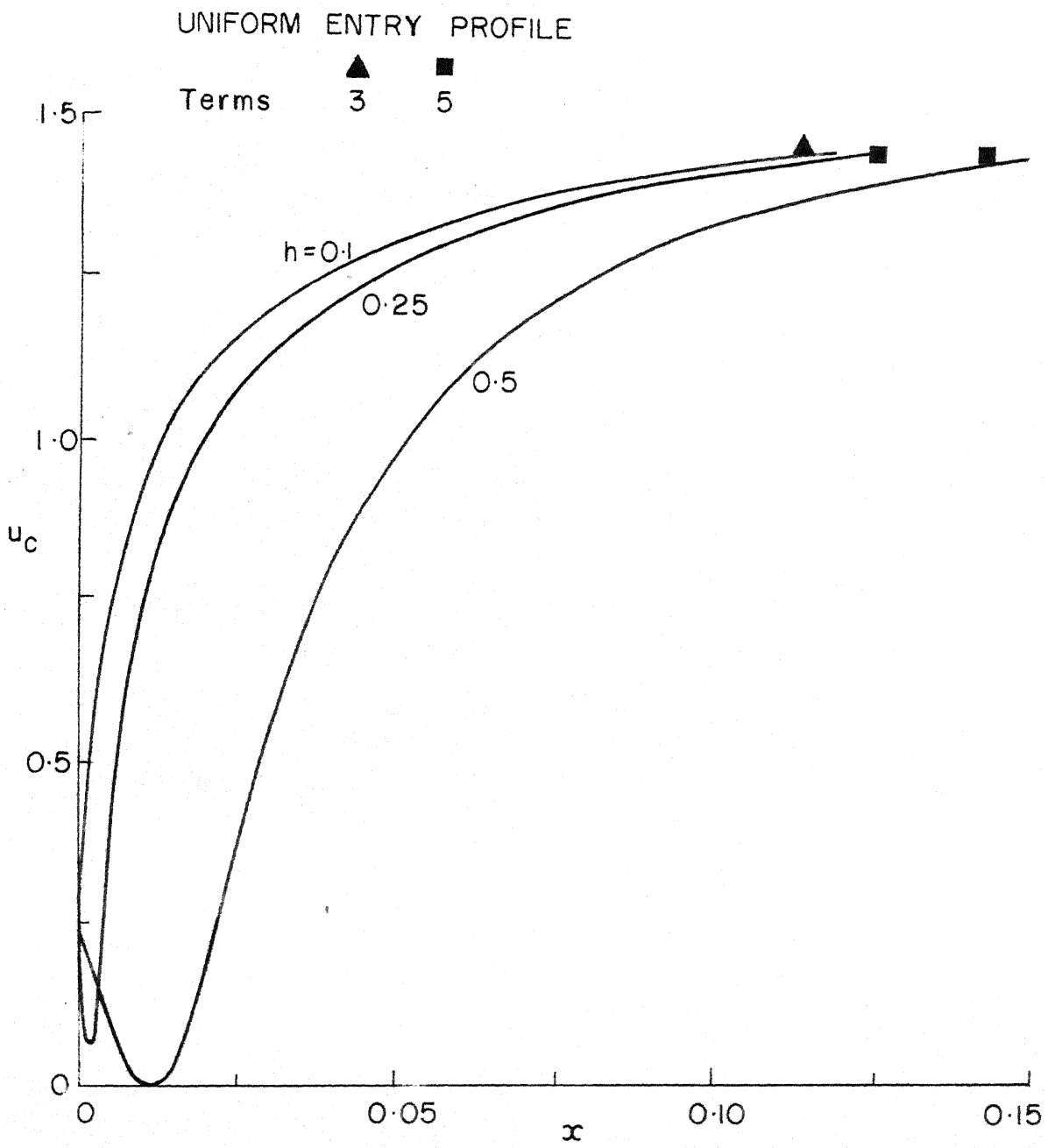

FIG. 39 CENTRELINE VELOCITY DISTRIBUTION FOR THE BASE IN A CHANNEL

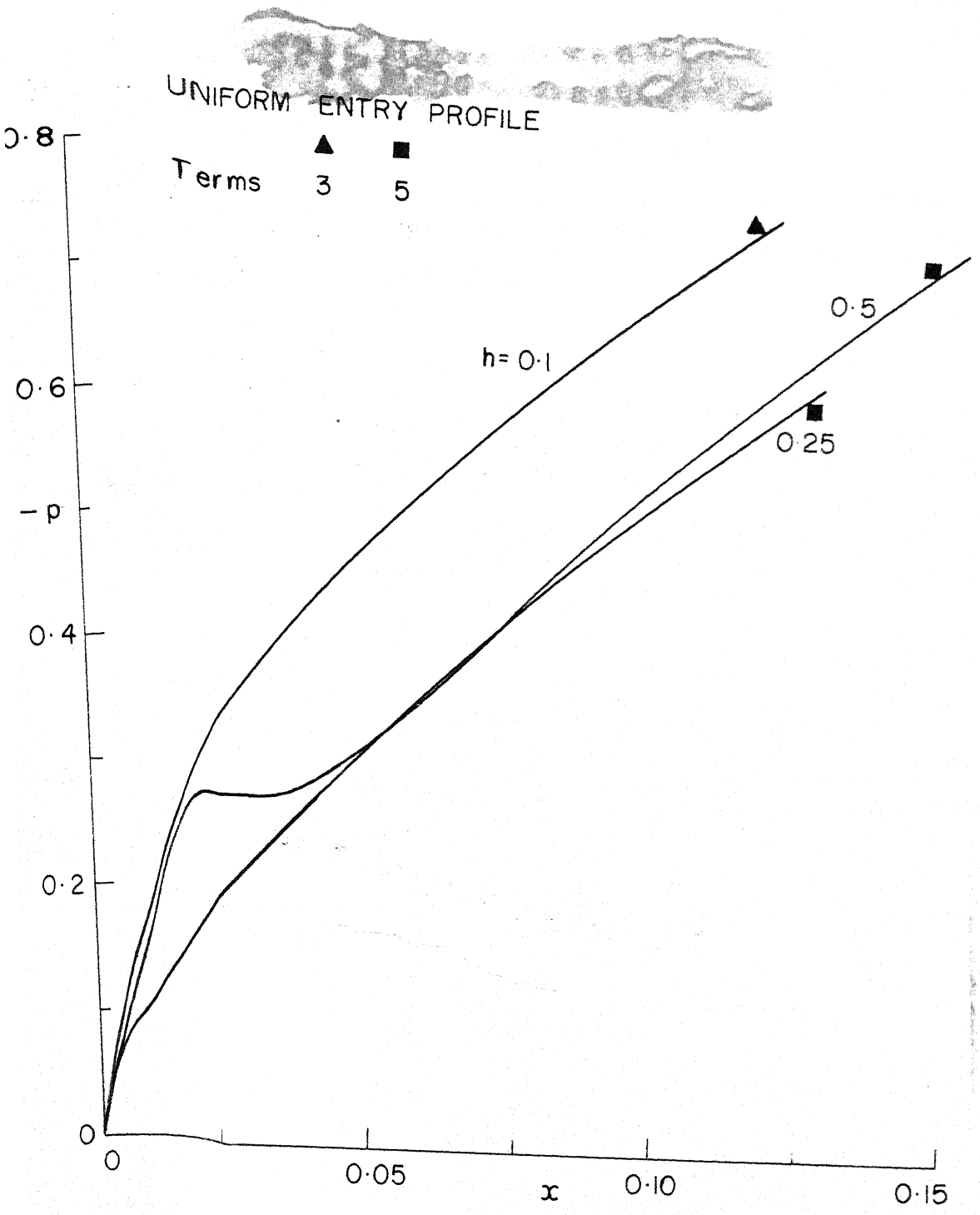

FIG. 40 PRESSURE DISTRIBUTION FOR THE BASE IN A CHANNEL

A 51152

Date Slip A 51152

This book is to be returned on the date last stamped.

CD 6 72.9

ME-1976-D-KUM-ANA.